

UNIVERSITY OF OKLAHOMA

GRADUATE COLLEGE

PERSONALIZED MEDICINE: DEVELOPING PRECISION ANTIVIRAL/

ANTICANCER THERAPEUTICS AND BIO-ANALYTICAL

CHEMOTHERAPEUTIC DRUG MONITORING

A DISSERTATION

SUBMITTED TO THE GRADUATE FACULTY

in partial fulfillment of the requirements for the

Degree of

DOCTOR OF PHILOSOPHY

By

RYAN BENSEN
Norman, Oklahoma
2020

PERSONALIZED MEDICINE: DEVELOPING PRECISION ANTIVIRAL/
ANTICANCER THERAPEUTICS AND BIO-ANALYTICAL
CHEMOTHERAPEUTIC DRUG MONITORING

A DISSERTATION APPROVED FOR THE
DEPARTMENT OF CHEMISTRY AND BIOCHEMISTRY

BY THE COMMITTEE CONSISTING OF

Dr. Anthony Burgett, Chair

Dr. Christina Bourne

Dr. Rakhi Rajan

Dr. Zhibo Yang

Dr. Cecil Lewis

Acknowledgments

I'd like to thank everyone in the Burgett lab for their continued support, numerous contributions, and overall friendly environment. A special thanks is needed for my mentor, Dr. Burgett, who continuously provided me training and guidance in all aspects of my scientific career. Furthermore, countless thanks are needed for Mr. Zachary Severance, who was my peer throughout all my studies, and I would not have been able to produce many of these results in chapter 2 without his assistance. On a similar note, a big thanks is need for Dr. Brett Roberts who produced many of the assays and data for chapter 2 as well. Thanks are also in order for Dr. Naga Rama Kothapalli for her continuing guidance and being a mentor.

None of these biological studies would have been able to be produced without the work from Dr. Anh Le – McClain, who isolated the OSW-1 compound, and synthesized both internal standards in chapter 4. Further thanks is needed for Mr. Cori Malinky for his synthesis in numerous molecules.

I'd also have to give a massive thank you to our collaborator, Dr. Yang, for his guidance and availability for using his laboratory equipment throughout chapter 4. Thanks is needed to Dr. Standke for her work, training, assistance, and mentorship throughout all of chapter 4, none of the produced work would have been possible without her assistance.

I'd also like to thank my other collaborator, Dr. Acar, for all her assistance with the production of chapter 3. Specifically, I'd like to thank Gokhan for his numerous contributions and would obviously not have been able to be produced without his help.

Thanks are also in order for the numerous professors which have graciously allowed me to use their equipment over the years: Dr. Duerfeldt, Dr. Cichewicz, Dr. Zgurskaya, Dr. Sims, Dr. Bourne, and Dr. Wu.

Lastly, I'd like to thank my committee for their support, guidance, and flexibility throughout my studies.

Table of Contents

| | |
|---|-------|
| List of Tables | xi |
| List of Figures..... | xii |
| Abstract..... | xviii |
| Chapter 1: Introduction to Personalized Medicine..... | 1 |
| 1.1 Personalized Medicine as a New Paradigm in the Clinical Treatment of Human Disease | 1 |
| 1.2 Current Practices in Clinical Bioanalytical Methods in Drug Administration..... | 2 |
| 1.3 The Oxysterol-Binding Proteins (OSBP/ORPs) As Potential Precision Drug Targets for Antiviral and Anticancer Drug Development..... | 4 |
| OSBP Biology | 5 |
| ORP4 Biology | 8 |
| 1.4 The Antiviral and Anticancer Compound OSW-1 Targets OSBP and ORP4..... | 8 |
| 1.5 Single Cell Bioanalytical Methods for Potential Use in Personalized Medicine . | 9 |
| The Single-Probe as a Personalized Drug Monitoring Method..... | 10 |
| 1.6 Summary of Dissertation Research: New Precision Compounds Targeting OSBP and ORP4 and New Single Cell Mass Spectrometry for Chemotherapy Drug Administration..... | 11 |
| Chapter 2: Molecular Pharmacology of Antiviral Compound Targeting OSBP, Including OSW-1..... | 13 |
| Abstract..... | 13 |
| Allocation of Contribution | 13 |
| 2.1 Introduction | 14 |

| | |
|---|----|
| 2.2 Methods | 16 |
| 2.2.1 Cell Lines and Viruses..... | 16 |
| 2.2.2 Cell Lysis..... | 16 |
| 2.2.3 Immunoblotting | 17 |
| 2.2.4 OSW-1 Compound Washout Treatments | 17 |
| 2.2.5 Deuterated OSW-1 | 18 |
| 2.2.6 OSW-1 Quantification..... | 18 |
| 2.2.7 Calpain Analysis..... | 20 |
| 2.2.8 Antiviral Analysis..... | 20 |
| 2.2.9 Competitive Binding Assay..... | 22 |
| 2.3 Results | 23 |
| 2.3.1 OSW-1 Treatment Selectively Degrades OSBP in Cells | 23 |
| 2.3.2 OSBP Repression is Independent of Residual OSW-1. | 24 |
| 2.3.3 OSBP Repression is independent of Calpain activity | 28 |
| 2.3.4 OSW-1 and THEV2 bind OSBP and ORP4..... | 30 |
| 2.3.5 OSW-1 selectively exhibits prophylactic activity | 33 |
| 2.4 Discussion..... | 35 |
| 2.5 Conclusions | 36 |
| Chapter 3: OSW-1 Compound Anti-cancer Development in Ovarian Cancer Targeting | |
| ORP4L Protein | 37 |
| Abstract..... | 37 |
| Allocation of Contribution | 37 |
| 3.1 Introduction | 38 |

| | |
|--|----|
| 3.1.1 Ovarian Cancer Background | 38 |
| 3.1.2 ORP4 Biology | 39 |
| 3.2 Methods | 41 |
| 3.2.1 Cell Culture | 41 |
| 3.2.2 2D Viability Assay | 41 |
| 3.2.3 Spheroid Development | 41 |
| 3.2.4 3D Viability Assay | 42 |
| 3.2.5 Cell Lysis..... | 43 |
| 3.2.6 Immunoblotting | 43 |
| 3.2.7 Trypan Blue Viability..... | 44 |
| 3.2.8 Delipidated FBS Media | 44 |
| 3.2.9 Statistical Analysis | 44 |
| 3.3 Results | 45 |
| 3.3.1 ORP4 is ubiquitously expressed in ovarian cancerous cells in vitro..... | 45 |
| 3.3.2 OSW-1 is a potent inhibitor of cancer cell proliferation. | 45 |
| 3.3.3 Ovarian cancer cells produce in vitro spheroids..... | 48 |
| 3.3.4 OSW-1 is a potent cytotoxic agent to ovarian spheroids in vitro..... | 50 |
| 3.3.5 OSW-1 toxicity is independent of OSBP degradation and correlates with ORP4L levels..... | 53 |
| 3.3.6 OSW-1 toxicity is regulated based on extracellular lipids. | 54 |
| 3.4 Discussion..... | 57 |
| 3.5 Conclusions | 58 |

| | |
|--|----|
| Chapter 4: Bio-Analytical Chemotherapeutic Drug Monitoring and Quantification of | |
| Gemcitabine in Single Cells | 60 |
| Abstract..... | 60 |
| Allocation of Contribution | 60 |
| 4.1 Introduction | 61 |
| 4.2 Methods | 64 |
| 4.2.1 Sample Preparation..... | 64 |
| 4.2.2 Single Probe Fabrication | 65 |
| 4.2.3 Glass Cell-Selection Probe Fabrication..... | 65 |
| 4.2.5 Single-Cell Mass Spectrometry Analysis | 66 |
| 4.2.6 Liquid-Chromatography Mass Spectrometry Analysis | 67 |
| 4.2.7 Isotopically-labeled Gemcitabine | 68 |
| 4.2.8 Statistical Analysis | 69 |
| 4.3 Results | 70 |
| 4.3.1 The Integrated Cell Manipulation System..... | 70 |
| 4.3.2 Adherent Cell Drug Identification..... | 74 |
| 4.3.3 Metabolomic Analysis..... | 75 |
| 4.3.4 Single-Cell Drug Quantification..... | 77 |
| 4.3.5 Clinical Single-Cell Patient Isolated Drug Quantification | 81 |
| 4.4 Discussion..... | 83 |
| 4.5 Conclusions | 84 |
| Chapter 5: Conclusions and Future Outlook | 85 |
| References | 88 |

| | |
|--|-----|
| Appendix 1: Chapter 2 Supplemental | 105 |
| Appendix 2: Chapter 3 Supplemental | 112 |
| Appendix 3: Chapter 4 Supplemental..... | 115 |

List of Tables

| | |
|--|----|
| Table 1: Quantification of intracellular gemcitabine in T24 and K562 cells using the Single-Probe (T24) or Single-probe/ICMP (K562) method..... | 76 |
| Table 2: Concentration of intracellular gemcitabine in K562 cells using SCMS and LCMS. | 81 |

List of Figures

| | |
|--|----|
| Figure 1: OSBP/ORP Binding Ligand 25-hydroxycholesterol (1) and OSW-1 (2)..... | 5 |
| Figure 2: Oxysterol-Binding Protein Family. ¹⁴² | 6 |
| Figure 3: Research Dissertation Schematic. Development of OSW-1 for antiviral/ anticancer therapeutic and methodology for gemcitabine chemotherapeutic monitoring. | 11 |
| Figure 4: OSW-1 competitive binding to the human OSBP and ORP4 protein against 25-OHC. | 23 |
| Figure 5: OSW-1 degrades the OSBP protein in a time and concentration dependent manner in HCT-116 cells A) The OSW-1 molecule. B) OSBP and ORP4 Western blot following 1 nM OSW-1 treatment. C) A 6 h treatment of compound, followed by 3X wash and Western blot at the provided times. D) 1 nM OSW-1 treatment for the indicated time followed by 24 h recovery. E) 1 nM OSW-1 treatment for the indicated time followed by 24 h recovery. F) 1 hr treatment at indicated OSW-1 concentrations followed by 24 hr recovery..... | 25 |
| Figure 6: Liquid Chromatography Mass Spectrometry (LCMS) quantification of OSW- 1 at 0 h and 24 h post washout of a 100 nM treatment for 1 h. The deuterated OSW-1 analog (5 nM) is used as an internal standard for quantification..... | 26 |
| Figure 7: Chromatogram of LCMS quantification of OSW-1 (<i>m/z</i> 895.44) at 0 h and 24 h post washout of a 100 nM treatment for 1 h. The deuterated OSW-1 analog (<i>m/z</i> 898.46) (5 nM) is used as an internal standard for quantification..... | 27 |

| | |
|---|----|
| Figure 8: Single Cell Mass Spectrometry (SCMS) quantification of OSW-1 at 0 hr and 24 hr post-washout of a 100 nM treatment for 1 hr. The deuterated OSW-1 analog (5 nM) is used as an internal standard for quantification. | 28 |
| Figure 9: Chromatogram of SCMS quantification of OSW-1 (m/z 895.44) at 0 h and 24 h post washout of a 100 nM treatment for 1 h using an internal standard of deuterated OSW-1 (m/z 898.46). Phosphatidylcholine (m/z 782.56) is used as a marker of intracellular content being analysed. | 29 |
| Figure 10: Western blot analysis of OSBP levels in HEK-293 cells of A) 24 h co-incubation of OSW-1 1 nM and calpain inhibitor ALLN 10 μ M, and B) following 6 h 1 nM treatment of OSW-1, washout, recovery for 24 h and treatment with calpain inhibitor, ALLN for an additional 24 h. | 30 |
| Figure 11: Competitive binding of OSW-1, THEV, TTP and ITZ to OSBP and ORP4 using the 25-OHC competitive binding assay. Example of results from one independent experiment shown..... | 31 |
| Figure 12: Growth inhibition analysis of co-administration of OSW-1 with either 10 μ M of ITZ, TTP, or THEV2 following 48 h. | 32 |
| Figure 13: A. Antiviral activity of TTP (10 μ M), ITZ (10 μ M), THEV2 (10 μ M), or OSW-1 (10 nM). Cells were inoculated with virus at an MOI of 1 and treated with compound for 10 h. B. Prophylactic activity of each compound. Compounds were administered for 6 h, washed out, 24 h recovery, then infected with virus at MOI of 1 for 30 min infection with 10 h recovery. Data acquired by Dr. Blewit..... | 33 |
| Figure 14: The antineoplastic compound, OSW-1, protein binding partner, ORP4, is a selectively expressed cancer protein. A.) The OSW-1 compound. B.) RNA expression | |

| | |
|---|----|
| in human tissues from the FANTOM5 dataset. C.) Patient percentage that have at least medium expression of ORP4 in cancer tissue. Data collected from the Human Protein Atlas. Patient samples ≥ 9 . D.) Western blot of OSBP and ORP4 in all four ovarian cell lines. E.) Quantification of OSBP and ORP4 in ovarian cancer cell lines relative to SKOV-3..... | 46 |
| Figure 15: OSW-1 is a cytotoxic agent to monolayer ovarian cancer cells. A-D) Growth inhibition curves of Paclitaxel, OSW-1, and Cisplatin in four ovarian cell lines. E) Table of GI ₅₀ values. Error shown as SD (n = 3). | 47 |
| Figure 16: OVCAR-8 and SKOV-3 ovarian cancer cells form spheroids <i>in vitro</i> . A.) Schematic of spheroid formation in ovarian cell lines. B.) OVCAR-8 and SKOV-3 spheroid development over 7 days. White bar represents 250 μ M. C.) Quantification of spheroid size over 7 days..... | 49 |
| Figure 17: The OSW-1 compound is potent, cytotoxic agent to <i>in vitro</i> generated ovarian cancer spheroids. A.) OVCAR-8 spheroid images at 72 h post treatment. B.) SKOV-3 spheroid images at 72 h post treatment. C.) OVCAR-8 spheroid toxicity quantification relative to control using Cell-Titer Glo. (n = 3). D.) SKOV-3 spheroid toxicity quantification. (n =3)..... | 50 |
| Figure 18: OSW-1 cellular morphology and viability. A) 40X magnification of OVCAR-8 and SKOV-3 monolayer (2D) following the provided treatments of OSW-1. B) Viability of each condition using a cell count with trypan blue cell viability..... | 51 |
| Figure 19: Ovarian cancer viability is correlated with ORP4L degradation and independent of OSBP expression upon OSW-1 treatment. A.) OSBP and ORP4L | |

| | |
|---|----|
| protein expression in 2D and 3D following the provided treatments of OSW-1 for 48 h in SKOV-3 and B.) in OVCAR-8..... | 52 |
| Figure 20: OSW-1 toxicity is potentiated in the absence of extracellular cholesterol. A) Growth inhibition curves of 2D OVCAR-8 cells and B) SKOV-3 2D cells with OSW-1, Paclitaxel, or 25-hydroxycholesterol incubated in either normal media (RPMI with 10% FBS), Delipid media (RPMI with 10% Delipid FBS), or cholesterol media (RPMI with 10% Delipid FBS and 20 μ g/mL cholesterol). C) Fold change quantification of GI ₅₀ values relative to normal media..... | 55 |
| Figure 21: The Single-Probe/ICMP Setup. A) The integrated cell manipulation platform (ICMP) Single-Probe coupled with the Mass Spectrometer. B) Schematic Representation of the Single-Probe coupled with the ICMP. C) 40X magnification of the cell-selection probe with K562 suspended cells..... | 70 |
| Figure 22: Lipid composition of a single, suspended K562 cell. Zoomed-in mass spectrum from a single cell showing the representative species (m/z 750–850). Structure confirmation of the labeled ions were performed through MS/MS analysis..... | 71 |
| Figure 23: Mass Spectrum of Taxol from a single K562 cell. Zoomed-in mass spectra showing molecular profiles (m/z 800–900) for (A) untreated and (B) treated (100 nM Taxol for 24 hours) single K562 cells. | 72 |
| Figure 24: Mass spectra obtained from individual K562 cells. (A) Spectrum from a single cell treated with 1 μ M gemcitabine for 1 hr. (B) Spectrum for a cell exposed to 1 μ M Taxol for 1 hr. (C) An individual cell treated with 100 nM OSW-1 for 4 hr. | 73 |

| | |
|--|-----|
| Figure 25: Metabolomic Analysis of individual K562 cells. PCA showing the overall difference of metabolomic compositions of single K562 cells in the control and drug treatment (100 nM Taxol for 24 h) groups. | 74 |
| Figure 26: Quantification of intracellular gemcitabine. Scatter plot depicting the amount of drug (attomoles) measured at each treatment concentration for each gemcitabine-treated (1-h) cell. (A) T24 cells using the Single-probe method and (B) K562 cells using the Single-probe/ICMP method. | 75 |
| Figure 27: Gemcitabine spectra from patient isolated bladder cancer cell. Mass spectrum of gemcitabine and the inactive metabolite, dFdU, with 1 $\mu\text{M}^{15}\text{N}_3$ -gemcitabine from an individual cell isolated from the urine of a bladder cancer patient one hour after a 1000 mg/m ² infusion of gemcitabine. | 78 |
| Figure 28: Mass spectrum of a single cell isolated from a bladder cancer patient qualitatively detecting phospholipids. | 79 |
| Figure 29: MS/MS spectra of Gemcitabine. A) MS/MS spectra of gemcitabine analyzed from a single cell isolated from bladder cancer patient 1. B) MS/MS of gemcitabine from a spiked solution. | 80 |
| Figure 30: 40X magnification of (A) K562 cells and (B) bladder cancer patient urinary cells. | 82 |
| Figure 31: Full blots from Figure 5 | 105 |
| Figure 32: Full blots from Figure 5 | 106 |
| Figure 33: Full blots from Figure 5 | 107 |
| Figure 34: Full blots from Figure 5 | 108 |
| Figure 35: Full blots from Figure 5 | 109 |

| | |
|--|-----|
| Figure 36: Zoomed out spectra of Figure 8. | 110 |
| Figure 37: Spectra of LCMS 100pM OSW-1 sample for limit of quantification | 111 |
| Figure 38: Spheroid Cytotoxicity and Protein levels. A) Spheroid images of SKOV-3 and OVCAR-8 treated with the provided concentration of compound at the provided times. B) Protein quantification of OSBP and ORP4L spheroid (3D) levels relative to monolayer (2D). | 112 |
| Figure 39: Full blot of Figure 15. | 113 |
| Figure 40: Full blots of Figure 20..... | 114 |
| Figure 41: MS/MS verification of lipids with 10-40 manufacturer's unit energy. | 115 |
| Figure 42: MS/MS verification of lipids with 10-40 manufacturer's unit energy. | 116 |
| Figure 43: MS/MS verification of lipids with 10-40 manufacturer's unit energy. | 116 |
| Figure 44: MS/MS verification of lipids with 10-40 manufacturer's unit energy. | 116 |
| Figure 45: MS/MS verification of lipids with 10-40 manufacturer's unit energy. | 116 |
| Figure 46: Synthesis of stable-isotopically labeled Gemcitabine..... | 116 |
| Figure 47: ¹ H NMR spectra of non-labeled gemcitabine (top) and labeled gemcitabine (bottom). | 116 |
| Figure 48: Mass spectrum of gemcitabine and ¹⁵ N ₃ -gemcitabine. (A) Spectra from a single T24 cell following 1 h 10 μM Gemcitabine treatment. (B) Spectra from a single K562 cell following 1 h 10 μM Gemcitabine treatment. | 116 |
| Figure 49: Spectra of Gemcitabine depicting the limit of quantification (LOQ) utilizing the single probe in a 5nM gemcitabine/ 100nM ¹⁵ N ₃ -gemcitabine solution in acetonitrile. | 116 |

Abstract

Personalized medicine, also known as precision medicine, is a broad medical paradigm for tailoring patients' treatments based upon their individual biological makeup to produce the most effective, safest clinical outcomes. Personalized medicine has the potential for enhancing nearly all fields of human health but has gained particular traction in oncology, a disease characterized by heterogeneity within patient populations. The application of personalized medicine in oncology requires both bioanalytical methods capable of providing real-time, useful clinical information in individual patients and new precision drugs matched to individual patient's clinical disease. My dissertation research encompasses two main projects centered on personalized medicine. The first project is the study of the molecular pharmacology of the antiviral and anticancer compound OSW-1. OSW-1 induces its antiviral activity through targeting oxysterol-binding protein (OSBP) and its anticancer activity through targeting OSBP-related protein 4 (ORP4). My research has established ORP4 as a potential personalized drug target in ovarian cancer, and OSW-1 as a potential lead target with potent anticancer activity in ovarian cell lines through targeting ORP4. The second major development is a single cell mass spectrometry method capable of quantifying chemotherapy drug levels in individual cancer cells, including single cancer cells isolated from patients. These discoveries have clear potential for developing clinically relevant, better personalized medicine through the development of optimal precision drug design and administration.

Chapter 1: Introduction to Personalized Medicine

1.1 Personalized Medicine as a New Paradigm in the Clinical Treatment of Human Disease

Over the past few decades, an emerging amount of evidence have demonstrated the variability in drug responses between individuals.¹ This differential reaction to medication between individual patients has initiated the realization of the importance of individual biological makeup in human medicine.¹ The new movement in personalized medicine (also frequently referred to as precision medicine) encompasses a broad medical approach for tailoring patients' treatments based upon their individual biological makeup to produce the most effective, safest clinical outcomes.¹ In 2015, President Obama enacted the Precision Medicine Initiative with a mission to circumvent the “one pill treats all” approach through “enabling a new era of developing individualized care”. Although nearly all fields of human health could be enhanced through personalized medicine, oncology is particularly in need of personalized medicine approaches.² Cancer is a disease characterized by extensive patient and disease heterogeneity², and therefore, the “one pill treats all” approach to medicine is not suitable for cancer treatment.

The field of personalized medicine grew out of the development of genomic sequencing technologies and the full sequence of the human genome in the early 2000s. Although only about 0.1% of the 3 billion bases pairs of DNA differ from person to person, these genetic differences are a significant cause of the different individual responses to clinical medicine.¹ This understanding has introduced a new field of study called pharmacogenomics, which is a field of science determining how genetic variations in individuals affect their response to therapeutic intervention. Many different genes

could, in concert, contribute to individual drug responses, making identifying specific gene causing the responses difficult.³ A clear example of the genes that regulate a patient's response to medicine are genes that code for cytochrome P450 (CYP 450) enzymes responsible for metabolizing, distributing, and excreting the vast majority of currently available drugs.⁴ Minute changes in the genes coding these enzymes, such as single nucleotide polymorphism (SNPs), could have pronounced effects on P450 metabolism of drug compounds in individual patients.

Although the “one pill treats all” approach for disease treatment still dominates modern medicine, recently many examples of therapies targeted to select populations of patients have been developed. Potentially the best example of existing precision medicines is the treatment of chronic myeloid leukemia (CLL) using the targeted drug Gleevec.⁵ Most CLL cases arise from a chromosomal abnormality producing a BCR-ABL1 fusion protein, which is only present in the CLL cells.⁵ The Gleevec drug targets and inhibits the BCR-ABL1 enzyme, blocking the CLL cell proliferation.⁵ Many precision cancer drugs are monoclonal antibodies targeting cancer-specific cell surface protein, such as the drug Herceptin which targets the HER2 protein present in the cell surface of many breast cancer cells.⁶

1.2 Current Practices in Clinical Bioanalytical Methods in Drug Administration

Beyond the development of new precision therapeutics, a main obstacle halting the development of personalized medicine is the lack of bioanalytical technologies capable of providing clinically relevant information about an individual patient in real-time. The absence of methods capable of guiding the personalization of drug

administration and treatment monitoring continues the “one pill treats all” approach to medicine, especially in the treatment of cancer. Therapeutic Drug Monitoring (TDM) is the existing method used to monitor drug levels in patients.⁷ TDM is defined as a clinical laboratory technique of individualizing drug dosage through monitoring and maintaining plasma and blood concentrations within a therapeutic window.⁷ The advantages of TDM was established in the 1970’s when therapeutic ranges were established and the incidences of toxicity for digoxin, phenytoin, lithium, and theophylline could be reduced.^{8–10} Today, TDM is mostly performed on patient’s blood samples and quantified using a variant of immunobinding assay procedures such as fluorescent polarization immunoassay (FPIA), enzyme immunoassay (EMIT) or enzyme-linked immunosorbent assay (ELISA).^{7,11,12} Although these assays produce quick results through commercial products, due to their antibody targeting methodologies, they are susceptible to cross-reactivity creating falsely elevated drug concentrations.^{7,11,12}

The application of TDM is also hindered due to the vast degree of specialists needed to accurately administer a personalized treatment course.⁷ An interdisciplinary cohort of professionals consisting of scientists, clinicians, nurses, pharmacists, and analytical chemists are needed to work together to successfully administer an appropriate treatment course in a timely manner.⁷ Furthermore, a cost-effective methodology is needed to keep the price of treatment to a minimum.⁷ Because of these difficulties, the standard use of TDM is at a minimum in the clinical setting.⁷

Current applications of TDM in oncology are further hindered due to the lack of personalization through not considering an individual’s unique cancer and drug uptake into the cancerous tumor cells. Because of an individual’s pharmacokinetic/

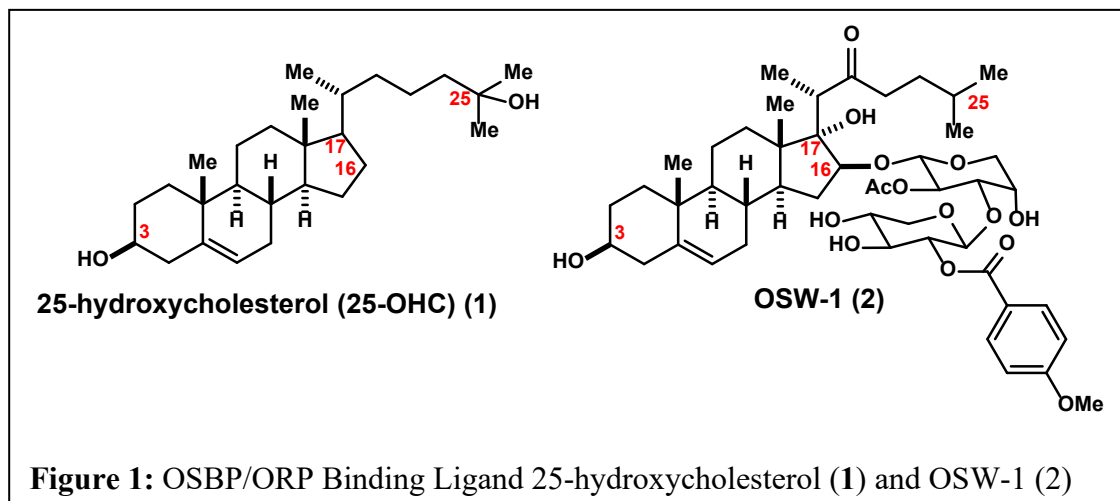
pharmacodynamic capabilities, the drug concentration measured in the plasma may not predict the drug concentration in the tumor and tumor cells.^{13,14} Furthermore, tumor cells are a complex, heterogenous mixture of cells consisting of multidrug-resistant (MDR) cancer and non-cancer cells.¹⁵ These (MDR) cells can engage P-glycoprotein pumps to extrude drugs outside of the cells, further creating a difference in drug concentration in the tumor cells compared to the blood serum.¹⁶ A bioanalytical method capable of quantifying drug compound in individual cancer cells in a time efficient and non-invasive manner would prove a valuable personalized tool for assessing individual TDM.

1.3 The Oxysterol-Binding Proteins (OSBP/ORPs) As Potential Precision Drug Targets for Antiviral and Anticancer Drug Development

Oxysterol-binding proteins (OSBP) and OSBP-related proteins (ORPs) comprise a family of proteins conserved in all eukaryotes, from yeast to humans.^{17,18} OSBP, the OSBP/ORP member first identified, was discovered as a high affinity binder of oxysterols *in vitro*.^{19,20} Oxysterols are 27-carbon products of cholesterol oxidation, mainly performed by hepatic cytochrome P450 enzymes (**Figure 1**, 25-hydroxycholesterol (**1**) as an example oxysterol).⁴

Oxysterols have a variety of biological activities including: inducing cytotoxicity, cholesterol regulation, and membrane integrity perturbation.^{21–26} Although the biological role of the individual member of the OSBP/ORPs are not completely elucidated, an overall idea is that these proteins are involved in cellular lipid sensing or transport, including sterols, and the preferential binding to oxysterols of the OSBP/ORP could control lipid homeostasis or specific cellular signaling events.^{17,27–30}

The OSBP/ORP protein family shares a conserved carboxy-terminal ligand binding domain (LBD) also referred to as OSBP related domain (ORD). The ORD structure consists of 19 anti-parallel beta sheets based upon protein structures of yeast homologs (**Figure 2**).^{18,31} Outside of the ORD, the N-terminal ~50 kDa contains two

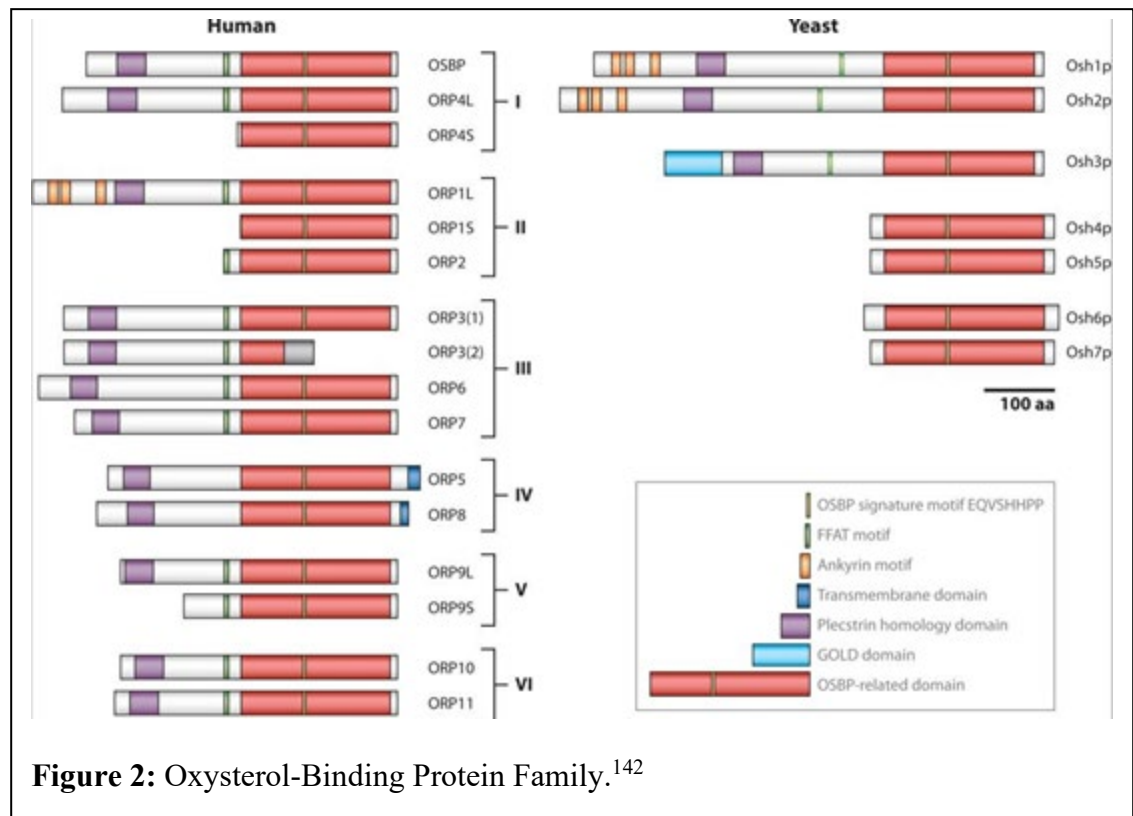


phenylalanines in an acidic tract (FFAT) domain and an amino terminal pleckstrin homology (PH) domain (**Figure 2**).¹⁸ The OSBP PH domain is reported to interact with phosphatidylinositols in cell membranes, specifically PI4P and PI2P, for trans-Golgi localization.^{32,33} The FFAT motif is able to interact with the ER resident vesicle-associated membrane proteins (VAPs) providing a tether between OSBP and the ER.³⁴

OSBP Biology

OSBP has been reported to bind to 25-hydroxycholesterol with a much higher affinity than cholesterol.^{17,23,35–37} OSBP is also reported to bind phosphatidylinositols with unclear affinity.^{17,23,35–37} OSBP is reported to be located at the Golgi/endoplasmic reticulum (ER) membrane contact site (MCS), where it traffics cholesterol from the ER to the Golgi, while retroactively trafficking phosphatidylinositol 4-phosphate (PI4P) from the Golgi to the ER.^{38,39} This process is believed to be fueled by a PI4P lipid pool

produced by the phosphorylation of phosphatidylinositol by PI4KIII β kinase at the Golgi and the hydrolysis of PI4P by SAC1 on the ER membrane.^{17,30} OSBP mediates this transfer keeping the concentration gradient intact in both organelle membrane.⁴⁰ Further studies also suggested that OSBP is able to recruit CERT to the Golgi-ER interface for ceramide transport and sphingomyelin production. In this model, PI4KIII β is stimulated to increase PI4P production, producing another level of lipid regulation at cellular membranes.⁴¹



Phosphorylation of OSBP by Protein kinase D (PKD) inactivates OSBP by masking the PH domain and inhibiting the translocation of OSBP to the Golgi.⁴² Furthermore, PKD can activate and inhibit PI4KIII β and CERT, respectively.⁴² This leads to a potential mechanism of action of OSBP where PKD phosphorylation of PI4KIII β leads to increased PI4P in the Golgi and recruitment of OSBP through its PH domain and

activation of ARF1. This leads to more production of PI4P and recruitment of CERT to the MCS. OSBP's transportation of cholesterol from the ER to the Golgi and counter transport of PI4P from the Golgi to the ER leads to CERT shutting ceramide leading to Sphingomyelin (SM) production. Together, this represents a lipid homeostasis mechanism controlled by PKD phosphorylation.⁴²

OSBP is reported to regulate ERK1/2 signaling activity through modulating the activity of phosphatases that regulate ERK.⁴³ In this model, OSBP is believed to be a scaffold protein for the tyrosine and serine/threonine phosphatases, HePTP and PP2A, and the OSBP/phosphatase activity is controlled by sterol binding to OSBP. Under normal cholesterol level conditions or the absence of oxysterols, OSBP is bound to cholesterol and undergoes a conformation change masking the PH domain, producing an inactive phosphatase complex, which keeps ERK1/2 activity repressed. Upon low cholesterol levels or oxysterol binding, the conformation of OSBP is changed, unmasking the PH domain, removing the phosphatases, translocating OSBP to the Golgi to replenish cholesterol levels and thereby activating ERK1/2 signaling activity.⁴³

An additional study found that OSBP interacts with JAK2/STAT3 signaling leading to the expression of profilin-1.⁴⁴ In this model, 7-ketocholesterol leads to the production of profilin-1 through STAT3 activation by JAK2 and OSBP. Upon OSBP binding with 7-ketocholesterol, OSBP interacts with JAK2 and becomes phosphorylated leading to STAT3 interacting with OSBP/JAK2. STAT3 is then able to translocate to the nucleus to induce transcription of profilin-1.⁴⁴ This demonstrates another example of OSBP acting as a lipid sensor regulating signaling in the cells.

Recently, OSBP was discovered to be required for the replication of dozens of currently untreatable human pathogenic RNA viruses, including members of the *Enterovirus* genus of viruses, Zika virus, Dengue fever virus, and hepatitis.^{45–48}

ORP4 Biology

ORP4, the most similar family member to OSBP, shares none of OSBP's biological regulation or cellular localization.^{36,49} Unlike the ubiquitous tissue expression of OSBP, ORP4 is selectively expressed in a limited amount of normal tissues including the brain, retina, and testes.⁵⁰ Of importance, the ORP4 protein has recently been demonstrated to be essential for cancer cell proliferation in immortalized cell lines, and essential for cellular proliferation in T-cell acute lymphoblastic leukemia (T-ALL) patients.^{51,52} ORP4 is reported to promote mitochondrial respiration in immortalized immune cells by regulating calcium release from the endoplasmic reticulum through mediating a G-protein activation of PLC3 β .⁵¹ Knockdown of ORP4 in cancer cell lines results in increased apoptosis, autophagy, and mitochondrial dysfunction, which phenocopies OSW-1 treatment.^{51,53–57} The limited, selective expression of ORP4 in normal tissue while being essential for cancer proliferation, signifies ORP4 as a potential cancer precision therapeutic target.

1.4 The Antiviral and Anticancer Compound OSW-1 Targets OSBP and ORP4

The natural product OSW-1 (3 β ,16 β)-3,17-Dihydroxy-22-oxocholest-5-en-16-yl-2-O-acetyl-3-O-[2-O-(4-methoxybenzoyl)- β -D-xylopyranosyl]- α -L-arabinopyranoside) is a potent anticancer compound isolated from the bulbs of the *Ornithogalum saundersiae*

plant.⁵⁸⁻⁶⁰ OSW-1 and other OSBP-targeting compounds were found to have broad-spectrum antiviral activity against many different RNA viruses.⁶¹⁻⁶⁴ In addition to its antiviral activity, the OSW-1 compound has potent anticancer activity through putatively binding OSBP-Related Protein 4 (ORP4).^{51,54-56,60} OSW-1 treatment induces the degradation of cellular OSBP and ORP4.⁶⁰

1.5 Single Cell Bioanalytical Methods for Potential Use in Personalized Medicine

The development of single-cell mass spectrometry methods has been a major focus in bioanalytical research.⁶⁵ These analytical methodologies have investigated heavily on the “omics” of individual, single cells discovering which genomic, transcriptomic, proteomic, and metabolic changes trigger oncogenic progression, rather than drug quantification.⁶⁶⁻⁶⁸ Mass spectrometry is becoming the dominant technology for single-cell metabolite analysis due to its low sample preparation, high sensitivity, and high-throughput, label free ability. Multiple mass spectrometry ionization techniques (e.g. matrix assisted laser desorption/ionization (MALDI)^{65,69-71}, electrospray ionization (ESI)⁷²⁻⁷⁵, electron ionization (EI)⁷⁶) coupled with numerous mass analyzers (e.g. time of flight (TOF), quadrupole, Orbitrap) have been successful for the analysis of metabolites from single cells. The techniques broadly fall under two categories, ambient ionization or non-ambient ionization. MALDI is a well-established, commonly utilized, non-ambient technique used for detecting and quantifying metabolites from single cells.^{68,77} Due to the soft ionization, molecules remain intact, ideal for metabolomic analysis. MALDI, however, requires fixation of cells on a solid matrix and the use of a vacuum, resulting in the lack of analyzing live cells and the addition of interfering MALDI Matrix with the

small weight metabolites (<500 daltons).⁶⁷ Due to this, the development of ambient techniques has been the preferred method development to analyze live, single cells resulting in near native environment of the cells.

Ambient ionization techniques can be broadly grouped into either laser desorption/ionization or microprobe extraction methods. Laser desorption/ionization methodologies have been used to mainly study embryos but have also been utilized to perform in situ metabolomic analysis of individual, single cells including oocytes, plant cells, and mammalian cells.⁷⁸⁻⁸¹ Microprobe extraction methodology stems from the initial live-video single cell mass spectrometry technique from Masujima's lab.⁸² These methods take advantage of analyzing the metabolites of individual, live cells either through the use of a probe that penetrates the cells capable of analyzing sub-cellular compartments, or a larger probe capable of lysing the entire cell. Furthermore, multiple separation techniques (e.g., capillary electrophoresis, ion mobility) are able to be coupled to these methods and applied on the single cell level.^{66,83}

The Single-Probe as a Personalized Drug Monitoring Method

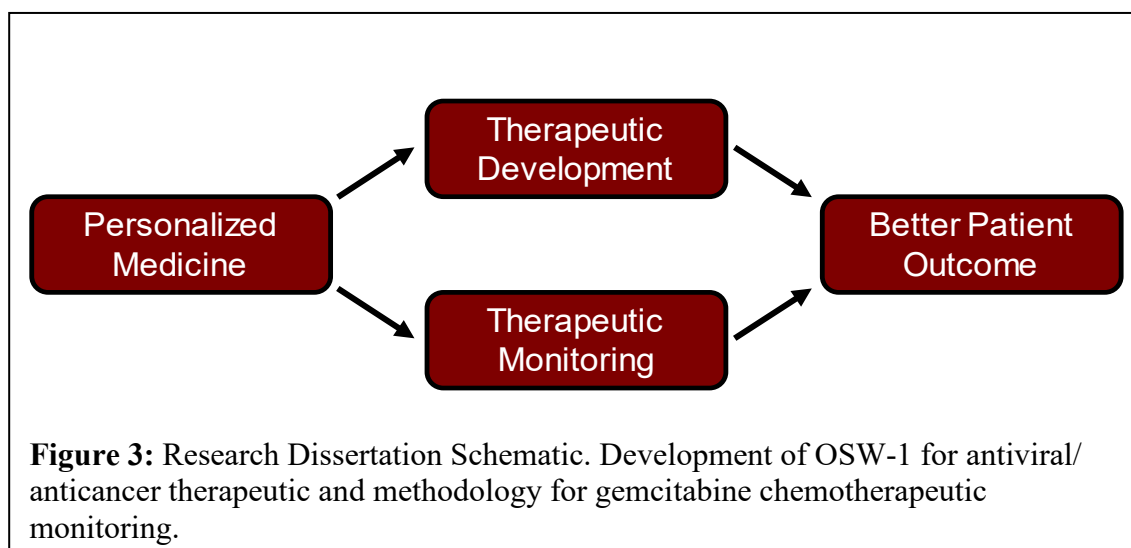
The Single-Probe is a developed sampling and ambient ionization device designed by the research group of Prof. Zhibo Yang in the Dept. of Chemistry and Biochemistry at the University of Oklahoma.⁸⁴ The Single-Probe is a microprobe extraction mass spectrometry technique uniquely capable of analyzing live, single cells with little to no sample preparation in real time.⁸⁴ It consists of a dual-bored quartz tubing with a sharp tip (<10 μ M) capable of a continuous flow of ionized solvent.⁸⁴ Once the Single-Probe is in contact with a single cell, the solvent flows through the tip, creates a micro lysis of the

cell and forms a liquid junction.⁸⁴ The cellular contents are extracted toward the nano-ESI emitter and ionized for MS analysis.⁸⁴

The Single-Probe MS technique has been modified and utilized for multiple applications, including MS imaging (MSI) analysis of multicellular spheroids, and detection of intracellular compounds from algal and adherent mammalian cells.^{85–89}

1.6 Summary of Dissertation Research: New Precision Compounds Targeting OSBP and ORP4 and New Single Cell Mass Spectrometry for Chemotherapy Drug Administration

The development of clinical cancer personalized medicine is limited by: 1) the lack of precision drugs and therapies that target cancer specific protein targets identified



in individual patient's cancer; and 2) the lack of clinical bioanalytical methodology capable of personalizing the administration of chemotherapy drugs to ensure the most effective outcomes in the individual patients. To address this dilemma, my dissertation research encompasses the study of OSBP and ORP4 as druggable targets for the

development of new antiviral and anticancer drug therapeutics. Further, I have worked to develop new applications of the single cell mass spectrometry technology to measure of the intracellular drug levels in single cancer cells from patients.

The three major projects of my doctoral research included in this dissertation are: 1) determining the prophylactic antiviral activity of the OSW-1 compound through targeting OSBP (**Chapter 2**); 2) characterizing ORP4 as a precision cancer target in ovarian cancer and OSW-1 as a potential precision cancer drug through targeting ORP4; (**Chapter 3**), and; 3) development of single cell mass spectrometry application for the quantification of drugs in individual cancer cells isolated from patients undergoing chemotherapy (**Chapter 4**).

Chapter 2: Molecular Pharmacology of Antiviral Compound

Targeting OSBP, Including OSW-1

Abstract

Oxysterol-binding protein (OSBP) is a conserved lipid regulator and lipid transport protein essential for the replication of several classes of RNA pathogenic viruses, including the *Enterovirus* genus of viruses. These RNA viruses that use OSBP to replicate in cells are responsible for many untreatable human diseases. Our research group has studied the molecular pharmacology of antiviral small molecules targeting OSBP, especially the natural product compound OSW-1. We've identified that the OSW-1 compound is a potent inhibitor of enterovirus replication *in vitro* through binding and degradation of the OSBP protein. We have shown that a short-term exposure (i.e., 1- 6 h) at a low dose (i.e., 1 nM) results in a long-term reduction of the OSBP protein for up to 72 hours with no changes in cellular viability, morphology, or proliferation, but correlates with the inhibition of viral replication. This multiday, multigeneration repression of the OSBP protein is independent of residual OSW-1 compound remaining in cell, nor is it caused by transcription inhibition, proteasome degradation, calpain activity, or autophagy. This long-term reduction and repression of OSBP presents a new opportunity for broad spectrum anti-*Enterovirus* activity, and a new route for prophylactic treatment through targeting of a host protein. We have also studied the molecular pharmacology of other reported antiviral compounds that target OSBP, including the steroidal compound T-00127-HEV2 (THEV2). I am co-author on both papers from our research group studying the molecular pharmacology of OSBP-targeting antiviral compounds, and my individual experimental research contributions to this overall published research project are reported here.

Allocation of Contribution

This chapter is a partial recapitulation results from two published articles: the 2018 *ACS Chemical Biology* paper⁹⁰ and the 2019 *Antiviral Research* paper.⁴⁵ The published articles was created from a group effort and has many co-authors, the major contributors were myself, Dr. Brett Roberts, and Mr. Zachary Severance. In this dissertation chapter, I have included only results from this paper that I produced, with the exception of the antiviral experiments (**Figure 13**), which were produced by our molecular virology collaborator Prof. Earl Blewett at Oklahoma State University Center of Health Sciences. The binding experiments (**Figure 4, Figure 11**) were jointly performed between myself and Mr. Zachary Severance. Furthermore, all mass spectrometry data acquisition was conducted through our established collaboration with the research group of Prof. Zhibo Yang lab at the University of Oklahoma. I worked with Dr. Shawna Standke, a graduate student in the Yang lab, to produce the mass spectroscopy results in **Figure 6, Figure 7, Figure 8, and Figure 9**. The mass spectroscopy studies used the deuterated version of the OSW-1 compound produced by Dr. Anh Le-McClain in our research group.

2.1 Introduction

OSBP is a required non-enzymatic host protein for the broad replication of the *Enterovirus* genus of virus responsible for many untreatable illnesses including: the common cold, acute respiratory infections, pneumonias, myocardial infections, hand, foot, and mouth disease, acute hemorrhagic conjunctivitis, and the paralytic condition acute flaccid myelitis.^{91–94} In addition, OSBP is known to be essential for hepatitis C virus, encephalomyocarditis, dengue, and zika virus replication.^{48,95,96} These viruses replicate in the cytosol of host cells through the hijacking of host proteins to produce replication organelles (RO).⁹⁷ RO are membrane bound structure made by stealing the membrane components of host ER and Gogi organelles.^{98–102} The human OSBP protein is reported to be critical for the formation of RNA virus's replication organelle formation.⁴⁶ For example, the enteroviral 3A protein recruits host ARF1 and GFB1 protein to the RO, in turn recruiting PI4KIII β and leading to PI4P accumulation. OSBP is able to localize to the RO through its interactions with PI4P and ARF1, and presumably shuttles essential cholesterol to the RO similar to its endogenous function between the Golgi and ER.^{100–102}

The essentiality of the OSBP protein for viral replication has led to the development of multiple OSBP targeting compounds for antiviral development. OSBP has been identified as the cellular target of the anti-enteroviral compounds, TTP-8307 (TTP)⁶², the FDA approved antifungal itraconazole (ITZ)⁶⁴, the steroidal compound T-00127-HEV2 (THEV2)⁶³, and the anti-cancer compound, OSW-1⁶¹. ITZ is a promiscuous compound with multiple cellular targets showing anti-fungal, cancer, and viral activity.^{103–105} It's broad range antiviral activity is believed to occur through its reported

binding to OSBP (K_d of 430 nM) which alters its cellular localization and inhibits cholesterol and PI4P counter transport.⁶⁴ TTP-8307 was also demonstrated to inhibit OSBP trafficking and to change the cellular localization of the protein.⁴⁸ THEV2 similar to both ITZ and TTP also changed the localization of OSBP and inhibited the transfer function.⁶³ Furthermore, THEV2 showed increased antiviral activity upon OSBP knockdown.⁶³ OSW-1 is unique compared to the other OSBP-targeting compounds as it targets both OSBP and ORP4, and that OSW-1 treatment caused a unique proteasomal degradation of OSBP.⁶⁰ OSW-1's broad antiviral activity is correlated to OSBP binding and perturbation rather than ORP4 binding.^{46,64}

Herein, this chapter describes my contributions to the identification of OSW-1 as a broad-spectrum prophylactic compound that works through a non-toxic, selective, and long-term degradation of the host OSBP protein. I show that the multiday repression of OSBP is independent of residual OSW-1 compound present in the cell. I also shown that the OSBP repression is not due to OSBP cleavage by activation of calpain protease activity. Further, my results demonstrate that the other OSBP-targeting antiviral activity THEV2 binds at an overlapping site to OSW-1, but unlike OSW-1, THEV does to induce the repression of OSBP in cells. My research contributions have clear applications for potentially developing new OSW-1-derived antiviral prophylactics and therapeutics.

2.2 Methods

2.2.1 Cell Lines and Viruses

HCT116 (ATCC CCL-247) colon cancer cell line was cultured in McCoy 5A media (Thermo 16600108) supplemented with 10% Hyclone and 1% penicillin streptomycin. HEK293 embryonic kidney cell line was cultured in DMEM (Thermo 11995073) supplemented with 10% Hyclone (Fisher Sci SH3006603) and 1% penicillin-streptomycin (Thermo 15140122). K-562 (ATCC CCL-243) was cultured in RPMI 1640 (Thermo 22400105) media supplemented with 10% Hyclone and 1% penicillin streptomycin. Coxsackievirus A9 (strain CoxA9-01) and Echovirus 2 (strain Echo2- 01) were obtained from the Oklahoma State Department of Health Laboratory. They are clinical isolates, obtained from OK residents and typed by the OK State Department of Health and/or the Center for Disease Control and Prevention. All other identifiers have been stripped off. These viruses were passaged twice in RD cells, aliquoted in 1.0 mL amounts and stored in complete medium at -80 °C. Each virus was titered on RD cells using a TCID-50 assay¹. To allow m.o.i. to be determined a conversion factor of 0.7 was used to change TCID-50 to pfu/mL.

2.2.2 Cell Lysis

Adherent cells were lysed by aspiration of media, wash with 1X PBS, addition of TrypLE™ Express (Gibco 12605- 010), and neutralized through the addition of media. Cells were spun at at 14,000 RCF for 0.45 min at 4C. Supernatant was aspirated, cell pellet washed with 1X PBS, and resuspended in 50 µL of AC lysis buffer (150 mM NaCl, 1.5 mM MgCl₂, 5% glycerol, 0.8% NP40, 1mM DTT, 50 mM HEPES, 25 mM NaF, 1

mM Na₃PO₄) with 3X HALT/EDTA protease inhibitor (Thermo 78438) and 0.2 mM phenylmethanesulfonylfluoride (Goldbio). Cells were freeze/ thawed (X3) with LN₂ and centrifuged for 15 min at 14,000 RCF at 4C. Resulting cell lysate was Bradford for protein concentration.

2.2.3 Immunoblotting

SDS-PAGE gels (8.5%) were loaded with 25 µg of protein, transferred to nitrocellulose membrane ((Bio-Rad 1620115) with a constant voltage of 100V for 1 h at 4C. The membrane was blocked in 5% milk for 0.5 h. Following washing with TBST (X3), the membrane was incubated with 1:500 ORP4 antibody (Santa Cruz sc-365922) or 1:1000 OSBP antibody (Santa Cruz sc-365771) overnight at 4C. Following washing, the membrane was incubated with 1:3000 Secondary antibody (Santa Cruz sc-2060) for 1 h at RT. Following washing, the membrane was developed with ClarityTM Western ECL substrate (Bio-Rad 1705061) and imaged on the Bio-Rad ChemiDocTM Touch Imaging System. The membrane was incubated with 1:1000 β-actin HRP (Santa Cruz sc-47778 HRP) after washing and developed as previously described.

2.2.4 OSW-1 Compound Washout Treatments

Cells were treated with 1 nM OSW-1, 1 nM Taxol, or DMSO media for 6 hr or the indicated time period. Media was removed and the cells were gently washed with 5 mL of complete media 3 times and then 10 mL of fresh, OSW-1-compound free media was added back to the cells. The cells were then allowed to recover for the indicated times (0-72 hrs) and were lysed as described above and analyzed by Western blot.

2.4.5 Deuterated OSW-1

The deuterated OSW-1 analog (Fig. 1A, 2) was produced via total synthesis of OSW-1 adapted from literature procedure. During the synthesis of the xylose component, a benzoate group containing the deuterated methyl substituent was introduced. ¹H NMR (400 MHz, Acetonitrile-d₃) δ 8.02 (d, J = 9.0 Hz, 2H), 7.02 (d, J = 8.9 Hz, 2H), 5.31 (d, J = 4.9 Hz, 1H), 4.84 (t, J = 8.2 Hz, 1H), 4.73 (dd, J = 8.3, 6.2 Hz, 1H), 4.61 (d, J = 7.7 Hz, 1H), 4.20 (s, 1H), 4.01 (d, J = 6.2 Hz, 1H), 3.92 (dd, J = 11.5, 4.9 Hz, 1H), 3.88 (s, 1H), 3.76 (dd, J = 12.4, 4.2 Hz, 1H), 3.67 (dt, J = 8.2, 4.2 Hz, 2H), 3.64 – 3.50 (m, 2H), 3.42 (dd, J = 12.4, 2.3 Hz, 1H), 3.38 – 3.22 (m, 2H), 2.86 (q, J = 7.3 Hz, 1H), 2.69 (s, 1H), 2.46 (ddd, J = 18.2, 9.0, 6.5 Hz, 1H), 2.23 – 2.08 (m, 5H), 1.99 – 1.90 (m, 1H), 1.85 – 1.76 (m, 1H), 1.75 – 1.68 (m, 2H), 1.67 (s, 3H), 1.64 – 1.38 (m, 5H), 1.32 (dt, J = 13.1, 6.6 Hz, 1H), 1.29 – 1.14 (m, 3H), 1.07 (d, J = 7.4 Hz, 3H), 1.04 – 1.01 (m, 1H), 1.00 (s, 3H), 0.94 – 0.83 (m, 1H), 0.82 – 0.74 (m, 9H). ¹³C NMR (101 MHz, Acetonitrile-d₃) δ 220.09, 169.95, 165.66, 164.73, 142.44, 132.79, 123.64, 121.86, 114.81, 102.92, 100.98, 88.19, 86.20, 80.82, 75.74, 74.47, 71.90, 71.72, 70.49, 67.67, 66.46, 65.22, 50.89, 49.20, 46.94, 46.54, 43.07, 39.71, 38.13, 37.35, 35.74, 33.19, 32.86, 32.69, 32.63, 32.37, 28.19, 22.88, 22.67, 21.34, 21.04, 19.79, 13.56, 12.16. HRMS calcd for C₄₇H₆₅D₃O₁₅Na: 898.4639 [M + Na]⁺, found 898.4611.

2.2.6 OSW-1 Quantification

LCMS: HCT-116 cells (1.5x10⁵) were seeded in a 6-well plate. Upon 60% confluency, cell lysate was created following a 1 hr treatment of 100 nM OSW-1, with or without a 24 hr post wash recovery. Trypsin (0.5 mL) was used to detach the cells, with

additional McCoy's media (0.5 mL) to stop digestion. Cell count was performed using a Bio-Rad TC20™ Automated Cell Counter with trypan blue viability staining. Cells were spun at 500 xg for 5 min followed by a 1-mL PBS wash. The cell pellet was lysed using 1 mL of 50 nM d-OSW-1 dissolved in cold acetonitrile and methanol (1:1) with brief vortexing on ice for 10 min. The cell pellet was spun at 15000 xg at 4°C for 15 min. The supernatant was transferred to a new tube and dried using a speed vacuum (Savant SPD11V, Thermo Scientific) at 70°C. Prior to analysis, cells are resuspended in 150 µL of ACN: H₂O (1:10). Analysis was performed using a Waters nanoAQUITY BEH C-18 column (100 µm x 100 mm, 1.7 µm) coupled with a mass spectrometer (Thermo LTQ Orbitrap XL, Waltham, MA) using a flow rate of 0.3 µL/min. Mobile phase A is ACN with 0.1% formic acid, and mobile phase B is H₂O with 0.1% formic acid. The time/%A are as follows: 0/0, 1/50, 2/100, 3/100, and 4/0 for a total runtime of 5 minutes.

SCMS: HCT-116 cells (1.5×10^5) were seeded on to a glass microchip (18 mm diameter) with chemically-etched microwells (55 µm diameter; 25 µm deep) placed into each well of a 6-well plate. Upon 60% cell confluency, cells were treated as described for nano-UPLC/MS. Following treatment, the microchip was washed with 5 mL of FBS-free McCoy's media and placed on an X, Y, Z-translational stage for quantification. MS analysis was performed as previously described.⁴ Briefly, singleprobes were coupled to the mass spectrometer by using a flexible arm clamp to position the nano-ESI emitter in front of the inlet. The solvent-providing capillary was connected to the solvent through the conductive union. For quantification, 50 nM d-OSW-1 was added into the solvent. High voltage (~4.5 kV) was used for SCMS experiments in the positive ion mode with a mass resolution ($m/\Delta m$) of 60,000. A flow rate of ~5 nL/s was used (the actual flowrate

is optimized for each Single-probe). Data was collected using Xcaliber software and exported into Excel for analysis.

2.2.7 Calpain Analysis

For the continual treatment, HeLa cells were seeded out in a 6 well plate. Upon 70% confluency, cells were treated with DMSO, DMSO and ALLN (10 μ M), OSW-1 (1nM), or OSW-1 (1nM) and ALLN (10 μ M) for 24 hr. Cells were lysed and analyzed following the 6-well lysis method and the western blot protocol. Under the washout experimental conditions, cells were treated with DMSO or OSW-1 (1nM) for 6 hr. Cells were washed out according to the washout experimental method. After 24 hr recovery, one set of DMSO and one set of OSW-1 was lysed following the 6 well lysis method. At the same time (24hr post-wash), ALLN (10 μ M) was added to one set of DMSO and one set of OSW-1. The cells continued to incubate until 48 hr post-wash, at which point they were lysed and analyzed using the western blot method.

2.2.8 Antiviral Analysis

Antiviral assays were done in the research group of Prof. Earl Blewett at Oklahoma State University Center for Health Sciences (OSU-CHS). HeLa cells were grown to <75% confluency (healthy log phase cells) in complete media, DMEM (Hyclone SH30081.0) with 10% FBS (Atlanta Biological S11550) and 1% penicillin-streptomycin (Gibco 15140-122). For experiments, cells were trypsinized, counted using a hemocytometer and seeded into 20 wells of two 24-well trays (Falcon 3047) with 2.0 x 10⁵ cells per well, in 1.0 mL complete media. Each treatment is performed using

quadruplicate wells (n=4) and each virus was on a separate plate. After seeding, cells were incubated 20 hr at 37 °C, 5% CO₂, at which point cells have grown to a near confluent monolayer. For the OSW-1 compound continual treatment experiments, (Fig. 6A), the media was gently removed from each well, and 1mL of media was added with the desired OSW1-compound concentration to each well, without disturbing the cells. Cells were incubated for 6 hr, after which time the media was removed and cells were gently washed three times with 1.0 mL of FBS-free DMEM media. After the media was removed, CoxA9-01 or Echo2-01 viruses, diluted in serum-free DMEM with a M.O.I. of 1.0 was added to the culture. The 2.0×10^5 cells per well was assumed to double during incubation so 4.0×10^5 pfu/well of virus was used for an M.O.I. of 1.0. The virus and cells were incubated for 30 minutes at 37 °C 5% CO₂. Then, the virus inoculum was removed, and the culture washed one time with 1.0 mL of serum-free media per well. Then, 1.0 mL of complete media with the indicated concentration of OSW-1 was added to the well, and the infected cells were then incubated for 10 hr at 37 °C, 5% CO₂. After 10 hrs the plate was stored at -80 °C until the TCID-50 titration. This experiment was performed independently three times to generate the data in the figure. For the OSW-1 compound washout treatment experiments, cells were seeded as above. After 20 hr incubation the media was gently removed from each well, and 1mL of media was added with the desired OSW-1-compound concentration to each well, without disturbing the cells. Cells were incubated for 6 hr, after which time the media was removed and cells were gently washed three times with 1.0 mL of FBS-free DMEM media. This was replaced with complete media and cells allowed to incubate for 20 hrs. After the media was removed, CoxA9-01 or Echo2-01 viruses, diluted in serum-free DMEM with a

M.O.I. of 1.0 was added to the culture. The 2.0×10^5 cells per well was assumed to double and double again during incubation so 8.0×10^5 pfu/well of virus was used for an M.O.I. of 1.0. The virus and cells were incubated for 30 minutes at 37 °C 5% CO₂. Then, the virus inoculum was removed, and the culture washed one time with 1.0 mL of serum-free media per well. Then, 1.0 mL of complete media was added to the well, and the infected cells were then incubated for 10 hr at 37 °C, 5% CO₂. After 10 hr incubation, the plate was stored at -80 °C until processing. Then, the plates were rapidly thawed, the cells in media were scrapped from the wells into sterile 1.5 mL centrifuge tubes and the suspension then centrifuged at 10,000 g at 4°C to produce the virus containing supernatant, which is assayed for TCID-50 titration on sub-confluent RD cells. This experiment was performed independently three times to generate the data in the figure.

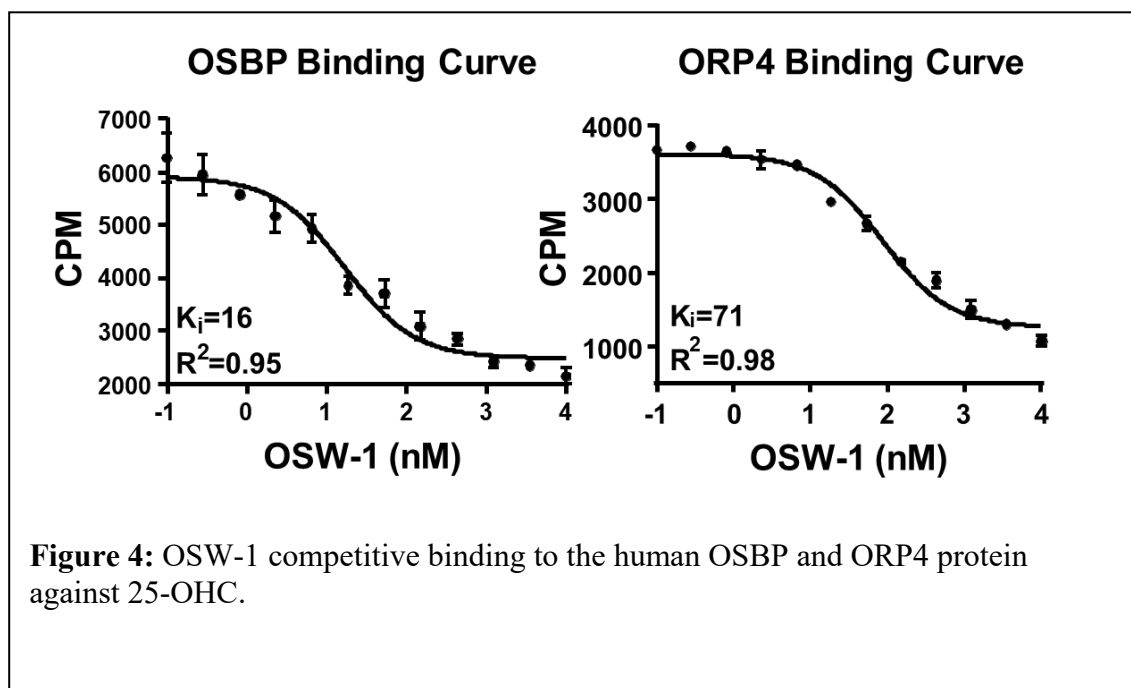
2.2.9 Competitive Binding Assay

OSBP and ORP4L were cloned into pcDNA 3.1 vector. ORP4L contained a Myc-His tag, whereas OSBP did not. The vectors were transfected into HEK-293T cells with lipofectamine 2000. Following a 48 hr incubation, cells were lysed with M-per-HALT with EDTA. Protein lysate was isolated through ultracentrifugation at 100,000g for 1 hr. Lysate was diluted to a working concentration of 0.2 mg/ mL The lysate was incubated with [³H] 25-OHC at 4 °C for 16 hr followed by a 30 min RT incubation with charcoal dextran and centrifuge for 15 min at 1,900 g. The cleared lysate was added to scintillation fluid and quantified using a TopCount scintillation counter.

2.3 Results

2.3.1 OSW-1 Treatment Selectively Degrades OSBP in Cells

The OSW-1 compound (**Figure 5**) is known to bind to both OSBP and ORP4 with high affinity (**Figure 4**) and induce degradation of OSBP.⁶⁰ I also showed that OSW-1-induced degradation of OSBP in HCT-116 cells in a time time-dependent manner (**Figure 5B**). An OSW-1 treatment of 1 nM induced a rapid reduction in OSBP levels, starting at 4 hours of treatment, until ~90% of OSBP had been reduced at after 24 hours treatment. Interestingly, I showed for the first time that although ORP4 levels were also reduced upon 1 nM OSW-1 treatment, the reduction of ORP4 levels were much slower and less significant, leading to only a ~50% reduction of ORP4 after 24 hours treatment (**Figure 5B**).



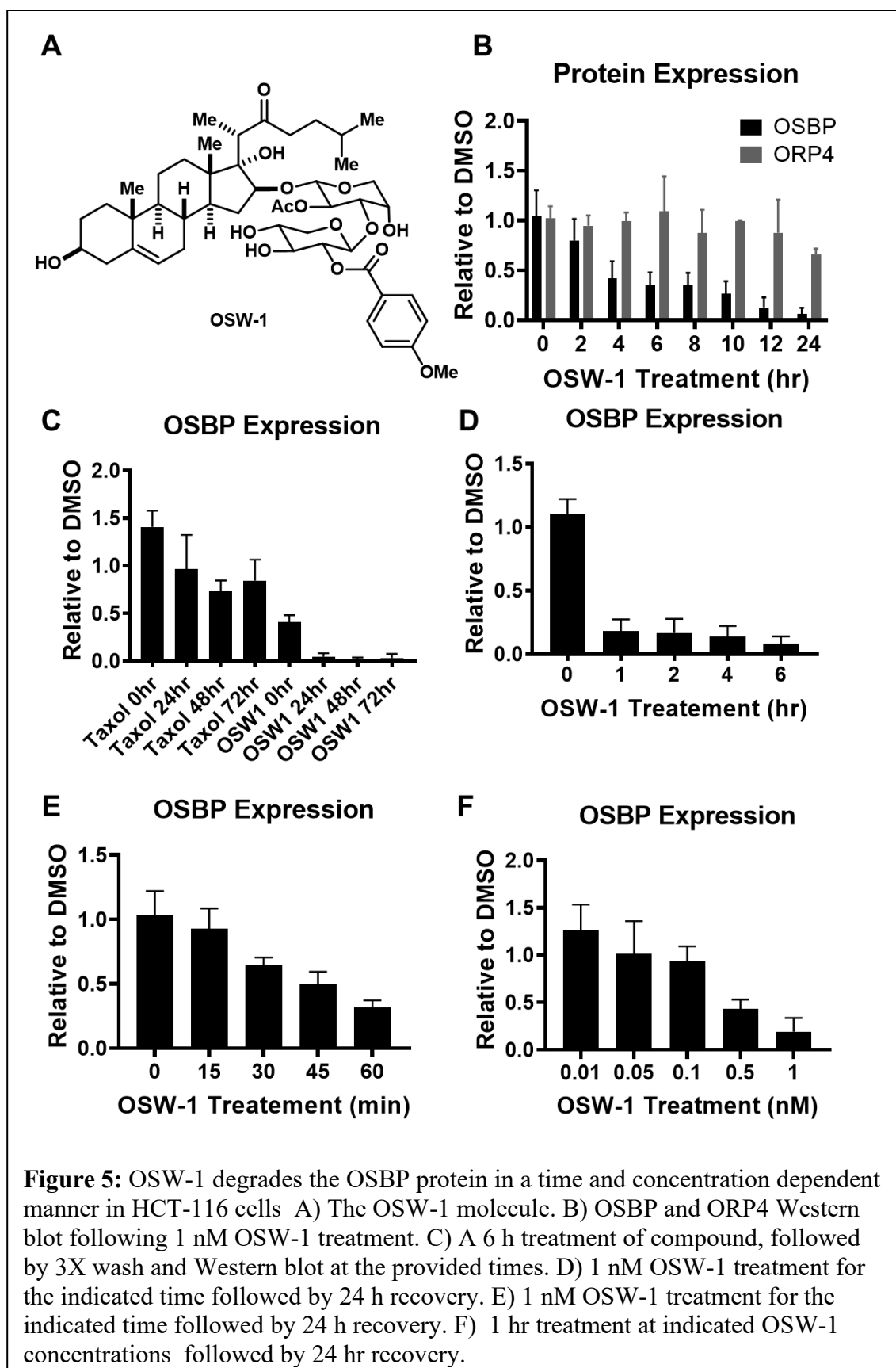
Having established the OSW-1-induced reduction of OSBP, experiments were then performed to determine how quickly OSBP levels returned to normal levels once OSW-1 treatment stopped. These ‘washout experiments’ were performed through

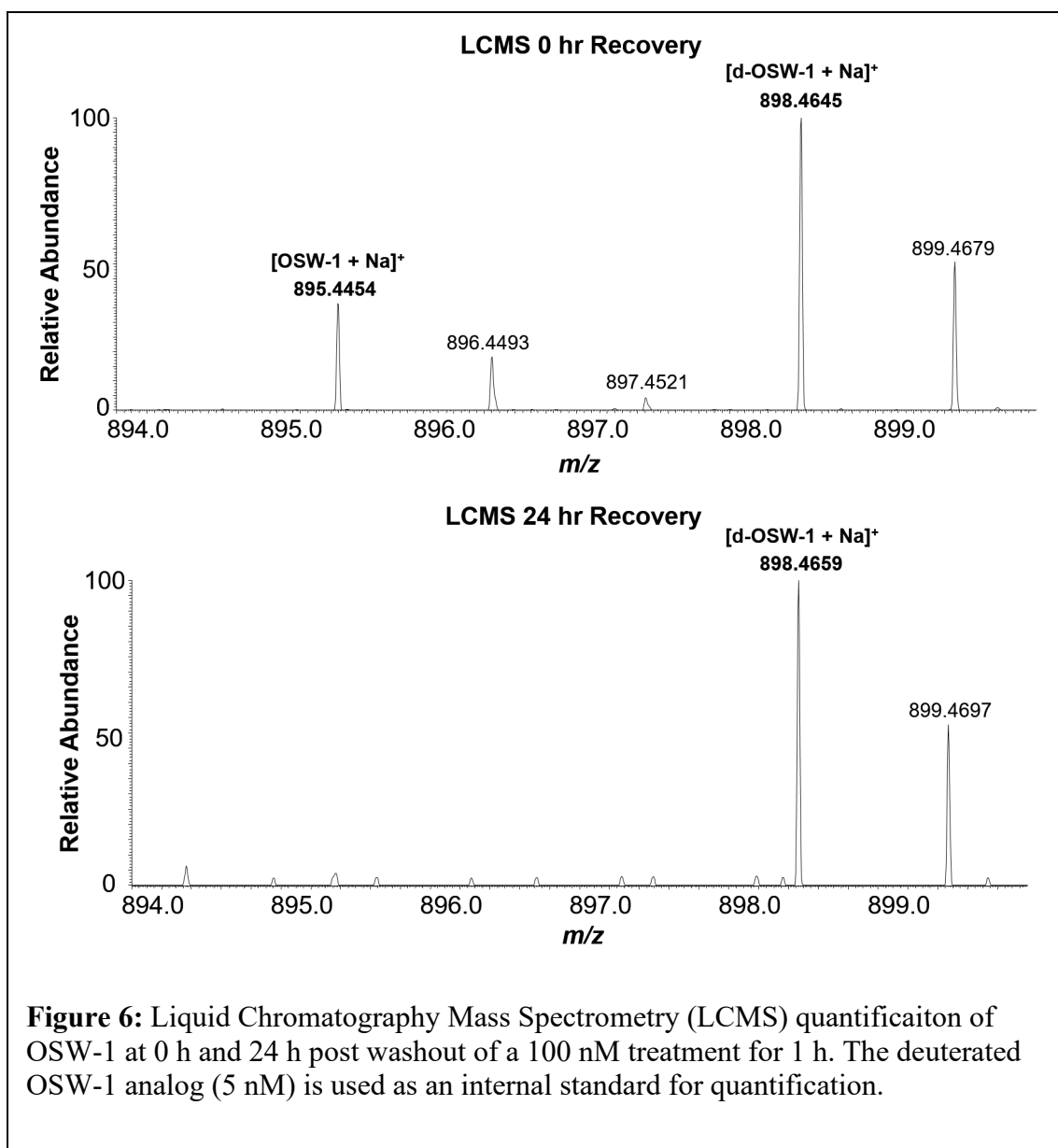
treating the cells with 1 nM of OSW-1 for 6 hours, followed by removal of the compound-containing media, washing the cells with fresh media three times, and then incubating the cells several days in OSW-1 free media. The washout experiment showed that 1 nM, 6 hr treatment induced a ~90% reduction of OSBP that remained reduced for 72 hours after compound treatment stopped (**Figure 5C**). This response is selective only to the OSW-1 compound and not due to a cytotoxic event (e.g., taxol treatment). for up to 72 hr (**Figure 5C**).

This repression of OSBP upon washout conditions is shown to be both concentration and time dependent in HCT-116 (**Figure 5D-F**). Treatments as short as 1 hour with 1 nM transient treatment of OSW-1 is sufficient to induce the 90% reduction in OSBP levels 24 hours later (**Figure 5D**), and a 30 min 1 nM OSW-1 treatment induces a partial reduction of OSBP (**Figure 5E**). Furthermore, as little as 0.5 nM OSW-1 for 1 hr is capable of producing significant degradation and repression of OSBP at 24 hours post-washout. (**Figure 5E**). Multiple other cells lines treated with low-dose, transient OSW-1 concentration showed similar long term reduction in OSBP levels.⁹⁰

2.5.2 OSBP Repression is Independent of Residual OSW-1.

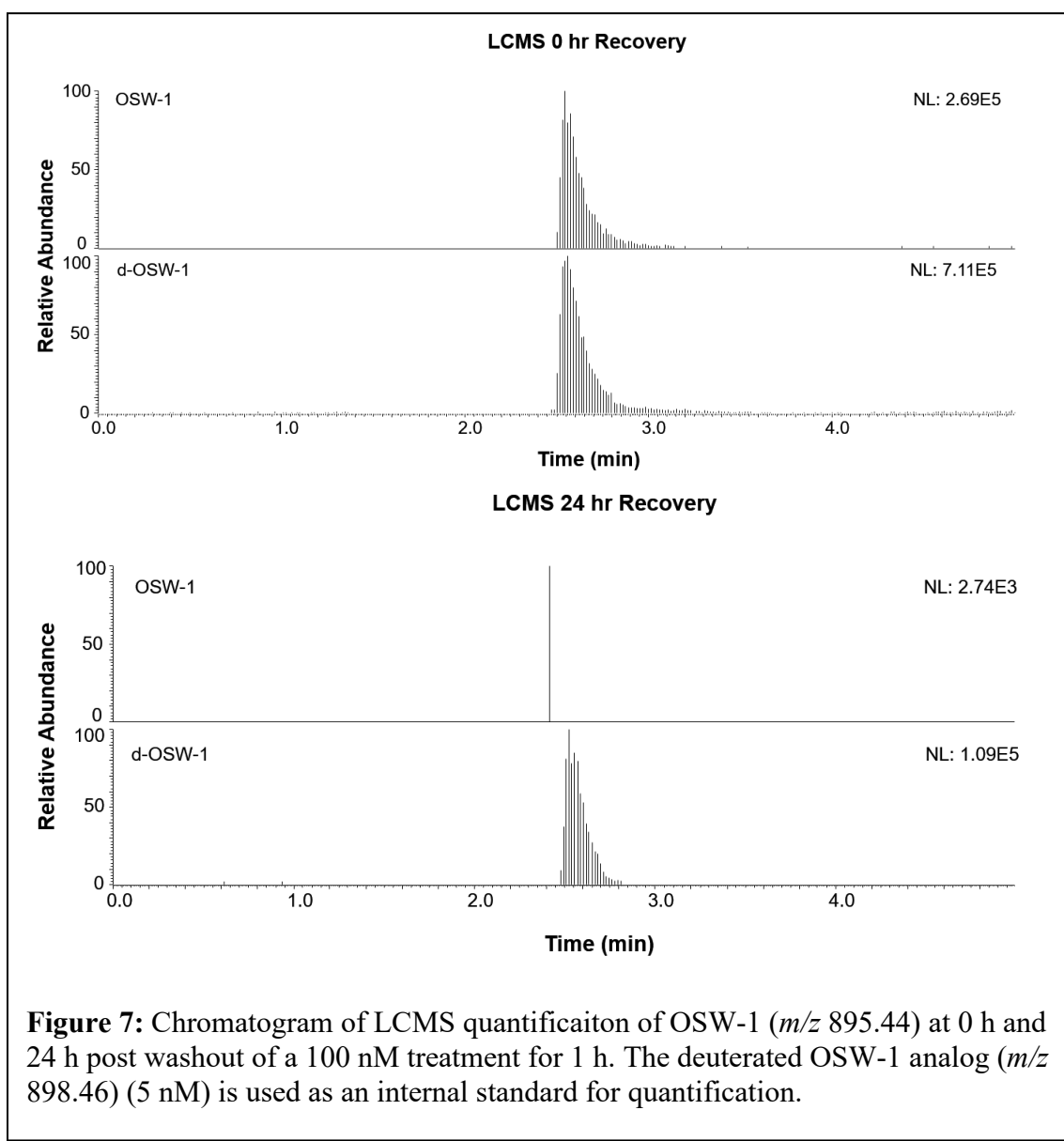
Mass spectrometry quantification was used to determine if the long term (**Figure 5C**) repression of OSBP is due to residual intracellular OSW-1 remaining post-washout. A liquid-chromatography mass spectrometry (LCMS) analysis was first performed on cellular lysate from OSW-1-treated HCT-116 cells. Cells were treated with 100 nM OSW-1 for 1 hr, compound-containing media was removed, the cells were washed three times and incubated in compound-free media for either 0 hr or 24 hr. An internal standard





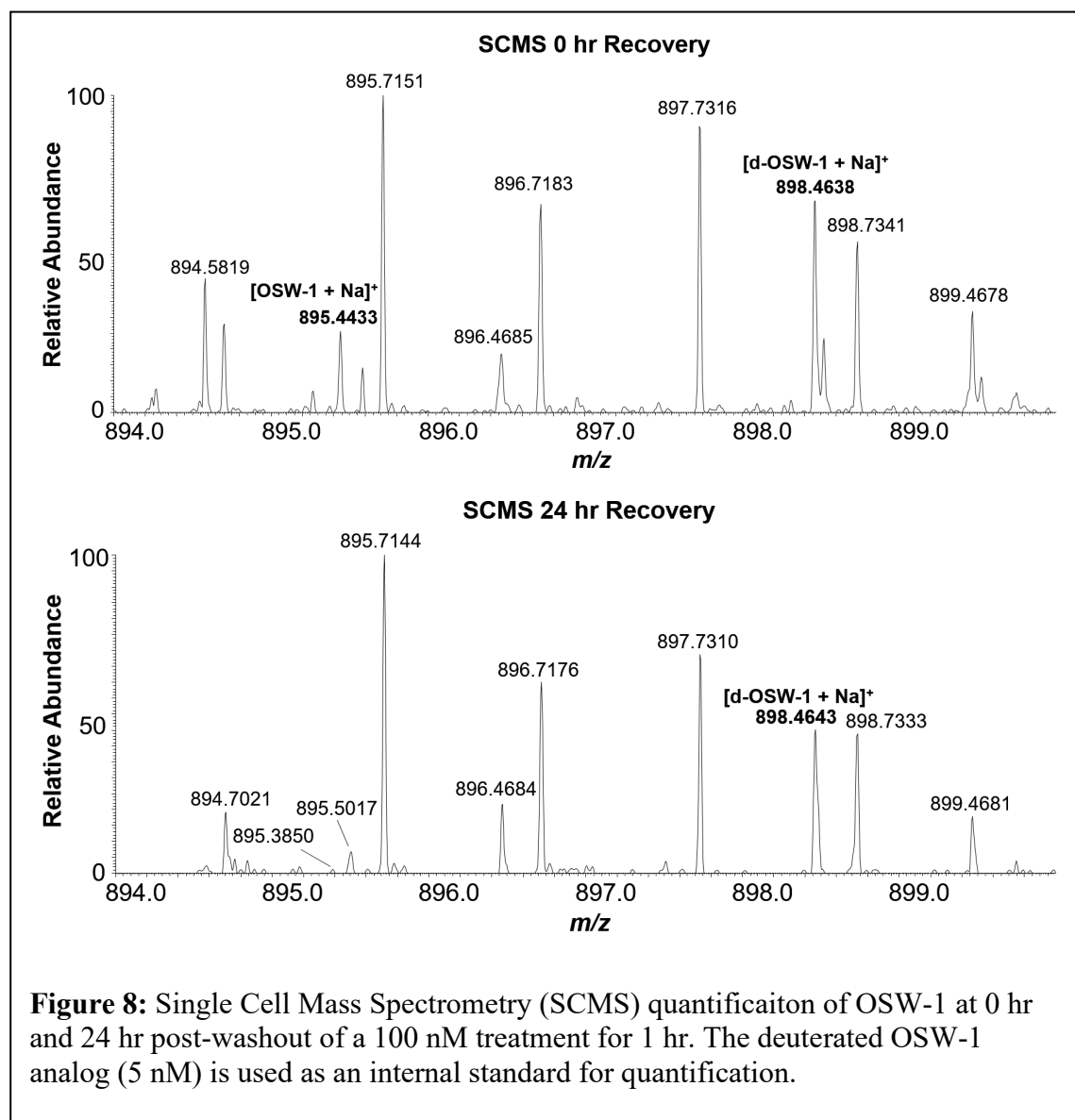
of deuterated OSW-1 added to the lysate in order to quantify the amount of OSW-1 compound present in the lysate. Following the 1 hr treatment, an OSW-1 intracellular concentration of $1.74 \pm 0.74 \mu\text{M}$ was measured (**Figure 6, Figure 8**). However, following 24 hr recovery post-washout, the OSW-1 compound was undetected (**Figure 6, Figure 8**). Furthermore, a complementary analysis using the Single-Probe single cell mass spectrometry technology developed by our collaborator, Dr. Yang, was used to validate the LCMS results.⁸⁴ The ability of the Single-probe system to detect intracellular OSW-

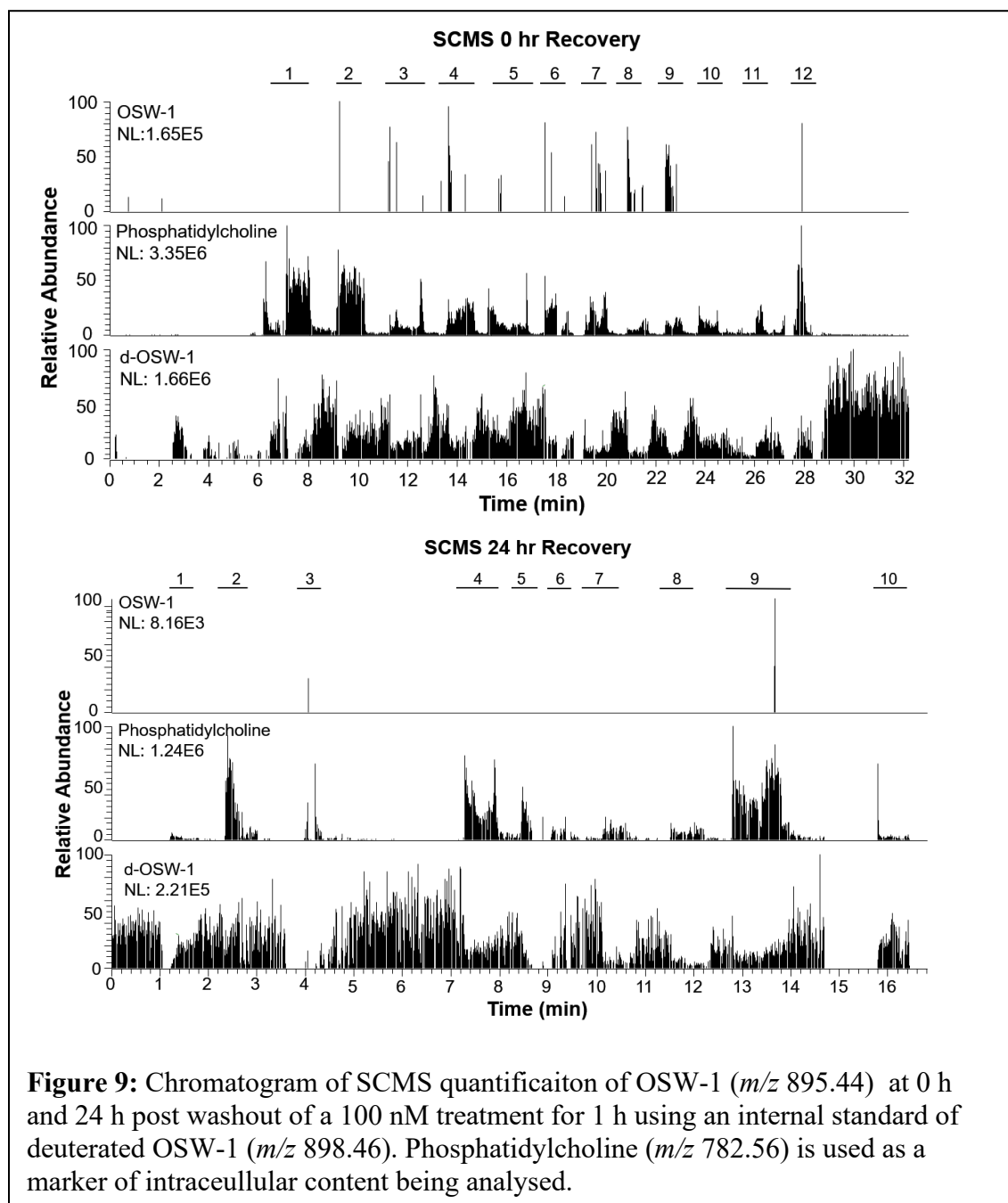
1 in single cells has been previously demonstrated.⁸⁴ In individual HCT-116 cells, the OSW-1 compound was detected following the 1 hr treatment but was not detected following a 24 hr recovery after washout (**Figure 7, Figure 9**). Together, this suggests that the OSBP repression is independent of prolonged intracellular amounts of the OSW-1 compound.



2.3.3 OSBP Repression is independent of Calpain activity

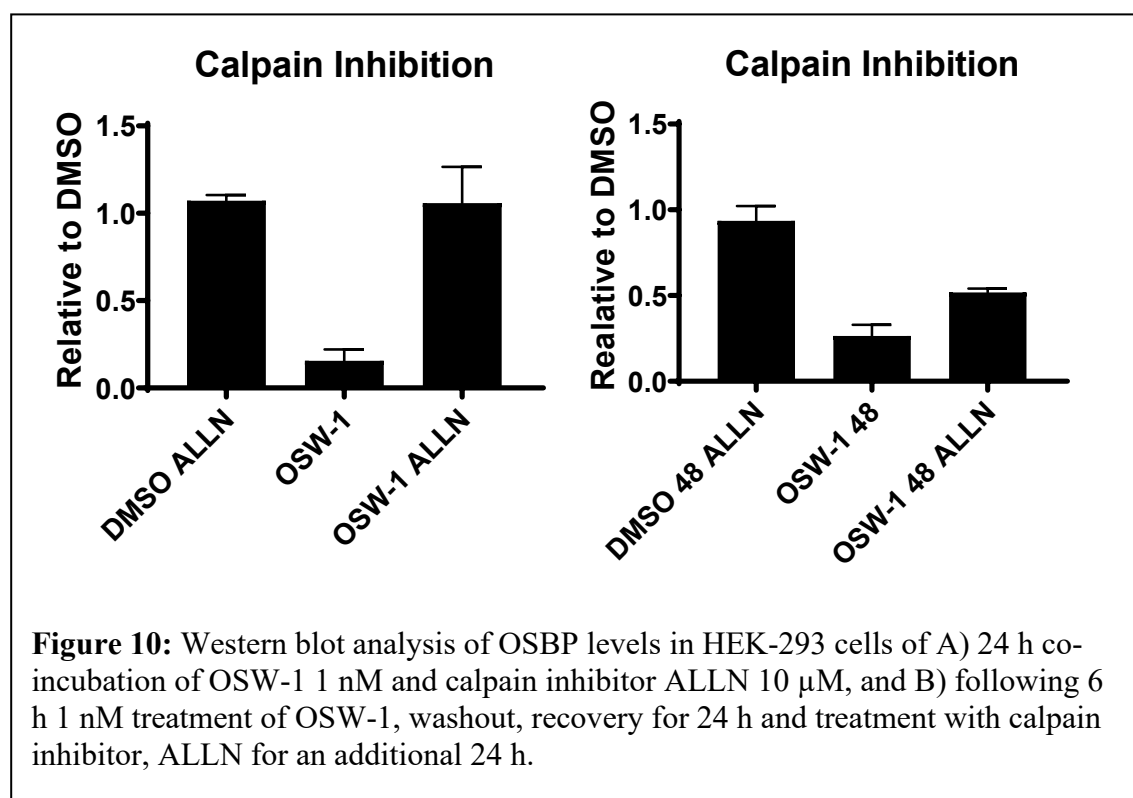
The OSW-1 compound has been shown to influence calcium regulation in lymphoblastic leukemia cells.⁵⁷ Because of this, I tested if the calcium-activated protease calpain could be responsible for the long-term repression of OSBP upon OSW-1





treatment. Co-administration of the calpain inhibitor ALLN at 10 μ M with 1 nM of OSW-1 in HEK-293 cells did prevent the initial degradation of OSBP, but addition of the ALLN inhibitor in cells with already reduced OSBP levels did not significantly rescue the OSBP levels (**Figure 10**). These results indicates that the longterm repression of OSBP was not

due to the calpain protease. The long-term repression of OSBP was also shown to be independent of OSBP transcription inhibition, proteasome activity, or autophagy.⁹⁰



2.5.4 OSW-1 and THEV2 bind OSBP and ORP4

In addition to OSW-1, the antiviral compounds ITZ, TTP, and THEV2 were reported to function through targeting OSBP.^{62–64} To compare these other compounds to OSW-1, binding of the ITZ, TTP, and THEV2 to OSBP and ORP4 using the well-established 25-OHC competitive binding assay was performed.^{60,106} We demonstrated

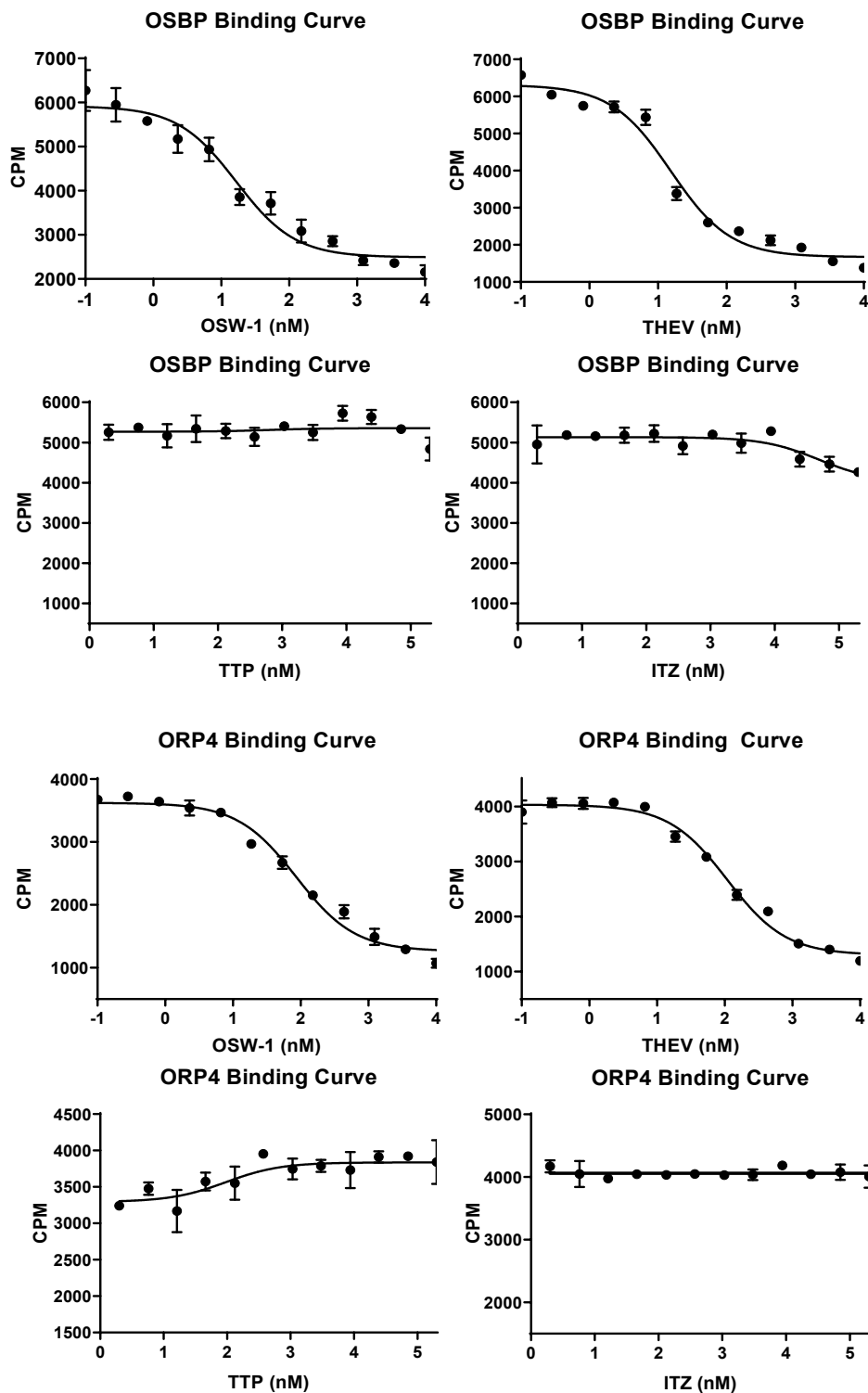
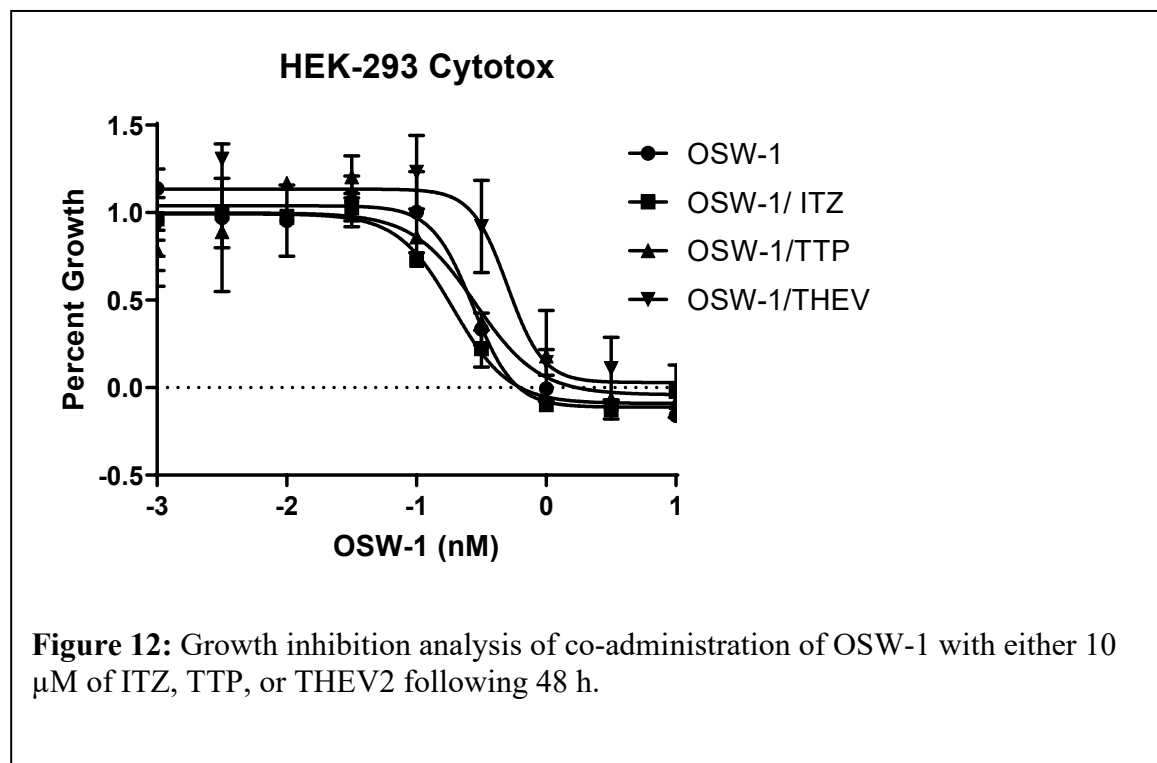


Figure 11: Competitive binding of OSW-1, THEV, TTP and ITZ to OSBP and ORP4 using the 25-OHC competitive binding assay. Example of results from one independent experiment shown.

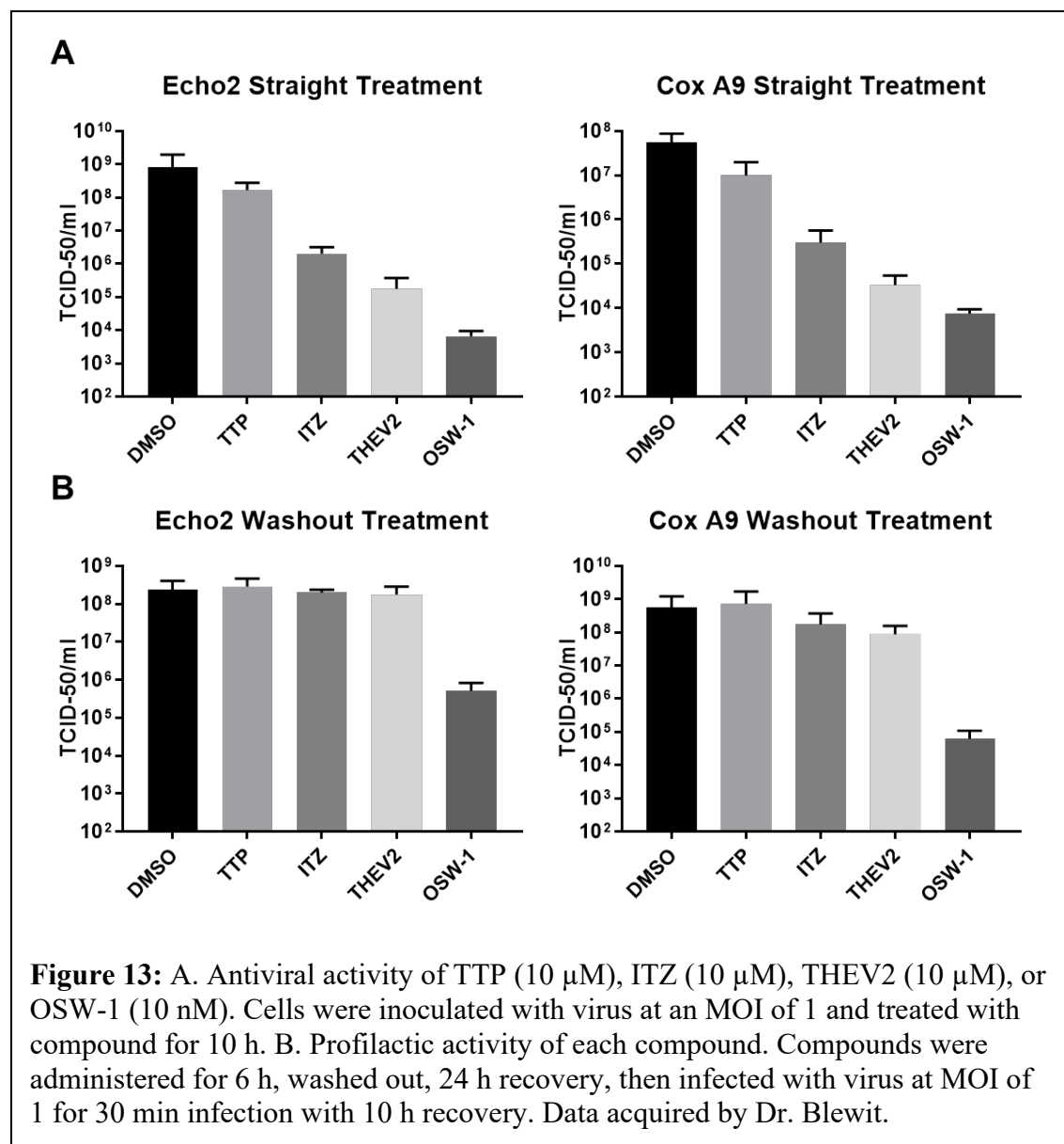
that the OSW-1 molecule and THEV2 were the only two compounds to displace 25-OHC binding to OSBP and ORP4; TTP and ITZ shown no competitive binding to 25-OHC (**Figure 11**). The OSW-1 OSBP $K_i = 16 \pm 4$ nM and ORP4 $K_i = 22 \pm 15$ nM. THEV2 OSBP $K_i = 71 \pm 6$ nM and ORP4 $K_i = 98 \pm 14$ nM. Furthermore, OSW-1 was the only compound capable of reducing OSBP levels in cells (data not shown).⁴⁵



THEV2 binds to OSBP and ORP4 with an affinity similar to OSW-1, but unlike, OSW-1, THEV2 shows no cytotoxicity at concentrations up to 10 μ M. (data not shown).⁴⁵ Co-incubation of 10 mM of THEV2 with OSW-1 in HEK-293 cells induces a slight, non-significant decrease in OSW-1 cytotoxicity with OSW- (Figure 12). Co-incubation of OSW-1 with TTP or ITZ had no effect on the OSW-1 cytotoxicity curve (Figure 12). The apparent shift of the OSW-1 growth curve upon co-incubation with THEV2 supports the compounds bind in overlapping binding sites in OSBP and ORP4, as shown in Figure 11.

2.5.5 OSW-1 selectively exhibits prophylactic activity

To evaluate the extent of antiviral activity of the OSBP-targeting compounds, HeLa cells infected with two *Enterovirus* pathogenic viruses (i.e., echovirus2 and coxsackievirus 9a), and were treated with each of the compounds. Cells were treated with 1 nM OSW-1 and 10 μ M THEV2, TTP, and ITZ. All compounds had antiviral activity, although OSW-1, THEV2, and ITZ were all more potent at inhibiting viral replication



than TTP in both virus models (**Figure 13**). To evaluate the prophylactic ability of each of the compounds, cells were pretreated with each compound for 6 hours. Then, the compound-containing media was removed, the cells washed three times with media, and incubated for 24 h in drug-free media. Then, the cells were infected with virus for 10 hours. (**Figure 13**). Viral count was performed from the supernatant through TCID-50 titration. OSW-1 was the only compound to exhibit prophylactic activity against both of the viral models (**Figure 13**).

2.4 Discussion

These results demonstrate that a short, transient, low dose treatment of the OSW-1 compound is sufficient to induce the selective degradation (>90%) and repression of the OSBP protein for multiple days after the compound treatment has stopped in multiple immortalized cell lines (**Figure 5**). The 72 hour repression of OSBP following removal of the compound demonstrates a stable biological effect transferable to multiple generations of cells. The OSW-1 induced repression of OSBP proceeds through an unidentified cellular mechanism. The long term repression of the OSBP did not correlate to any signs of toxicity or morphological changes in cells, which might be expected if OSBP is an essential protein responsible for transferring lipids between organelle membranes (data not shown).¹⁰⁷ Although the initial degradation of the OSBP protein is coordinated through the proteasome, the multi-day repression of the protein is independent of transcription repression, proteasome activity, the OSW-1 compound, autophagy, or calpain activity (**Figure 10**).¹⁰⁷ Furthermore, because OSBP repressed cells do not exhibit any signs of cytotoxicity, growth arrest, or morphology changes, it can be concluded that this repression is specific to the OSBP protein and independent of global protein repression. Furthermore, confirming this, a global iTRAQ proteome analysis did not detect any systematic global protein changes.¹⁰⁷

This long-term repression of OSBP is also specific to OSW-1 and not any other known putative OSBP targeting compounds, ITZ, TTP, or THEV2 (data not shown).¹⁰⁸ Although all four compounds exhibited antiviral activity, only OSW-1 and THEV-2 complete for binding with 25-OHC (**Figure 11, Figure 13**). These results suggest ITZ and TPP bind OSBP in another pocket other than the oxysterol binding site. Furthermore,

OSW-1 was the only compound to degrade OSBP and exhibit prophylactic activity against enteroviral replication *in vitro*, most likely due to OSBP long term repression (Figure 13).

2.5 Conclusions

These results demonstrate that targeting the host protein OSBP with a low dose, transient treatment of the OSW-1 compound causes a non-toxic degradation and long-term repression of the protein, which correlates with inhibition of *Enterovirus* replication. This unique, unidentified regulator mechanism of OSBP repression has obvious therapeutic effects and demands to be continually explored for designing a new class of non-toxic, OSBP degrading therapeutics.

Chapter 3: OSW-1 Compound Anti-cancer Development in Ovarian

Cancer Targeting ORP4L Protein

Abstract

Oxysterol-binding protein (OSBP)-related protein 4 (ORP4) is a cancer-specific driver of cellular proliferation and a regulator of cellular metabolism. The natural product OSW-1 targets ORP4 and its closely related paralog OSBP producing potent antiproliferative properties through an incompletely understood mechanism. Although reported to have limited to no expression in normal tissue, ORP4 is putatively expressed in the majority of cancers, with specifically high expression in ovarian cancer. We demonstrate that ORP4 is strongly expressed in all ovarian cancer cell lines tested, including in three-dimensional spheroid tumor-models. The nanomolar antiproliferative activity of the OSW-1 compound was correlated to ORP4 expression levels in the different ovarian cancer cell lines, both in monolayer and in spheroid models. The correlation of ORP4 levels and OSW-1 potency suggests a precision targeting of the cancer-specific ORP4 protein. Importantly the OSW-1 compound had comparable superior cytotoxicity in the ovarian cancer three-dimensional spheroids models compared to cisplatin and paclitaxel. OSW-1 compound treatment induces the degradation of ORP4, and the cytotoxicity correlated to the amount of ORP4 degradation, further supporting the identification of ORP4 as a potential precision cancer target in ovarian cancer. Further, the absence of extracellular lipids dramatically potentiated the cytotoxic effects of OSW-1 in monolayer cells, and this increase in OSW-1 potency was rescued by addition of extracellular cholesterol. These results suggest that ORP4 is a potentially druggable precision cancer target for ovarian cancer, and that the increased potency of the OSW-1 compound in the absence of lipids presents an opportunity for the compound to possibly selectively target nutrient/lipid deprived tumors *in vivo*.

Allocation of Contribution

This chapter is from a manuscript in preparation. I am co-first author on the manuscript. The results presented here are a collaborative effort between the Burgett lab and the research group of Dr. Handan Acar, in the Department of Biomedical Engineering at the University of Oklahoma. The manuscript writing was conducted by myself with assistance from Mr. Gokhan Gunay and edits from both Dr. Burget and Dr. Acar. I was responsible for all the data accumulation and figure making of **Figure 14, Figure 15, Figure 18, Figure 19, and Figure 20** (Mr. Gokhan Gunay was responsible for producing spheroid lysate). Mr. Gokhan Gunay was responsible for the data accumulation and figure making of **Figure 16 and Figure 17**. Support from both Mr. Matthew Finneran and Isha Jhingan were also provided throughout the project.

3.1 Introduction

3.1.1 Ovarian Cancer Background

Ovarian cancer is the deadliest gynecological malignancy, with a 50% five-year survival rate causing over 14,000 deaths per year in the United States.¹⁰⁹ The high morbidity and mortality of ovarian cancer is due to diagnosis commonly occurring after the metastatic spread of the cancer (Stage III or IV), at which point the treatment options are often limited and inefficient.¹¹⁰ The major type of epithelial ovarian cancer (EOC) is high-grade serous carcinoma (HGSC).¹¹¹ Standard of care treatment of metastatic HGSC is a combination chemotherapy of a platinum-based drug (e.g., cisplatin or carboplatin) and an anti-mitotic agent (e.g., paclitaxel).¹¹² HGSC malignancies are complicated due to an atypical route of metastasis. Unlike most epithelial cancers, HGSC disseminates through a transcoelomic route rather than a hematogenous or lymphatic route.¹¹¹ The transcoelomic HGSC metastasis results in the dissemination of the cancer cells to vital organs throughout the abdomen cavity, which affects the gastrointestinal and genitourinary systems. This cancer pathophysiology also leads to ascites formation, increasing patient morbidity rates.^{111,113} Transcoelomic metastasis requires the HGSC cells to avoid anoiks (i.e., cell detachment programmed cell death) through formation of tumor spheroids, which provides the required cell-to-cell adhesion for the cancer cells.^{113,114} HGSC spheroid formation depresses the efficacy of the standard of care chemotherapy and promotes drug HGSC resistance.¹¹³ Also, the three dimensional HGSC spheroid structure is deficient in nutrient distribution, producing concentric gradients, resulting in an inner necrotic core surrounded by a layer of viable quiescent cells with an outer proliferating layer of cells.^{115,116} The clinical relevance of HGSC spheroids,

especially in the therapeutic treatment, has led to the development of three-dimensional (3D) cell culturing methods in the study of ovarian cancer. Ovarian cancer cell lines 3D spheroids models created in the research labs mimic the *in vivo* HGSC spheroid, including the cell-extracellular matrix (ECM) composition, requirement for cell-cell interactions, and transcriptome alteration, all of which cannot be achieved by traditional 2D culture^{117–121}. As a useful proxy of the clinical HGSC, 3D spheroid cell culture models, including ovarian cancer, has been used to test and identify new anticancer agents.^{122–124}

3.1.2 ORP4 Biology

The natural product compound OSW-1 (**Figure 1**) is an exceptionally potent cytotoxic agent against a wide range of *in vitro* cancer cell lines (NCI 60 Avg. GI₅₀ = 0.78 nM).⁵⁹ OSW-1 induces its cellular effects through binding to oxysterol-binding protein (OSBP) and OSBP-Related Protein 4 (ORP4)^{60,125}. OSBP and ORP4 are cytoplasmic, non-enzymatic proteins belonging to a 12-member family of lipid transport and lipid regulatory proteins.^{126–129} OSBP is reported to be required for ER-Golgi lipid transport and for the replication of several classes of RNA pathogenic viruses.^{48,64} OSBP has no known role in cellular viability, cellular proliferation, or cancer biology.^{46–48,90} In contrast, ORP4 is an identified precision cancer target and driver of cancer cell proliferation. ORP4L is selectively expressed in patient-isolated T-cell acute lymphoblastic leukemia (T-ALL) cells and drives the leukemia proliferation, including in leukemia stem cells.^{51,53} ORP4 is reported to promote mitochondrial respiration in immortalized immune cells by regulating calcium release from the endoplasmic reticulum through mediating a G-protein activation of PLC3β.⁵¹ Knockdown of ORP4 in cancer cell

lines results in increased apoptosis, autophagy, and mitochondrial dysfunction, which phenocopies OSW-1 treatment.^{51,53–57} Unlike the ubiquitous expression of OSBP, ORP4 is reported to have limited selective expression in only parts of the brain, retina, and testes (Figure 14).⁴⁹ ORP4^{-/-} mice develop normally, aside from male sterility, signifying the limited role of ORP4 in non-transformed tissue.¹³⁰

Herein, we describe the ORP4 expression in a series of ovarian cancer cell lines, including ovarian cancer cells cultured as three-dimensional spheroids. We demonstrate that the ORP4-targeting compound OSW-1 shows potent cytotoxicity relative to SOC chemotherapy agents cisplatin and paclitaxel in both monolayer (2D) and spheroid (3D) ovarian cell line models. To produce these results, we provide extensive characterization of spheroid development in multiple ovarian cancer cell lines, producing an ideal *in vitro* model for investigating small-molecule pharmacology on *in vivo* tumors and circulating spheroids. The toxicity of the OSW-1 compound is suggested to have a unique biological mechanism of ORP4L protein degradation due to OSW-1 compound binding resulting in cell death independent of OSBP protein degradation. Lastly, the absence of extracellular lipids, modeling a nutrient deprived tumor, significantly potentiated the cells specific to the OSW-1 compound with the addition of extracellular cholesterol attenuating this effect, suggesting the applicability of OSW-1 as a tumor-specific-targeting small molecule.

3.2 Methods

3.2.1 Cell Culture

OVCAR-3 (ATTC # HTB-161), OVCAR-8 (NCI-Vial Designation 0507715), and OVSAHO (JCRB-1046) were cultured in RPMI Medium (Thermo 22400105) with the addition of 10% Hyclone (Fisher Sci SH3006603) and 1% penicillin-streptomycin (Thermo 15140122). SKOV-3 (HTB-77) were cultured in McCoy 5A media (Thermo 16600108) supplemented with 10% Hyclone and 1% penicillin-streptomycin. All mammalian cell lines were cultured at 37 °C in 5% CO₂ in either Nunclon Delta 10 cm² dishes (VWR 10171744), T25 flask (CellStar 690160) or T75 flask (TPP 90076).

3.2.2 2D Viability Assay

Cells were seeded out in a 96-well plate in 75 µl of media at a cell number of 5.0e³ per well. Compounds were serial diluted at 4X concentration in medium. 25 µl of compound containing media was added to 75 µl of cells, resulting in a 1X dilution of drug. Following a 72 h incubation, CellTiter-Blue was added for 20 h, and fluorescence was measured (544nm excitation; 590nm emission) using a plate reader. Growth relative to untreated cells were calculated expressed as IC₅₀ values on Graphpad Prism software utilizing the four-parameter-dose-response curve.

3.2.3 Spheroid Development

Spheroid formation was induced by the ultra-low attachment technique. Briefly, round bottom 96-well plates (CELLTREAT 229590) were treated with anti-adherence rinsing solution (STEMCELL 07010) by centrifuging the plates at 1300 g for 5 min. The

solution was aspirated, and wells were washed with basal medium. OVCAR-8 or SKOV-3 cells were seeded in 200 μ l of media at the desired cell number and plates were centrifuged at 100 g for 3 min. For OVCAR-8 spheroids 100 μ l of medium is removed and 100 μ l of fresh medium was added every 24 h. For SKOV-3 spheroids, 100 μ l of medium was removed on day 4 and 100 μ l of fresh medium was added until day 7. Spheroid formation was observed for 7 days by monitoring the formation every 24 h with bright field imaging. Spheroids were characterized for their surface area, circularity, and solidity by using ImageJ.

3.2.4 3D Viability Assay

Spheroid viability was measured by using CellTiter-Glo3D. The solution was thawed overnight prior to experiments. 96-well plates and CellTiter-Glo3D solution were equilibrated to room temperature prior to use. Briefly, 100 μ l of CellTiter-Glo3D solution was added on top of 100 μ l spheroid solution. Contents were vigorously mixed to induce lysis of the spheroid and efficient extraction of ATP. Plates were incubated at room temperature for 25 minutes for stabilization of luminescent signal. After the incubation period luminescence was recorded by using an integration time of 1 second per well, accordingly with the manufacturer's instructions. Toxicity was calculated relative to an untreated control group. No spheroids were formed on the outside wells of the 96 well plate to avoid edge effect.

3.2.5 Cell Lysis

Adherent cells were lysed by aspiration of media, wash with 1X PBS, addition of TrypLETM Express (Gibco 12605- 010), and neutralized through the addition of media. Cells were spun at 14,000 RCF for 0.45 min at 4°C. Supernatant was aspirated, cell pellet washed with 1X PBS, and resuspended in 50 µL of AC lysis buffer (150 mM NaCl, 1.5 mM MgCl₂, 5% glycerol, 0.8% NP40, 1mM DTT, 50 mM HEPES, 25 mM NaF, 1 mM Na₃PO₄) with 3X HALT/EDTA protease inhibitor (Thermo 78438) and 0.2 mM phenylmethanesulfonylfluoride (Goldbio). Cells were freeze/ thawed (X3) with LN₂ and centrifuged for 15 min at 14,000 RCF at 4°C. Resulting cell lysate was Bradford for protein concentration.

3.2.6 Immunoblotting

SDS-PAGE gels (8.5%) were loaded with 25 µg of protein, transferred to nitrocellulose membrane ((Bio-Rad 1620115) with a constant voltage of 100V for 1 h at 4°C. The membrane was blocked in 5% milk for 0.5 h. Following washing with TBST (X3), the membrane was incubated with 1:500 ORP4 antibody (Santa Cruz sc-365922) or 1:1000 OSBP antibody (Santa Cruz sc-365771) overnight at 4°C. Following washing, the membrane was incubated with 1:3000 Secondary antibody (Santa Cruz sc-2060) for 1 h at RT. Following washing, the membrane was developed with ClarityTM Western ECL substrate (Bio-Rad 1705061) and imaged on the Bio-Rad ChemiDocTM Touch Imaging System. The membrane was incubated with 1:1000 β-actin HRP (Santa Cruz sc-47778 HRP) after washing and developed as previously described.

3.2.7 Trypan Blue Viability

Following compound treatment, media was transferred to a new 15 mL falcon tube. Adherent cells were washed with 1X PBS, addition of 2.5 mL TrypLE™ Express, and neutralized by addition of used media. Cell count and viability was performed using Trypan Blue (Thermo 15250061) with a TC20™ automated cell counter (BioRad).

3.2.8 Delipidated FBS Media

FBS was delipidated through a Brown and Goldstein modification of the method developed by Cham and Knowles. Briefly, 50 mL of FBS was added to a mixture of n-butanol and di-isopropyl ether in a 40:60 (v:v) ratio. The solution was incubated for 20 min at RT followed by a 20 min incubation on ice. The solution was centrifuged at 2000 rpm for 2 min. The lower aqueous fraction was isolated and re-extracted with 50 mL of di-isopropyl ether followed by centrifugation. The resulting aqueous phase was evaporated to 20 mL under Nitrogen gas and dialyzed to PBS O/N and filter sterilized. The 20 mL of delipidated FBS was added to 500 mL of media supplemented with 1% penicillin-streptomycin.

3.2.9 Statistical Analysis

All results are displayed as mean \pm SD. A minimum of $n = 3$ was performed for each experiment. Statistical analysis was performed in GraphPad Prism 8.3.) using 2-way ANOVA with a follow up Dunnett's test, p value ≤ 0.05 .

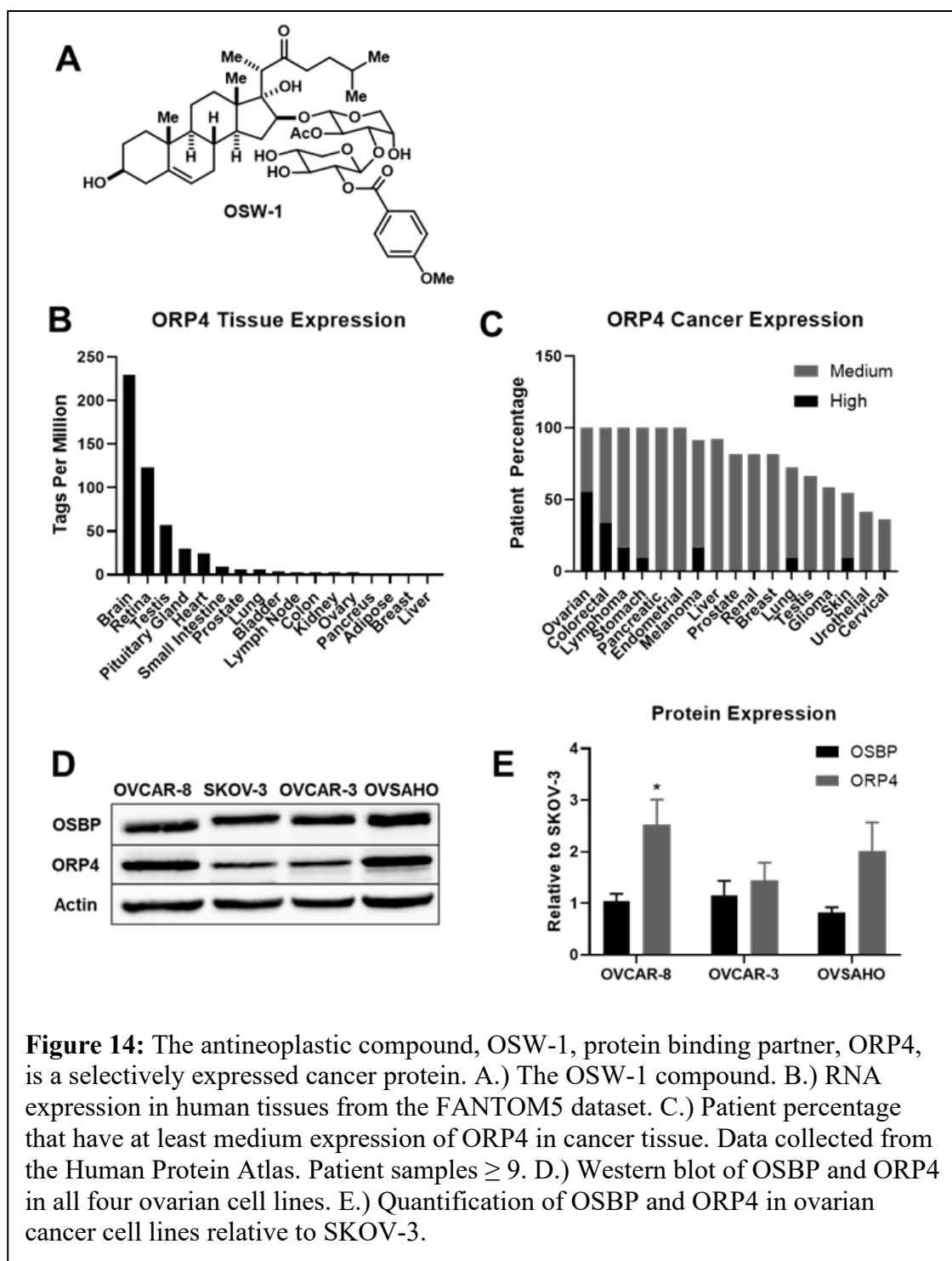
3.3 Results

3.3.1 *ORP4 is ubiquitously expressed in ovarian cancerous cells in vitro.*

Analysis of the publicly available human RNA expression datasets shows that ORP4 has minimal expression in normal ovarian tissue but is highly expressed in ovarian cancers (Figure 14). We evaluated the expression of ORP4 relative to OSBP in four HGSC immortalized cell lines: SKOV-3, OVCAR-8, OVCAR-3 and OVSAHO. SKOV-3, OVCAR-3, and to a lesser extent, OVCAR-8, are extensively used ovarian cell line model systems reported to be genetically dissimilar to patient derived ovarian cancer samples.¹³¹ Conversely, OVSAHO is reported to more closely recapitulate ovarian cancer patient samples, and therefore OVSAHO would be a more informative pre-clinical model system for studying ovarian cancer than the other established cell lines.¹³¹ Although all four ovarian cancer cell lines expressed ORP4, there were significant relative differences in expression of ORP4 in the individual cell lines. The OVCAR-8 and OVSAHO cell lines showed approximately two-fold more ORP4 expression than SKOV-3 and OVCAR-3 (**Figure 14**). In contrast, the level of relative OSBP expression did not vary between the four cell lines (**Figure 14**).

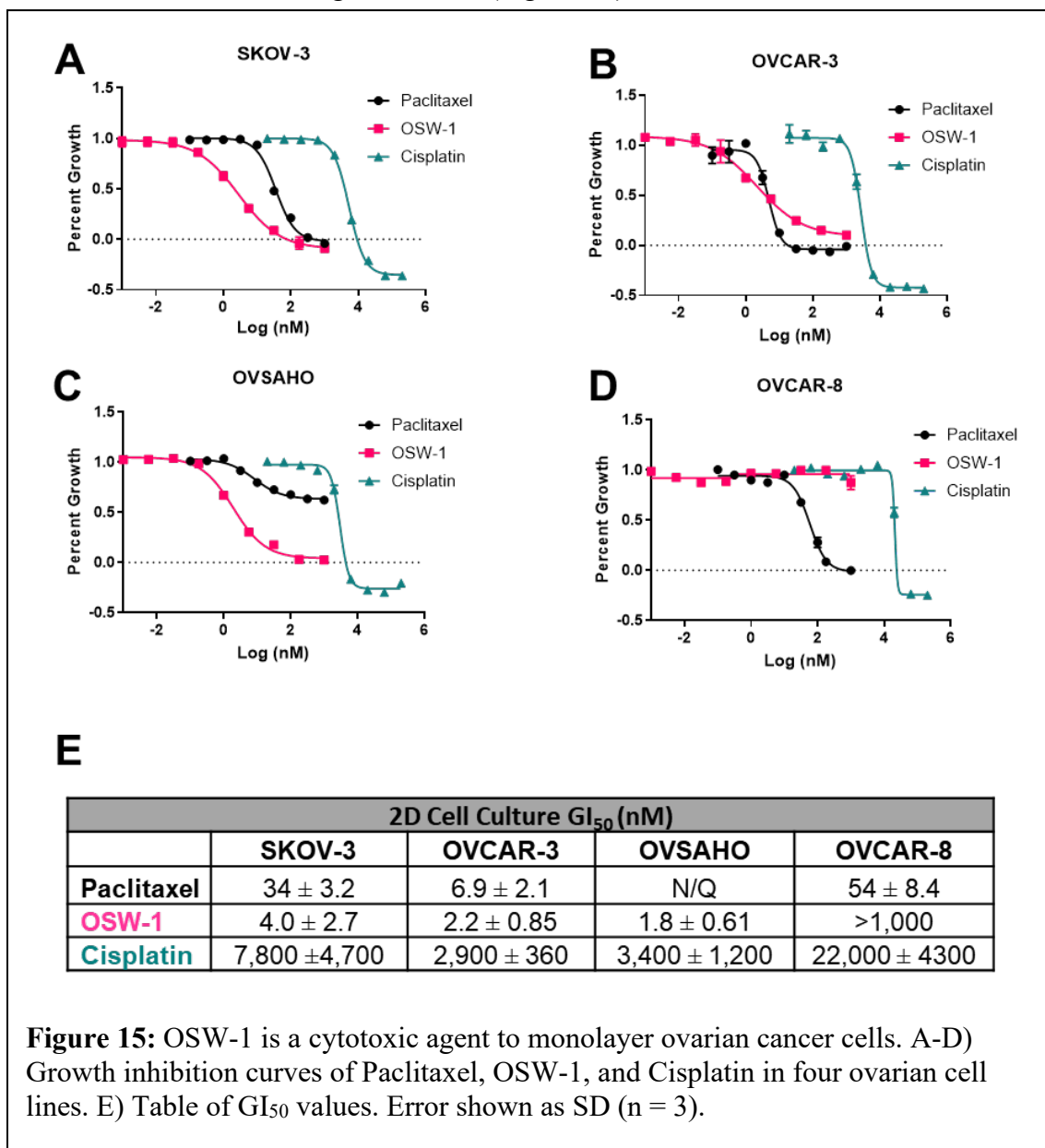
3.3.2 *OSW-1 is a potent inhibitor of cancer cell proliferation.*

To assess the efficacy of the OSW-1 compound (**Figure 14**), it was compared to the clinically used ovarian anti-cancer compounds, paclitaxel and cisplatin, against our ovarian cancer cell line panel in a monolayer (2D) viability assay (**Figure 15**). Compounds were administered for 72 h at the provided concentrations and toxicity was quantified relative to vehicle control using cell titer blue. The OSW-1 compound



exhibited potent, low nanomolar toxicity against three of the four ovarian cancer cell lines (SKOV-3, OVCAR-3, and OVSAHO), showing a higher potency than both clinical drugs, paclitaxel and cisplatin (**Figure 15**). Unexpectedly, the OSW-1 compound was

ineffective at producing toxicity in OVCAR-8 cells up to 1 μM yet remained sensitive to paclitaxel and cisplatin treatment (**Figure 14**). It should be noted that the OSW-1 compound did induce morphological changes, exhibiting less cell-cell interactions, to the OVCAR-8 cell line starting at 1.0 nM (Figure 18), however, it did not correlate with

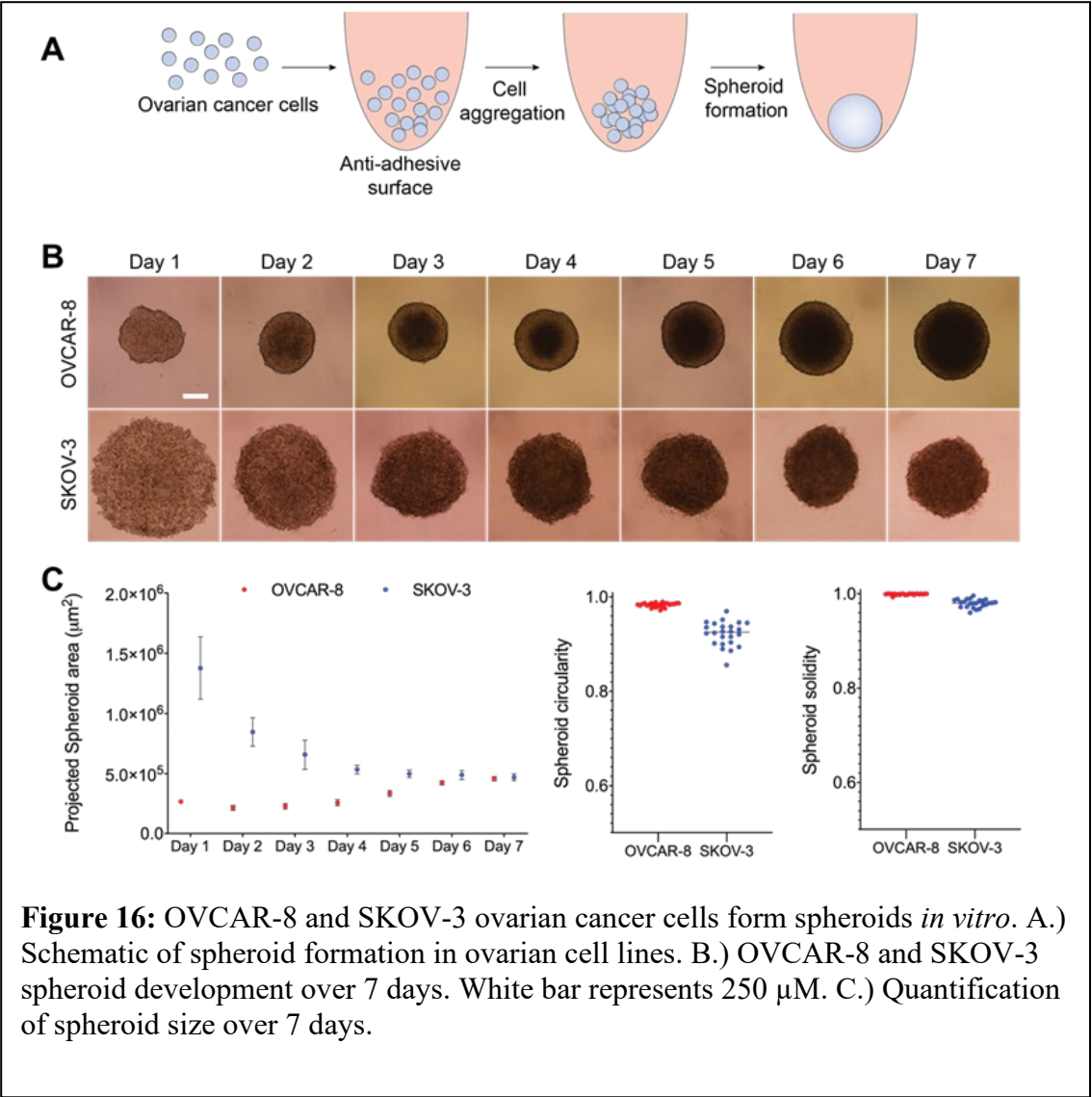


toxicity (**Figure 15, Figure 18**). Furthermore, the OVSAHO cell line showed resistance to paclitaxel (GI₅₀ N/Q) but was still sensitive to OSW-1 (GI₅₀ 1.8 nM). Together, these results suggest the OSW-1 is a potent, cytotoxic agent of ovarian cancer cells *in vitro*.

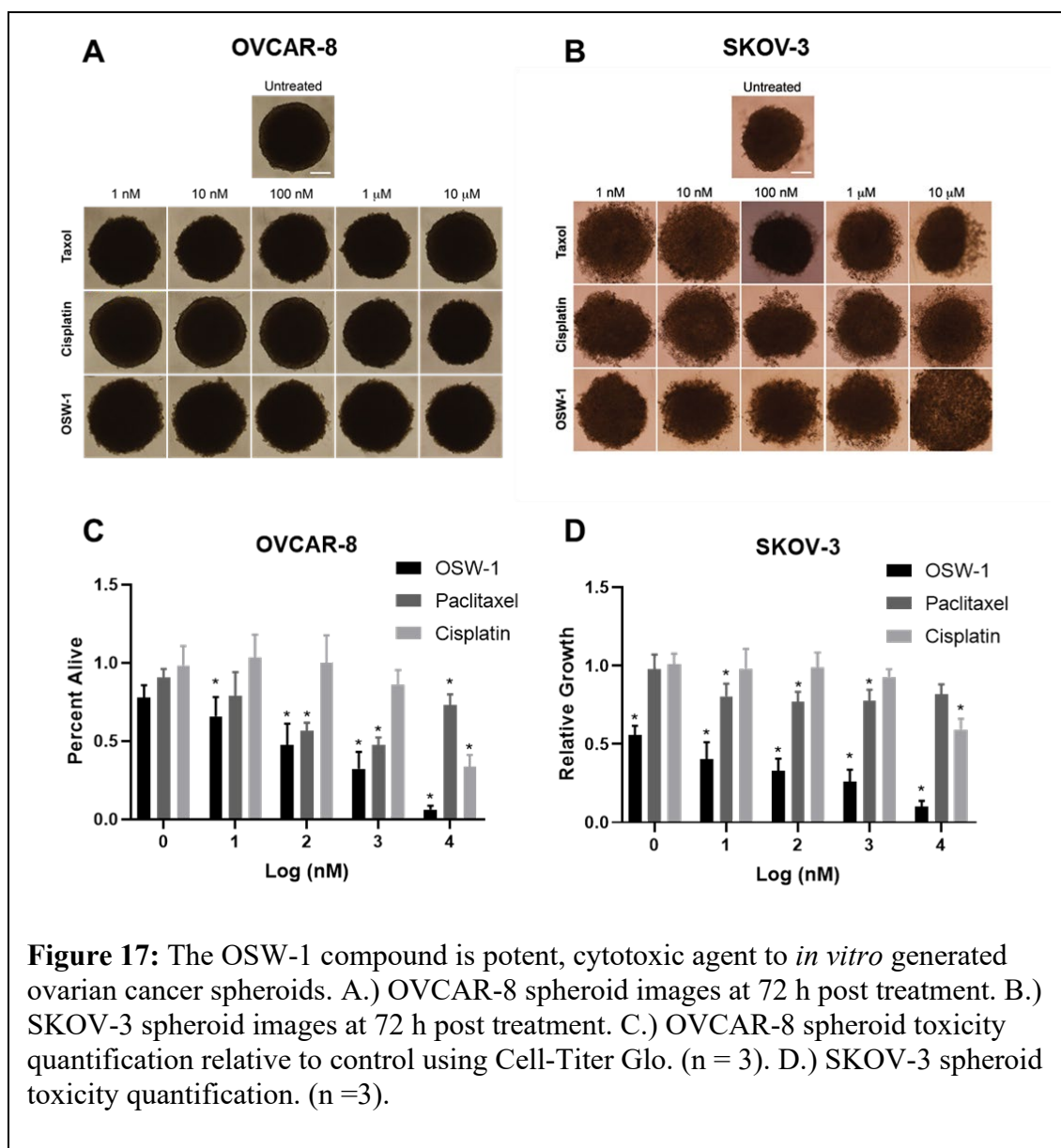
3.3.3 Ovarian cancer cells produce *in vitro* spheroids.

3D tumor spheroids provide a better representation of *in vivo* tumors compared to conventional 2D culture.¹²⁴ Spheroid formation occurs through aggregation of cells and has been developed by using different techniques; hanging drops^{132,133}, ultra-low attachment¹³⁴, spinner flasks¹³⁵, and agarose coating¹³⁶. Even though each technique results in spheroid formation, the specific spheroid generation technique has been shown to influence drug toxicity¹³⁷. OVCAR-8 and SKOV-3 spheroids were initiated with different cell numbers using the ultra-low attachment method and their growth for 7 days was monitored and their surface area was calculated by using ImageJ. OVSAHO and OVCAR-3 cells were unable to form compact spheroids using this method. Initial cell numbers for spheroid formation was selected to obtain similar sizes of spheroids at day 7. For both cell lines 5000, 10000, and 20000 cells were seeded on round bottom 96-well plates and monitored for their spheroid formation over 7 days. A total of 8 spheroids for each cell density seeding were analyzed for their surface area. OVCAR-8 spheroids initiated with 5,000 cells and SKOV-3 spheroids initiated with 20,000 cells resulted in similar sizes on day 7. Compared to SKOV-3 cells, OVCAR-8 cells aggregated within the first 24 h and formed spheroids even within 48 h. Additionally presence of FBS in the medium resulted in disruption of the spheroid formation around day 4 for SKOV-3 cells. Previously, spheroid formation has been described in serum-free conditions. Therefore, SKOV-3 spheroids were initiated without the presence of FBS and within 4 days spheroids had clear boundaries (**Figure 16**).

After obtaining the cell numbers resulting in similar spheroids size characterization of spheroids was carried out with these cell confluences. For 7 days, spheroids were characterized for their projected surface area (Figure 16). Circularity and

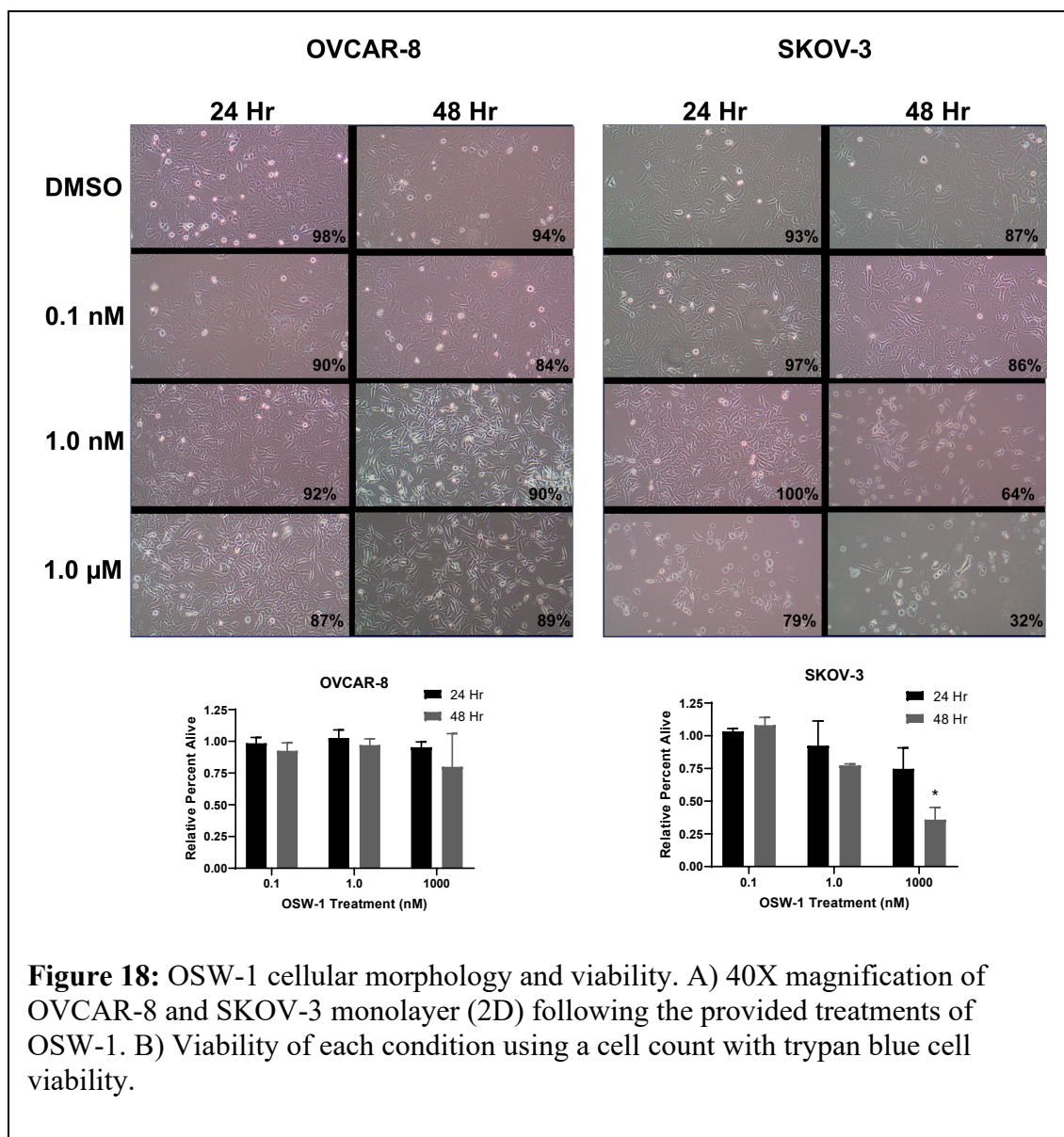


solidity measurements were carried out on day 7 (**Figure 16**). OVCAR-8 spheroids increase in size over the course of 7 days and had clear boundaries around day 2, while SKOV-3 cells formed spheroid boundaries around day 4 and did not increase in size due to lack of FBS in the media (Figure 16). Both spheroids had circularity more than 0.9 and had solidity more than 0.95 indicating the formation of dense and circular spheroids.¹³⁸



3.3.4 OSW-1 is a potent cytotoxic agent to ovarian spheroids *in vitro*

In order to test the OSW-1 compound in a more clinically relevant model, OSW-1, paclitaxel, and cisplatin were evaluated for their toxicity on a spheroidal (3D) assay generated from OVCAR-8 and SKOV-3 cells. **(Figure 17).** Toxicity of the compounds were analyzed by using CellTiter Glo 3D ATP detection mechanism instead of standard colorimetric methods which have been shown not applicable in 3D systems^{139,140}.



Following 7 days of growth, spheroids were treated with the provided concentration of compound and analyzed for viability following 72 h. OVCAR-8 spheroids were not as responsive to paclitaxel treatment (50% cell death at 100 nM) compared to the monolayer treatment (GI_{50} 58 nM) but exhibited similar sensitivity toward cisplatin treatment (50% cell death at 10 μ M in spheroids and GI_{50} 22 μ M in monolayer) (**Figure 17**). Interestingly, OSW-1 treatment resulted in a dose dependent loss of viability in OVCAR-8 spheroids with 50% cell death at 100 nM, in contrast to monolayer cells showing resistance up to 1

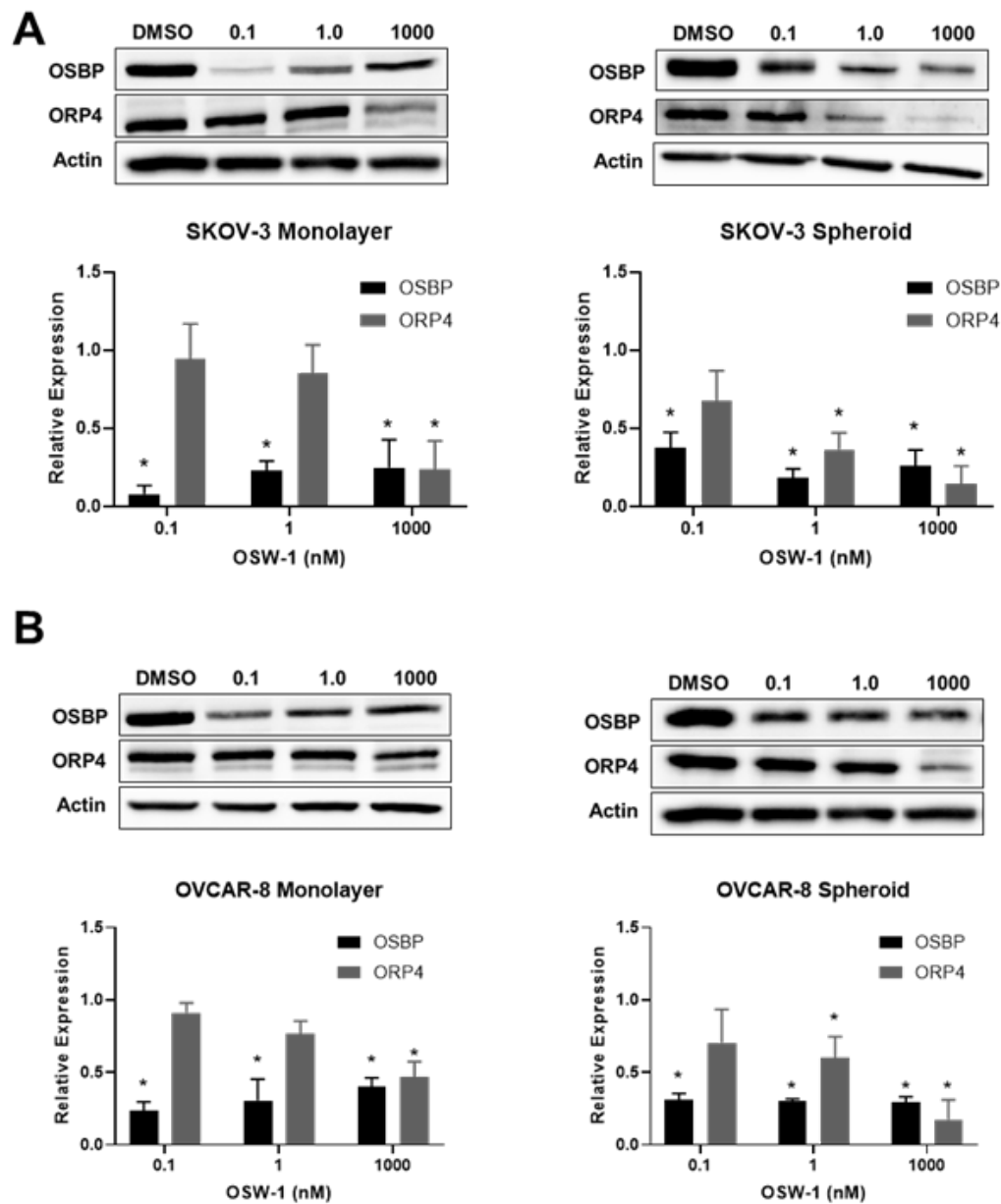


Figure 19: Ovarian cancer viability is correlated with ORP4L degradation and independent of OSBP expression upon OSW-1 treatment. A.) OSBP and ORP4L protein expression in 2D and 3D following the provided treatments of OSW-1 for 48 h in SKOV-3 and B.) in OVCAR-8.

μM . SKOV-3 spheroids were resistant to paclitaxel treatment exhibiting less than 25% cell death up to 10 μM and showed an increased resistance toward cisplatin treatment with less than 50% cell death at 10 μM . (**Figure 17**). Similar to OVCAR-8 spheroids,

OSW-1 inhibited SKOV-3 spheroid viability in a dose-dependent manner with 50% cell death at 1 nM, comparable to the 2D model (GI₅₀ 4.0 nM) (**Figure 17**). Furthermore, paclitaxel and cisplatin treated spheroids maintained their compact spheroid structure for the initial 48 h even at 1 mM concentration, however OSW-1 treatment clearly indicated disruption of spheroid boundaries around 10 nM which is 100-times lower than paclitaxel and cisplatin. These results indicate that OSW-1 is a potent cytotoxic agent of *in vitro* generated ovarian cancer spheroids, showing toxicity even when the SOC paclitaxel and cisplatin are incapable of inducing cell death.

3.3.5 OSW-1 toxicity is independent of OSBP degradation and correlates with ORP4L levels.

To address the mechanism of OSW-1 toxicity, both the OSBP and ORP4 levels were analyzed upon different concentration treatments of OSW-1 in both SKOV-3 and OVCAR-8 2D and 3D cultures following 48 h of treatment. Previous studies have demonstrated that low dose OSW-1 treatment (1 nM) results in selective degradation of the OSBP protein in a monolayer cell model^{60,90}. We also observed >60% OSBP degradation with as little as 0.1 nM OSW-1 for 48 h in both a 2D and 3D model with no signs of toxicity (**Figure 18**). An increasing amount of OSW-1 compound (i.e, 1.0 nM and 1.0 μ M) resulted in a non-significant difference in OSBP levels compared to the 0.1 nM treatment (p value > 0.05) (**Figure 18**). ORP4L protein levels, however, correlated closely with the viability of the cells in a 2D model, resulting in an OSW-1 concentration dependent degradation of the protein (**Figure 18**). The degradation of ORP4L was also evident in a 3D cell model correlating to viability in an OSW-1 dependent manner with

> 80% protein degradation at 1 μ M in both SKOV-3 and OVCAR-8 spheroids (**Figure 18, Figure 17**). The higher levels of degradation of the ORP4 protein upon 1.0 μ M treatment in OVCAR-8 spheroids (87%) compared to the monolayer (63%), could suggest a rationale into its increased toxicity to the OSW-1 compound in a 3D model. Furthermore, the lower, but not significant (p value > 0.05) levels of the OSBP and ORP4L protein in OVCAR-8 spheroids compared to monolayer could also influence the increase toxicity to OSW-1. Together, these results demonstrate an OSBP independent cytotoxicity mechanism of action, suggesting that the degradation of the ORP4L protein due to OSW-1 compound binding correlates with cellular viability *in vitro*.

3.3.6 OSW-1 toxicity is regulated based on extracellular lipids.

In vivo tumors are increasingly characterized by having hypoxic conditions and nutrient gradients in accordance with their distance from the nearest vasculature, this includes essential amino acids and sugars, but also lipids¹⁴¹. This absence of lipids demands a dependence on endogenous lipid biosynthesis. To further explore the discrepancy in OSW-1 toxicity between the 3D and 2D cell models of OVCAR-8, OSW-1 toxicity was monitored in both the presence and absence of extracellular lipids in a 2D model. OVCAR-8 and SKOV-3 cells grown in this delipidated condition exhibited little to no changes in growth and phenotype but exhibited a significant change in toxicity to the OSW-1 compound (**Figure 19**). OVCAR-8 cells exhibited a significant -200,000 fold change in sensitivity to the compound in delipidated media (GI₅₀ 0.06 nM) (Figure 19). This effect was also seen in SKOV-3 with a -180 fold change in sensitivity in delipid

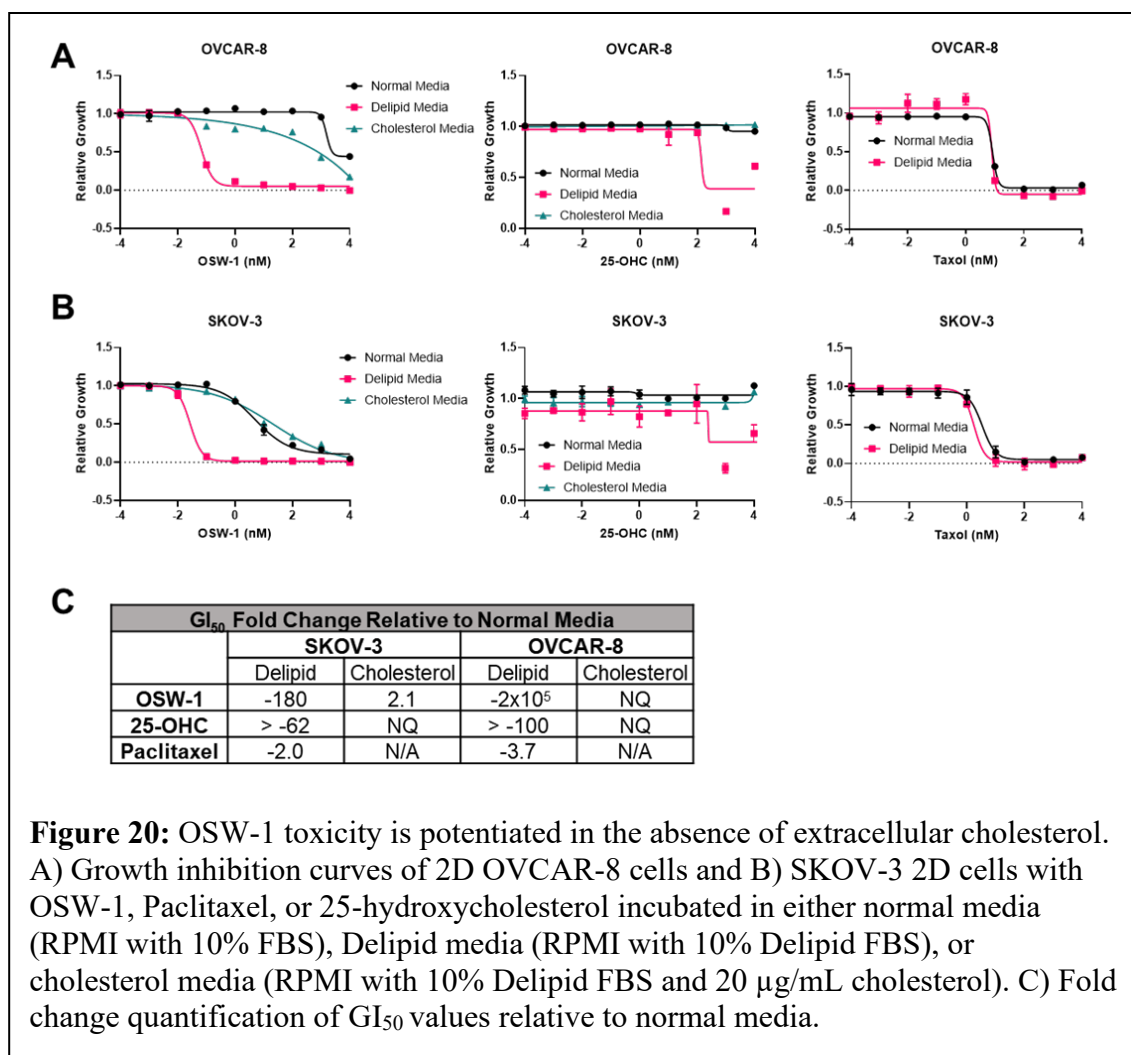


Figure 20: OSW-1 toxicity is potentiated in the absence of extracellular cholesterol. A) Growth inhibition curves of 2D OVCAR-8 cells and B) SKOV-3 2D cells with OSW-1, Paclitaxel, or 25-hydroxycholesterol incubated in either normal media (RPMI with 10% FBS), Delipid media (RPMI with 10% Delipid FBS), or cholesterol media (RPMI with 10% Delipid FBS and 20 $\mu\text{g/mL}$ cholesterol). C) Fold change quantification of GI₅₀ values relative to normal media.

media (GI₅₀ 0.02 nM) (Figure 19). Intriguingly, the addition of exogenous cholesterol to the delipid media attenuated the potency of the OSW-1 compound (**Figure 19**). 25-OHC, an endogenous ligand to the OSBP and ORP4 protein and also an inhibitor of β -Hydroxy β -methylglutaryl-CoA (HMG-CoA), an essential enzyme for endogenous cholesterol synthesis, also showed an increase in toxicity in the absence of lipids as expected, and the addition of cholesterol completely rescued the cells with no detectable toxicity up to 10 μM (Figure 19). Importantly, the change in toxicity in the delipid media was specific only to the OSW-1 compound and not due to a global cellular stress response (e.g. paclitaxel treatment). Together, these results demonstrate a unique mechanism of action specific to

the OSW-1 compound in the absence of exogenous lipids, potentially further explaining the increased sensitivity to the OSW-1 compound in 3D OVCAR-8 culture.

3.4 Discussion

We've identified the OSW-1 compound as a potent inhibitor of ovarian cancer growth in both a monolayer (2D) and spheroid (3D) cell model (**Figure 15**, **Figure 17**). The OSW-1 compound was able to induce cellular toxicity to ovarian cancer spheroids in the nano-molar range, whereas the clinically used therapeutics, cisplatin and paclitaxel were unable to induce a significant degree of toxicity under 10 μ M. The toxicity of the OSW-1 compound was correlated with the degradation of the ORP4L protein and was independent of OSBP degradation (**Figure 19**). Intriguingly, the OSW-1 compound was significantly more potent in the absence of extracellular lipids in a 2D model and the presence of exogenous cholesterol rescued this effect (**Figure 20**).

The OVCAR-8 cell line is the first cell line, to the best of our knowledge, to show resistance to the OSW-1 compound (**Figure 15**). The cell line does exhibit a significantly higher amount of the ORP4L protein, the proposed cytotoxic target of the OSW-1 compound, which could lead towards its resistance (**Figure 14**). However, the OVSAHO cell line also has a large amount of the ORP4L protein relative to SKOV-3, but remains sensitive to the compound, suggesting that OVCAR-8's resistance is not entirely due to elevated ORP4L levels. High dose OSW-1 treatment (1 μ M) for 48 h in 2D OVCAR-8 cells did not induce as much ORP4L degradation as in 3D (**Figure 19**), suggesting; 1) The ORP4L protein is essential for the viability of the cells; 2) the OSW-1 compound is able to cause the degradation of the protein, and; 3) this degradation could be regulated differently between 2D and 3D cultures, but could also be due to the difference, albeit not significant, OSBP and ORP4L protein levels between 2D and 3D. It should also be noted that 0.1 nM treatment of the compound was able to induce OSBP degradation in both 2D

and 3D cultures in each cell line tested, suggesting that the OSW-1 compound is able to penetrate into the cells, and the resistance of the OVCAR-8 cells is not due to compound entry.

The significantly lower pico-molar GI_{50} values of the OSW-1 compound in delipidated media compared to normal 10% FBS supplemented media (**Figure 20**) could be due to targeting of the OSBP protein, the strongest known binding protein to the compound. This would correlate with the degradation of the OSBP protein seen in both 2D and 3D culture as low as 100 pM treatment of the compound (**Figure 19**). Furthermore, the addition of cholesterol to the media rescuing this toxicity also suggests OSBP as the molecular target, since OSBP is known to traffic newly synthesized cholesterol from the Endoplasmic Reticulum to the Golgi Apparatus in addition to sensing cholesterol levels and controlling pERK activity, an essential pathway for cellular division^{43,142}. The degradation of the OSBP protein is independent of toxicity in the presence of extracellular lipids, however (**Figure 18**). This suggests that the OSW-1 compound would be a selective inhibitor for tumor growth by targeting both OSBP and ORP4. In this proposed model, 1. OSW-1 targets and degrades the cancer specific ORP4 protein resulting in cellular death, and 2. OSW-1 targets and degrades the ubiquitous tissue expressed OSBP protein, resulting in cellular death only in cholesterol deprived conditions (e.g., tumor tissue).

3.5 Conclusions

Taken together, our data suggests that the OSW-1 compound is a more potent inhibitor of ovarian cancer compared to the clinically used compounds, cisplatin and

paclitaxel, in both monolayer and spheroids *in vitro*. This toxicity is suggested to be due to ORP4L degradation, but in the absence of extracellular cholesterol, the targeting and degradation of the OSBP protein may be toxic to the cells in a sub nano-molar concentration, producing an ideal therapeutic for ovarian cancer with the potential of being applicable to multiple other cancers.

Chapter 4: Bio-Analytical Chemotherapeutic Drug Monitoring and Quantification of Gemcitabine in Single Cells

Abstract

The personalization of drug treatment requires capabilities to measure drug levels and efficacies in patients at the single-cell level since disease states are characterized by the biological activity of individual cells. Currently, there are no commonly used bioanalytical methods capable of real-time measurement of drug levels for the live single cells. The ability to quantify drug amount on the single-cell level is especially needed in the clinical treatment of cancer, because precisely measuring the amount of chemotherapy drug present in the individual cancer cells of a patient would allow for more adaptative and personalized administration of chemotherapy drugs. This would potentially lead to better clinical outcomes with fewer side effects. In this study, we report the quantification of the anti-cancer drug gemcitabine present in individual bladder cancer cells from both cell lines and patients undergoing standard chemotherapy. This bioanalytical innovation was achieved through development of a quantitative single cell mass spectrometry (qSCMS) sampling apparatus consisting of Single-probe mass spectrometry technology and an integrated cell manipulation platform (ICMP). The qSCMS analysis using the integrated Single-probe/ICMP system allows for the measurement of drug amount from individual cells. Particularly, the drug concentration can be obtained upon the measurement of cell size using the microscope of this integrated system. Our technique can potentially be developed into a rapid, real-time bioanalytical tool to more effectively and safely administer drug medications in patients.

Allocation of Contribution

This chapter is a submitted manuscript currently under review. I am co-first author on this manuscript. The data in this chapter is an accumulation of results from my collaborative work with Dr. Yang's lab at the University of Oklahoma. My collaborative work includes the 2019 *Analytical Chemistry* publication.¹⁴³ The research presented here was mainly conducted by myself and Dr. Standke, a former graduate student of Dr. Yang's lab. Dr. Standke contributed the analytical chemistry expertise to the project, including probe fabrication, instrument maintenance, and operation of the mass spectrometer. I was responsible for all mammalian and clinical cell culturing and preparation and drug treatment. I also assisted in the operation of analytical data accumulation (assisted with the operation of the mass spectrometer/ main operator of the ICMP/ LCMS). Dr. Standke and I contributed equally with data analysis and drug quantification. I was the main contributor for the creation of all publication figures shown (Dr. Standke was responsible for **Figure 21**). Mr. Devon Colby assisted throughout the project and was primarily responsible for probe fabrication.

4.1 Introduction

The current inability to quantify intracellular chemotherapy drug concentrations in cancer cells limits the personalization and overall effectiveness of drug administration in clinical cancer medicine. In this study, we report the development of a new quantitative single cell mass spectrometry (qSCMS) method capable of providing absolute drug amounts and concentrations (for spherical cells) in single cancer cells. Our qSCMS system is comprised of the Single-probe, a miniaturized sampling and ionization probe, combined with an integrated cell manipulation platform (ICMP). Using this qSCMS system, we conducted quantitative analysis of the intracellular drug gemcitabine present in individual bladder cancer cells, including those isolated from patients undergoing standard-of-care chemotherapy. The development of single cell pharmacology bioanalytical methods can potentially lead to more effective and safely administered drug medications in patients, especially in the treatment of cancer.

New single cell analysis techniques have recently emerged, including DNA and RNA sequencing, microfluidics, imaging, flow cytometry, and mass spectrometry (MS).^{144–156} The pursuit of single cell mass spectrometry (SCMS) technology has led to the development of new and innovative methodologies utilizing unique apparatuses, ionization technologies, and microscopy.^{157–167} Research into the treatment and study of cancer is a major potential application of SCMS methods. Understanding abnormal biology at the single cancer cell level is an increasing focus of cancer biology. Cancer stem cell theory and the clinical relevance of circulating tumor cells (CTC) are examples of the single cell focus of cancer research.^{168–170}

SCMS also has the potential to improve the administration of drug compounds in clinical cancer medicine. The use of SCMS in drug development and in drug administration will be especially important in the emergence of effective precision medicine. Ideally precision medicines in the clinical treatment of cancer should combine new targeted treatments with the capability of assessing, in a time-relevant manner, the efficacy of drug treatments in individual patients.¹⁷¹ The current lack of meaningful, real-time bioanalytical measurements in cancer patient drug administration limits the personalization and responsiveness of the treatment. Due to inter-individual pharmacokinetics/ pharmacodynamics (PK/PD), the amount of drug present in patient serum often does not report on the amount of drug present at tumor sites.^{172,173} The measurement of chemotherapy drug concentrations in biopsied tissue isolated from tumor sites might not represent the intracellular drug concentration in the tumor cells for multiple reasons. Tumor tissue samples are usually a complex, heterogenous mixture of cancer cells and non-cancer cells, and multi-drug resistant (MDR) cancer cells engage P-glycoprotein pumps to extrude therapeutic drugs into the extracellular tumor space.¹⁶ Due to these limitations in bioanalysis in drug administration, most chemotherapy drug dosage is determined by a patient's gross physical characteristics, such as body surface area, rather than any personalized or cancer-specific criteria.¹⁷⁴ Further, the chemotherapy drug regimen is commonly administered using a non-adapting, fixed schedule with efficacy determined from an endpoint analysis, such as an imaging scan (e.g., PET scan), after weeks or months of drug chemotherapy drug administration¹⁷⁵. Patients, therefore, are required to endure extensive, non-personalized chemotherapy dosing with its potential

associated adverse side effects before any determination if the treatment will have any efficacy.

The development and application of SCMS bioanalytical methods for the detection, quantification, and biological activity of drug compounds would be a powerful tool to provide real-time feedback of therapeutically-relevant treatment efficacy.¹⁷⁶ Our established Single-probe SCMS technology allows for the analysis of small molecules from individual cells, which are attached onto substrate (e.g., glass cover slip) surfaces, under ambient conditions.^{84,177} Using an isotopically-labeled deuterated irinotecan drug compound analog as an internal standard, we utilized the Single-probe system to successfully perform quantitative single cell mass spectrometry (qSCMS) in measuring the intracellular amounts of the anticancer drug irinotecan in single adherent cancer cells.¹⁷⁸ To further extend the SCMS analytical methods to non-adherent suspended cells with minimal interferences from complex sampling matrices, we coupled the Single-probe device with an integrated cell manipulation platform (ICMP) (Figure 21).¹⁷⁹ The ICMP, consisting of an inverted microscope, two cell manipulation systems, a microinjector, and a glass cell-selection probe, is capable of distinguishing cell types, morphologies, and sizes as well as capturing individual cells for analysis.¹⁷⁹

Here, we report the development and the application of the Single-probe/ICMP system to quantify the amount of standard-of-care cancer drug gemcitabine in single cancer cells. Using the Single-probe/ICMP system, we for the first time performed qSCMS measurement of the amount of an anticancer drug in bladder cancer cells isolated from patients undergoing intravenous chemotherapy.

4.2 Methods

4.2.1 Sample Preparation

Adherent Cell Line: For the adherent bladder cancer cell line model, T24, cells were plated (2×10^5) into each well of a 6-well plate containing a poly-D-lysine-coated glass microchip with chemically-etched microwells ($25 \mu\text{m} \times 55 \mu\text{m}$) and McCoy's Media 5a supplemented with 10% FBS and 1% penicillin-streptomycin. Approx. 36 h after initial seeding, the media in each well is replaced with Gemcitabine-containing media at the indicated concentrations and incubated at 37°C and 5% CO_2 for the duration of the treatment time (1 h). Prior to analysis, each glass microchip is rinsed with FBS-free media (5 mL) to avoid the detection of Gemcitabine from extracellular species. Cells were tested using the traditional Single-probe setup, modified for quantification

Suspended Cell Line: The human chronic myeloid leukemia cell line, K562, were grown in T25 flasks at 37°C and 5% CO_2 in RPMI media supplemented with 10% FBS and 1% penicillin-streptomycin. Prior to treatment (24 h), K562 cells (5×10^5) were seeded out in a T25 flask. The cells were spun at 1500 RPM for 5 min and treated with Gemcitabine at the indicated concentrations at a 4 mL volume in a 15 mL Falcon tube. After treatment, cells were pelleted at 1500 RPM for 5 min at 37°C and washed 3 times with PBS (10 mL). All tubes were resuspended in PBS (3 mL/tube) and were used for analysis in a 3 mL petri dish. K562 cells were analyzed using the integrated cell manipulation platform (ICMP) in conjunction with quantitative single cell mass spectrometry using the Single-probe mass spectrometry technique.

Patient Samples: Two separate groups of bladder cancer patients' urinary cells were analyzed in this study. One group ($n=2$) was not subjected to gemcitabine, while the

other (n=2) received 1000 mg/m² infusion of gemcitabine. The urine was collected in a specimen jar for the analysis of the non-treated patients and collected 1 h after infusion for the treated patients. The urinary sample was processed and analyzed within 3 h after collecting. Each sample was processed as followed: sample was spun at 1500 RPM for 5 minutes at 37°C, followed by washing with pre-warmed PBS (20 mL) 3 times. The cells were resuspended in PBS (2 mL), and the cell solution was placed into a 3-mL petri dish for analysis using the ICMP.

4.2.2 Single Probe Fabrication

Dual-bore quartz tubing (OD: 500 µm; ID: 127 µm) was pulled into a sharp needle (OD: ~5 µm) using a micropipette laser puller. Fused silica capillary (OD: 110 µm, ID: 40 µm) was placed into one bore as a solvent-providing capillary. The same diameter capillary was flame-pulled and placed into the other channel of the dual-bore quartz needle as a nano-ESI emitter. The probe was sealed using UV resin and secured on a glass slide with Epoxy glue for easy coupling to the flexible arm clamp of either the X, Y, Z-translational stage (adherent cells) or TransferMan manipulation system (suspended cells).

4.2.3 Glass Cell-Selection Probe Fabrication

Single-bore glass tubing (ID: 0.3 mm, OD: 1.1 mm) was transformed into a glass cell-selection device using a vertical pipette puller. Briefly, the glass was heated to create a tapered tip (~15 µm in diameter) to encompass an individual cell. Once the probe was pulled apart, it was placed in a Microforge MF-9 and bent ~45° from its original position.

4.2.4 Integrated Cell Manipulation Platform

The Single-probe setup has been modified to accommodate an Eppendorf cell manipulation system, which utilizes both a Single-probe and a cell-selection device that allows the analysis of samples from a complex matrix with minimal sample preparation. The system is composed of an Eppendorf TransferMan cell manipulation system, Nikon inverted microscope, a Tokai Hit ThermoPlate, and a glass cell-selection device. The cell-selection device was held in place and controlled through an Eppendorf TransferMan cell manipulation system. The Single-Probe was controlled through a second TransferMan system and stabilized with a flexible arm clamp. This system was constructed on a motorized table for convenient coupling to the Thermo LTQ Orbitrap XL mass spectrometer.

4.2.5 Single-Cell Mass Spectrometry Analysis

The Single-probe's nano-ESI emitter was aligned with the extended ion transfer tube's inlet. The solvent-providing capillary of the Single-probe was programmed to deliver solvent (internal standard dissolved in acetonitrile with 0.1% formic acid) at a flow rate of ~100 nL/min. Analysis was performed using a Thermo LTQ Orbitrap XL mass spectrometer. Positive ionization mode was used with a voltage of ~4.5 kV applied to the conductive union during analysis. (The flow rate and ionization voltage were optimized for each experiment due to varying tip size, emitter length, and emitter distance from the mass spectrometer's inlet). A resolution of 60,000 and 1 scan/100 ms maximum injection time were used.

Adherent Cell Line: The glass microchip was placed on an X, Y, Z-translational stage controlled through the LabView software package, which allows controlled movements in 0.1 μm increments. Cells are monitored using a top-view digital stereomicroscope. Once an individual cell is selected, the stage is lifted in the z-direction for insertion. Microscale extraction of cellular content occurs and is introduced to the mass spectrometer after ionization using the nano-ESI emitter.

Suspended Cell Line: Cells are placed in the lid of an 18-mm petri dish placed on a ThermoPlate at 37°C to mimic the cellular environment. During analysis, cells are monitored using an inverted microscope. Once a cell is chosen, suction is gently applied to the glass cell-selection device by changing the mineral oil in the CellTram Vario microinjector to secure a cell, and the cell-selection device is lifted in the Z-direction until aligned with the Single-probe tip. Once a liquid junction is formed between the two probes, suction from the cell-selection device is released for cell transfer. The cell undergoes microscale lysis and extraction and is taken up through drag force and capillary action before being sprayed into the mass spectrometer for analysis.

4.2.6 Liquid-Chromatography Mass Spectrometry Analysis

K562 cells (5×10^5) were seeded out in T25 flasks. After 24 h, cells were spun at 1500 RPM for 5 min and resuspended in 4 mL of RPMI media supplemented with Gemcitabine at the desired concentration. Following 1 h, cells were washed (X3) with PBS and resuspended to a total volume of 1 mL in PBS. Cells were counted using an automated cell counter (Bio-Rad TC20TM) and were lysed using 1 mL of cold acetonitrile spiked with 100 nM of isotopically-labeled gemcitabine for 10 min with brief vortexing.

Cell lysate was spun at 15,000 RCF for 15 min at 4 °C. Supernatant was transferred to a new tube and dried with a speed vacuum (Savant SPD11V, Thermo Scientific) at 70 °C for 1 h. Samples were resuspended in 150 µL 12: 88 Acetonitrile: water. Liquid chromatography was performed using a Waters nanoAQUITY BEH C-18 Column (100 µm x 100 mm, 1.7 µm) at 30 °C, a flow rate of 0.4 µL/ min, and a voltage of 2 kV. Mobile phase A is acetonitrile with 0.1% formic acid, and mobile phase B is water. A 15 min isocratic gradient was used with an A: B composition consisting of 12:88. Data acquisition was performed on a biological triplicate. (n=3).

4.2.7 Isotopically-labeled Gemcitabine

Stable-isotopically labeled gemcitabine was accessed through a short sequence of reactions following the synthetic route that scientists at Eli Lilly published in 1991.¹⁸⁰ The starting material 3,5-di-O-benzoate-2-deoxy-2,2-difluoro-D-ribofuranose 4.3 was purchased commercially as a mixture of both anomers. The hemiacetal mixture was then activated as glycosyl donor by conversion of the free hydroxyl group to a mesyl group in 4.4 with good yield (82%). The glycosyl acceptor was prepared from commercially available 2-¹³C, 1,3-¹⁵N₂ cytosine 4.5. Glycosyl acceptor 4.6 was prepared in situ from heating the mixture of cytosine 4.5 and hexamethyldisilane to reflux in presence of ammonium sulfate for 45 minutes. Utilizing the Vorbrueggen glycosylation method, the mesylated glycosyl donor 4.4 was reacted with silylated glycosyl acceptor 4.6 and trimethylsilyl trifluoromethanesulfonate as the activator in refluxing 1,2-dichloroethane for 48 hours. This reaction produced a mixture of protected isotopically labeled gemcitabine 4.7 (76% yield). The glycosylation reaction was presumed to proceed

through an SN1 pathway involving an oxonium ion intermediate, which resulted in a mixture of nucleoside anomers with the ratio of α : β being 1.3 : 1 as measured through ^1H NMR.

Treating the mixture 4.7 with ammonia in anhydrous methanol effectively removed both benzoyl protecting groups. The anomeric mixture of deprotected nucleoside were successfully separated through semi-preparative reverse-phase HPLC to afford desired β -anomer (4.8 in 34% yield) and α -anomer (4.9 in 4.0% yield). The desired β -nucleoside 4.8 was then converted to the hydrochloride salt of gemcitabine 4.10 in the presence of equimolar HCl in isopropanol. The molecular weight of the stable-isotopically labeled gemcitabine 4.10 was confirmed through high resolution mass spectrometry.

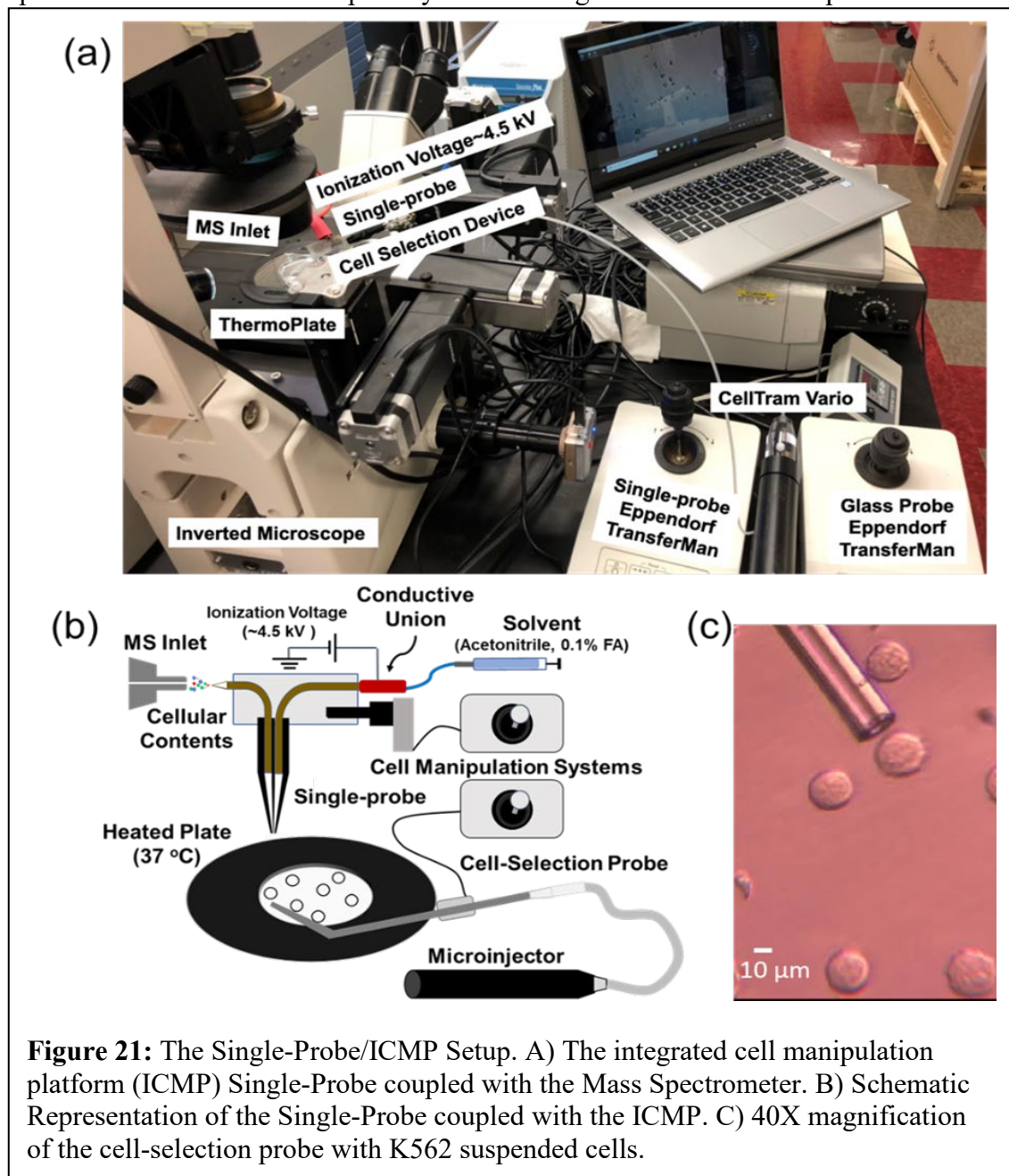
4.2.8 Statistical Analysis

All results are expressed as mean \pm SD with a minimum of three biological replicates. All statistical tests were performed on Graph Pad Prism 8 using a Mann-Whitney Test. The P values reported are as followed: * $p \leq 0.05$, ** $p \leq 0.01$ *** $p \leq 0.001$, and **** $p \leq 0.0001$.

4.3 Results

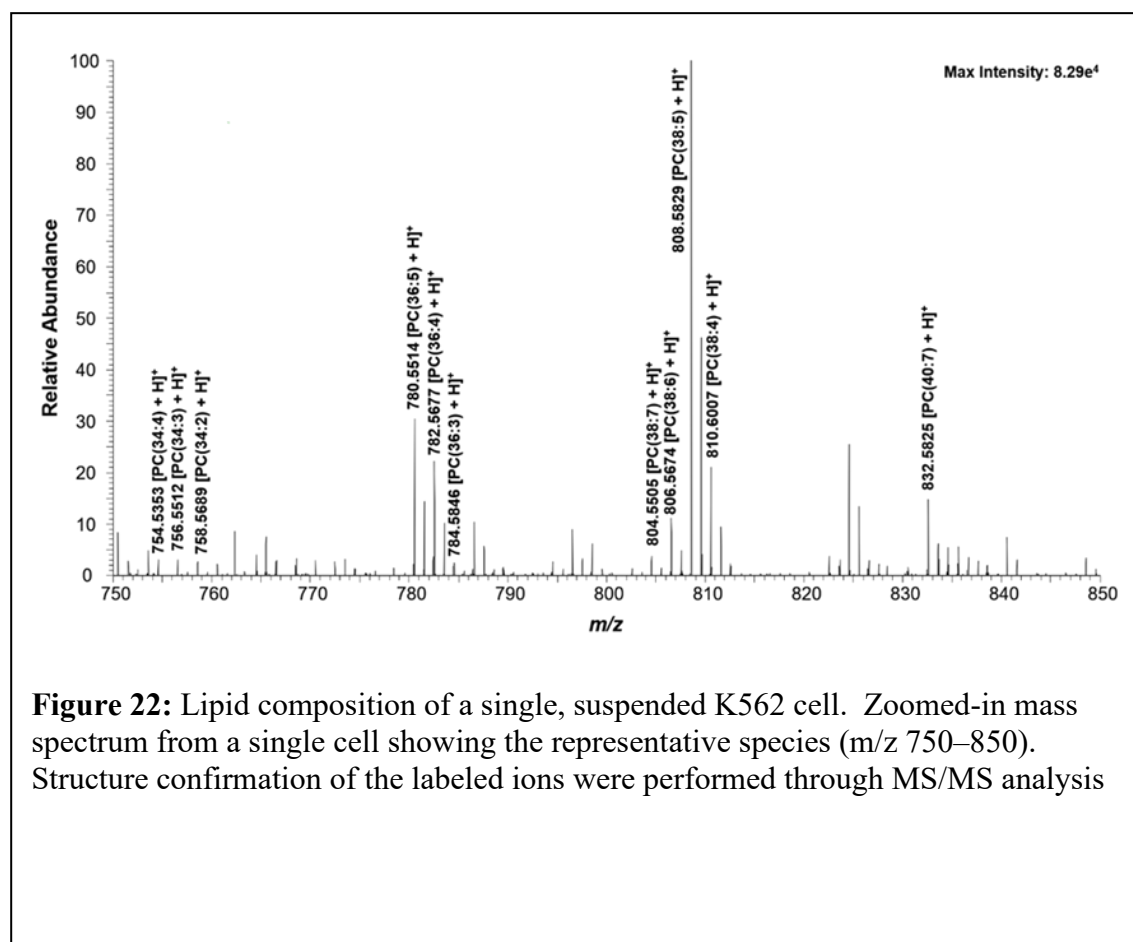
4.3.1 The Integrated Cell Manipulation System

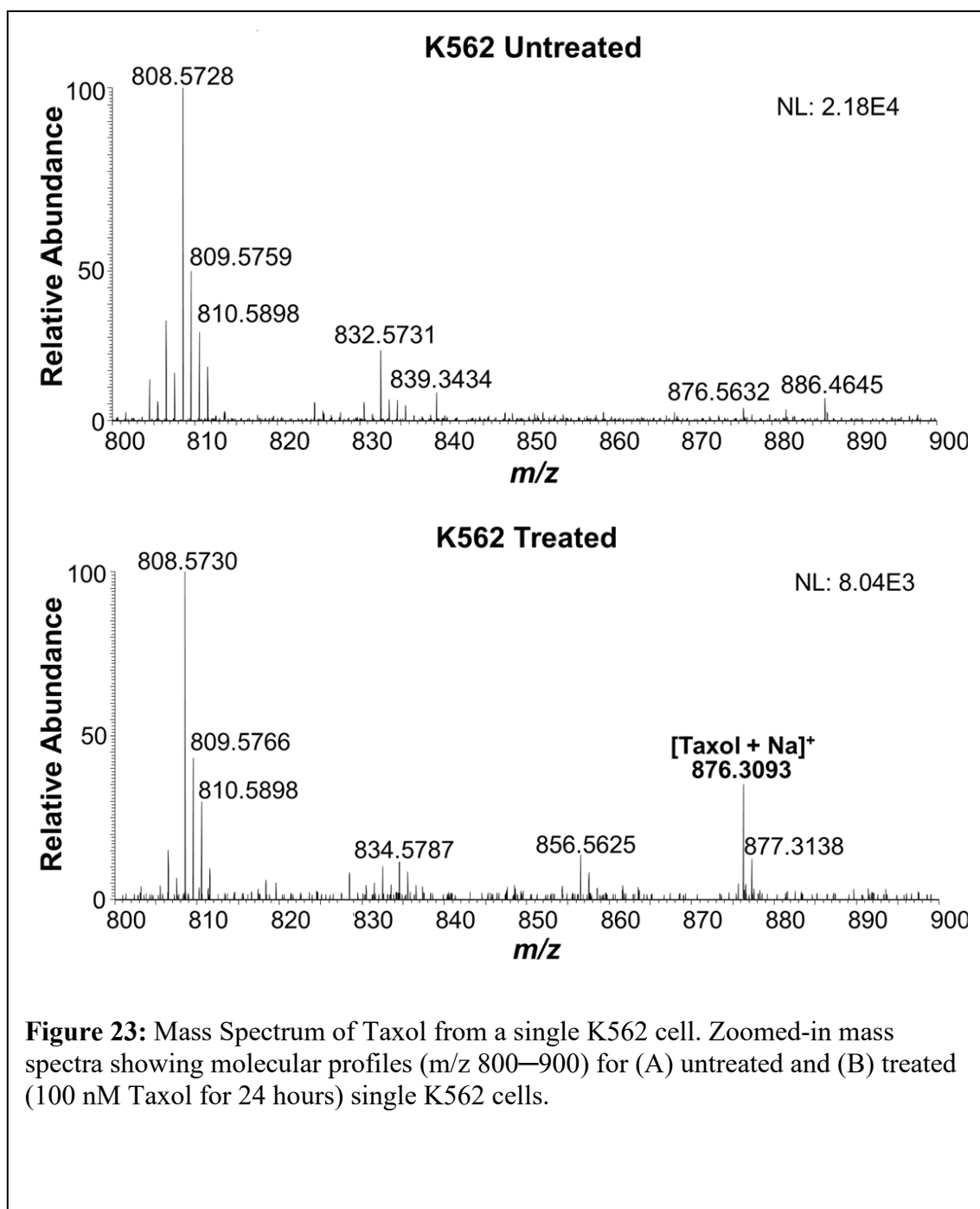
To analyze intracellular metabolites from single, suspended cells, the previously established Single-probe was coupled to an integrated cell manipulation platform (ICMP) (Figure 21). The ICMP system coupled to the Thermo LTQ Orbitrap XL mass spectrometer allowed the capability of selecting one individual suspended cell and



analyzing its intracellular metabolites by forming a liquid junction with the Single-probe, which serves as both a sampling and ionization device. The ICMP system consists of two Eppendorf TransferMan micromanipulation devices used to control both the cell selection device (small glass tubing with a small tip size) and the Single-probe. The Single-Probe nano-ESI was centrally aligned with the inlet of the extended ion transfer tube in order to interface with the mass spectrometer. The cell culture is placed on a Thermo Plate system set to 37°C on top of an inverted Nikon Eclipse TE300 inverted microscope to visualize the cells.

To operate the Single-probe/ ICMP system, the suspended cell culture (3 mL) is placed in a lid of a 35x12-mm petri dish. Cells were evaluated using the inverted





microscope. Using the TransferMan, the cell-selection probe was moved to a cell of interest. A gentle suction was applied using the CellTram Vario filled with mineral oil. A digital stereomicroscope was used to visualize the transfer of the cell from this culture to the Single-Probe. Once a junction was formed, the cell undergoes a micro-lysis and the cellular contents were carried by a continuous flow of acetonitrile solvent in the Single-

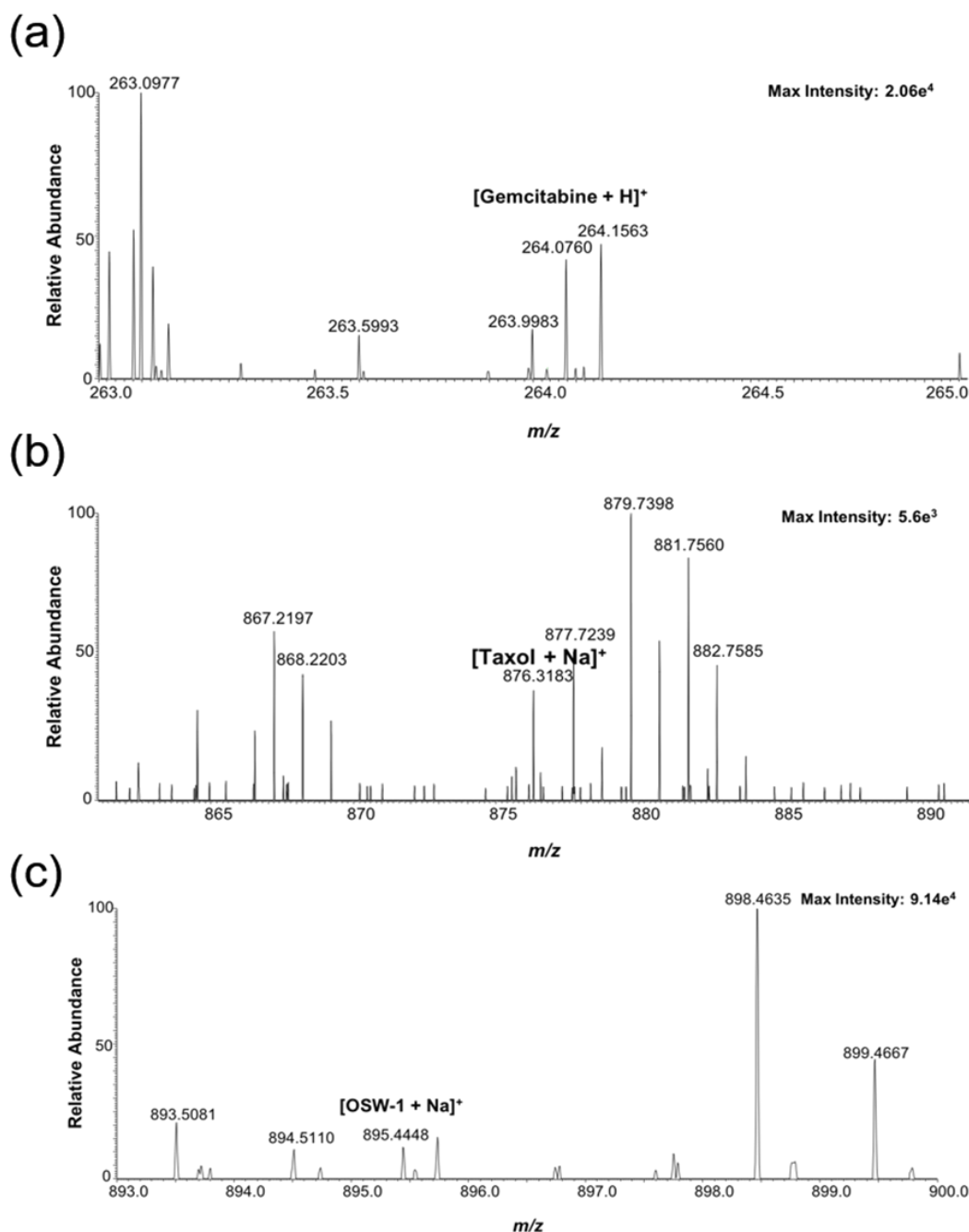


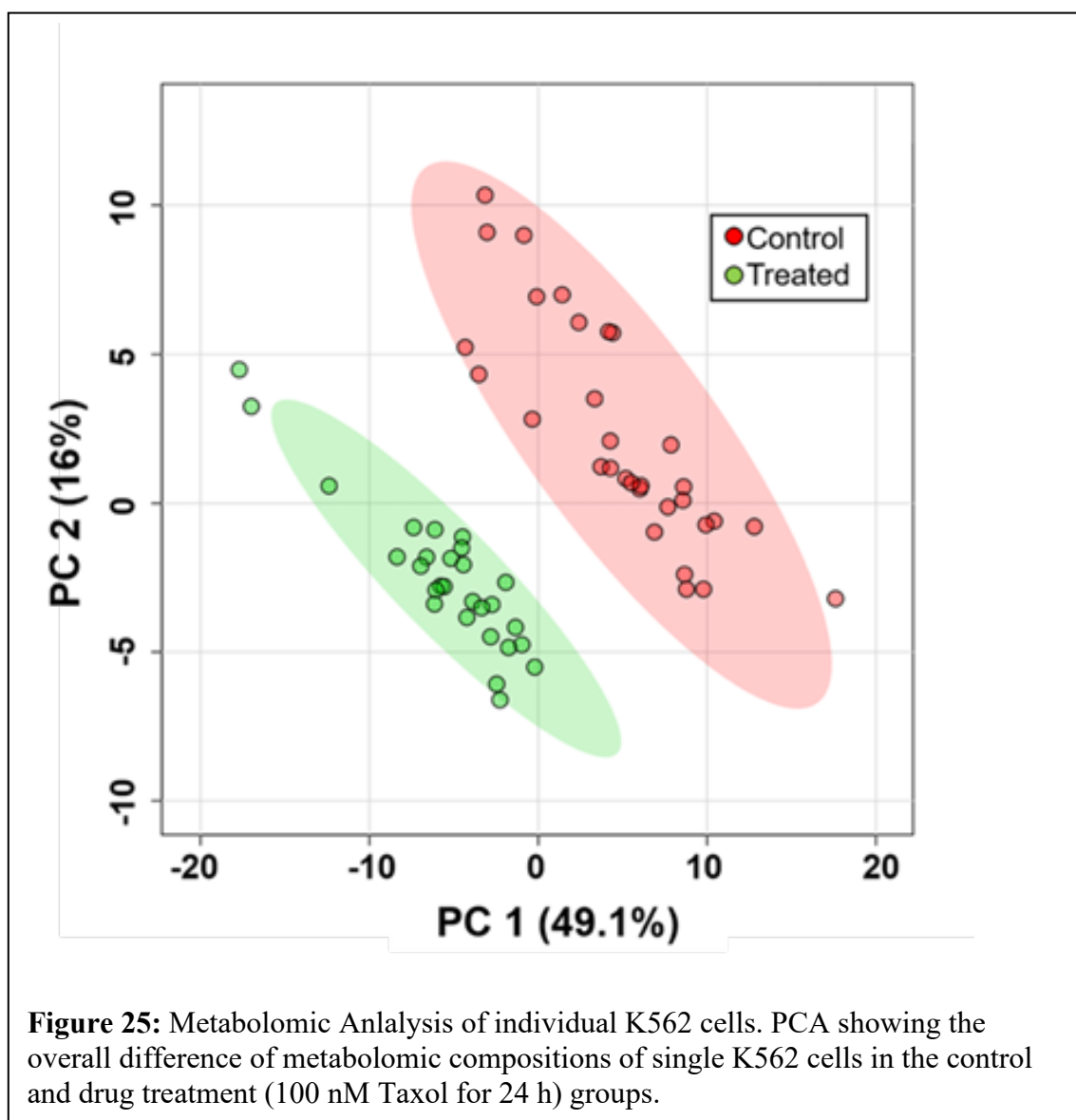
Figure 24: Mass spectra obtained from individual K562 cells. (A) Spectrum from a single cell treated with 1 μ M gemcitabine for 1 hr. (B) Spectrum for a cell exposed to 1 μ M Taxol for 1 hr. (C) An individual cell treated with 100 nM OSW-1 for 4 hr.

Probe, ionized, and sprayed in the mass spectrometer. The mass spectrometry parameters consisted of a 60,000 mass resolution at m/z 400, mass range of 100-1000, ionization

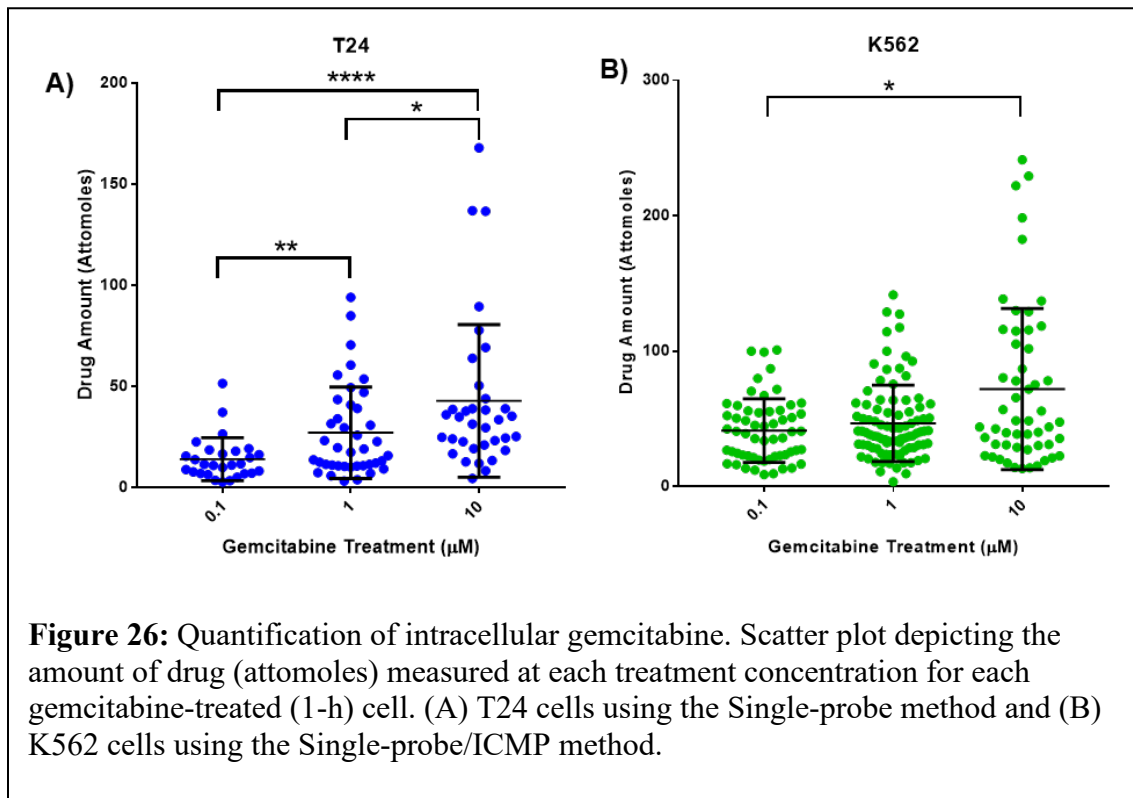
voltage of +4.5kV, 1 microscan, 100ms max injection time, and automatic gain control.

4.3.2 Adherent Cell Drug Identification

The Single-probe/ICMP system was used to detect the accumulation of different drug compounds (Gemcitabine, Taxol, and OSW-1) inside single chronic myeloid leukemia cells (K562 cell line). Cells were subjected to either Gemcitabine (1 μ M) or Taxol (1 μ M) for 1 h, or OSW-1 (1 μ M/ 100 nM) for 2 h/ 4h, respectively. The



Phosphatidyl Choline (PC) lipid peaks PC(34:4), PC(36:4), and PC(38:5) at m/z 754.536, 782.567, and 808.583, respectively, were highly ionizable and produced a reproducible signal depicting the analysis of cellular content in addition to numerous other PC identities (**Figure 22**). All PC peaks were subjected to MS/MS fragmentation to confirm the structures. In addition to these peaks, among many other detectable molecular



signatures, all three compounds were detected in individual K562 cells, but were not detected in the extracellular PBS solvent, indicating the compounds were released from the cell upon microlysis at the Single-Probe junction (**Figure 23, Figure 24**).

4.3.3 Metabolomic Analysis

In addition to identifying drug compound accumulation, the Single-probe/ICMP system was used to detect global metabolomic changes in individual K562 cells. K562 cells were subjected to either 100 nM Taxol or vehicle (DMSO) for 24 h. A minimum of

20 cells for each treatment condition was analyzed using the Single-Probe/ICMP setup. Following the 24 h treatment, the morphology of the cells did not change, however, the Taxol treated group had a significant change in the metabolomic composition of the cells (**Figure 25**). A principle component analysis (PCA) was formed through taking the single cell mass spec (SCMS) data and subjecting it to a background removal, noise reduction, peak alignment, and normalization using Geena2 prior to analysis with MetaboAnalyst. 73 metabolites were significantly changed ($p < 0.05$) upon drug treatment. To identify compounds of interest, a liquid chromatography mass spectrometry (LCMS) analysis of K562 lysate was performed and molecular identity was confirmed through MS/MS analysis. Monoglycerides (MG) and diglycerides (DG) comprised many of the significantly changed molecules. This data represents the capability of this method to both detect the amount of exogenously treated compound within the cell and perform a global analysis on the intracellular metabolites on a single-cell level.

Table 1: Quantification of intracellular gemcitabine in T24 and K562 cells using the Single-Probe (T24) or Single-probe/ICMP (K562) method

| Treatment Conc. | T24 (Attomole) | K562 (Attomole) |
|-----------------|-----------------|-----------------|
| 0.1 μ M | 13.9 ± 10.6 | 41.3 ± 23.5 |
| 1 μ M | 27.0 ± 22.6 | 46.7 ± 28.2 |
| 10 μ M | 42.8 ± 37.7 | 72.0 ± 59.5 |

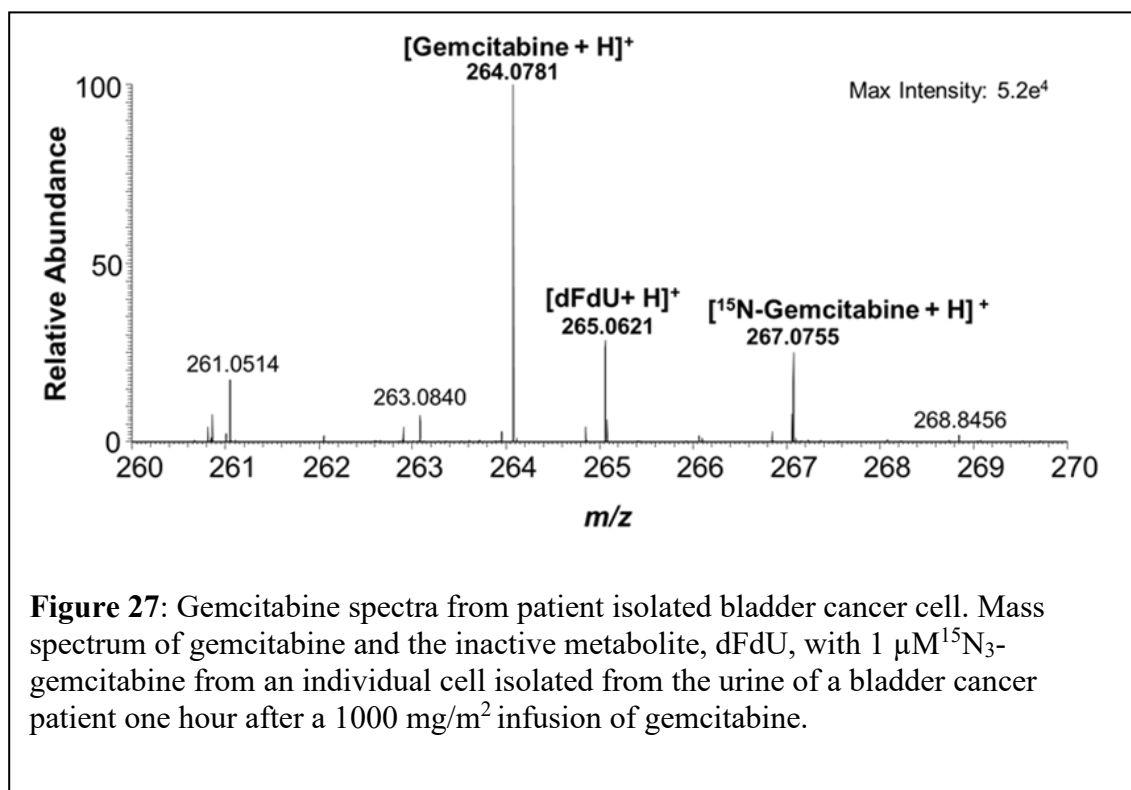
4.3.4 Single-Cell Drug Quantification

Following the development of this methodology for the detection of drug compounds and changes in intracellular metabolites upon drug treatment, we developed this technology to quantify the amount of drug compound accumulated inside single suspended cells. To begin this analysis, we utilized the established Single-Probe to quantify drug compound from the adherent bladder cancer cell line, T24. Cells were treated with the standard of care chemotherapeutic, gemcitabine, at either 0.1 μM , 1.0 μM , or 10 μM for 1 h and quantified using the Single-probe (**Figure 26, Table 1**). An internal standard of (^{13}C , ^{15}N -labeled) gemcitabine we prepared ($[\text{}^{13}\text{C}\text{C}_8\text{H}_{11}\text{F}_2\text{}^{15}\text{N}_2\text{NO}_4 + \text{H}]^+$, m/z 267.0703) was added into the sampling solvent (acetonitrile with 0.1% formic acid). The resulting continuous flow and detection of the known concentration of internal standard allowed the ability to quantify the amount of detected intracellular gemcitabine in the cell utilizing the following equation:

$$\frac{\Sigma A}{\Sigma B} = \frac{x}{c * t * v} \quad (\text{Equation 4.1})$$

A and B are the integration of the ion intensities for the target compound and standard, respectively, considering the internal standard concentration (c), time (t), and flow rate (v). This illustrated the ability to quantify the amount of gemcitabine inside single, adherent bladder cancer cells *in vitro*.

T24 cells were treated for 1 h with 1 μ M gemcitabine and trypsinized to release from the solid support. The resulting suspended cells were captured and quantified for intracellular gemcitabine using the Single-probe/IMCP system. The intracellular amount of gemcitabine in 20 suspended cells was determined as 37.2 ± 9.2 attomole, which is not



significantly different ($P > 0.05$) to the intracellular gemcitabine calculated in the T24 cells while adherent using the Single probe. This result demonstrated the reproducibility and viability of the Single-probe/ICMP in suspension cells versus the Single-probe in adherent cells. Further, K562 suspension leukemia cells were treated with 0.1, 1.0, or 10 μ M gemcitabine for 1 h and subjected to the qSCMS measurement using the Single-probe/ICMP setup (**Figure 26, Table 1**). The intracellular gemcitabine in individual K562 cells followed a similar trend to T24 cells. There is an increase of intracellular

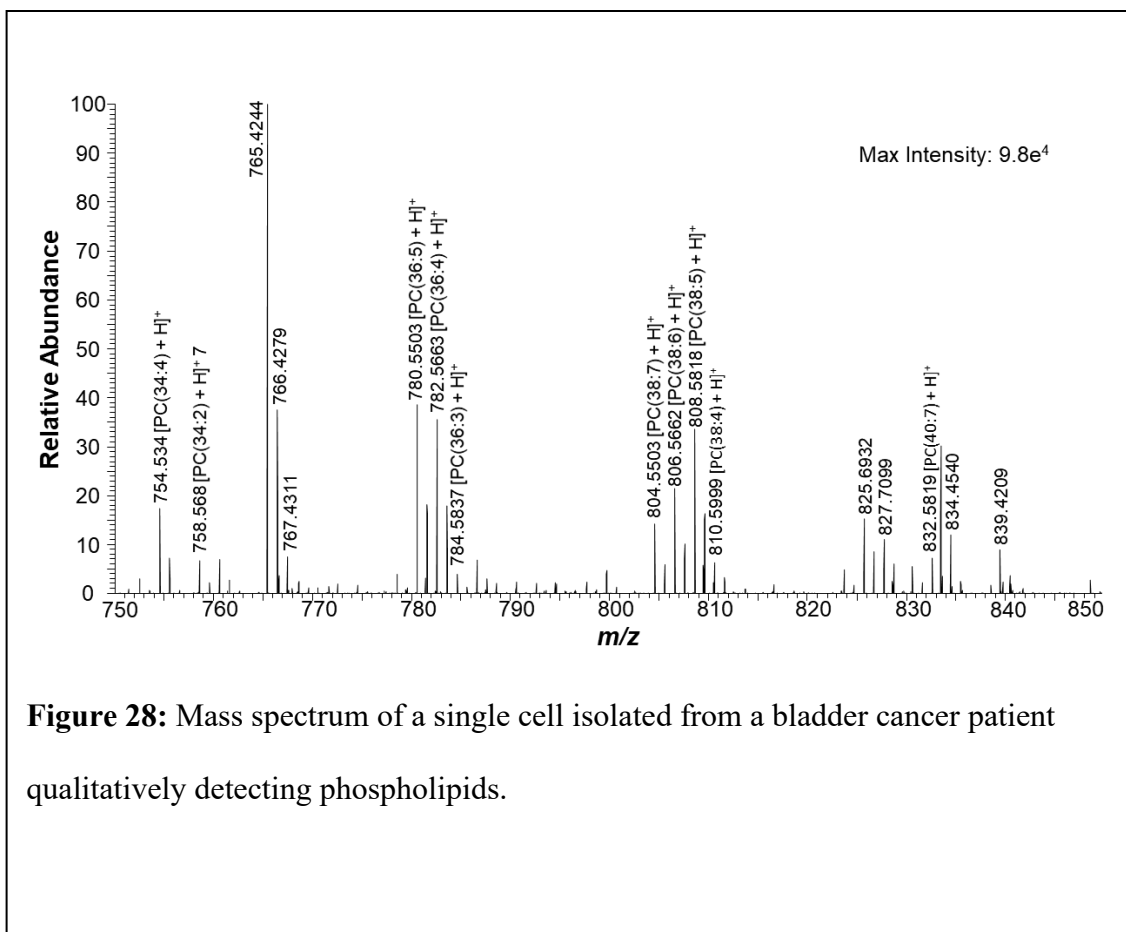


Figure 28: Mass spectrum of a single cell isolated from a bladder cancer patient qualitatively detecting phospholipids.

gemcitabine in both the adherent T24 cells, measured with the Single-probe system, and the suspension K562 cells, measured with the Single-Probe/ICMP system corresponding to an increase in cellular dose.

However, the increase in intracellular gemcitabine was not proportional with the increase in treatment condition (i.e., a 10 fold increase in treatment did not correlate with a 10 fold increase in intracellular amount). The 10 μ M treatment correlated with a significant increase in intracellular gemcitabine compared to the 1 μ M treatment in both treatments and methodologies.

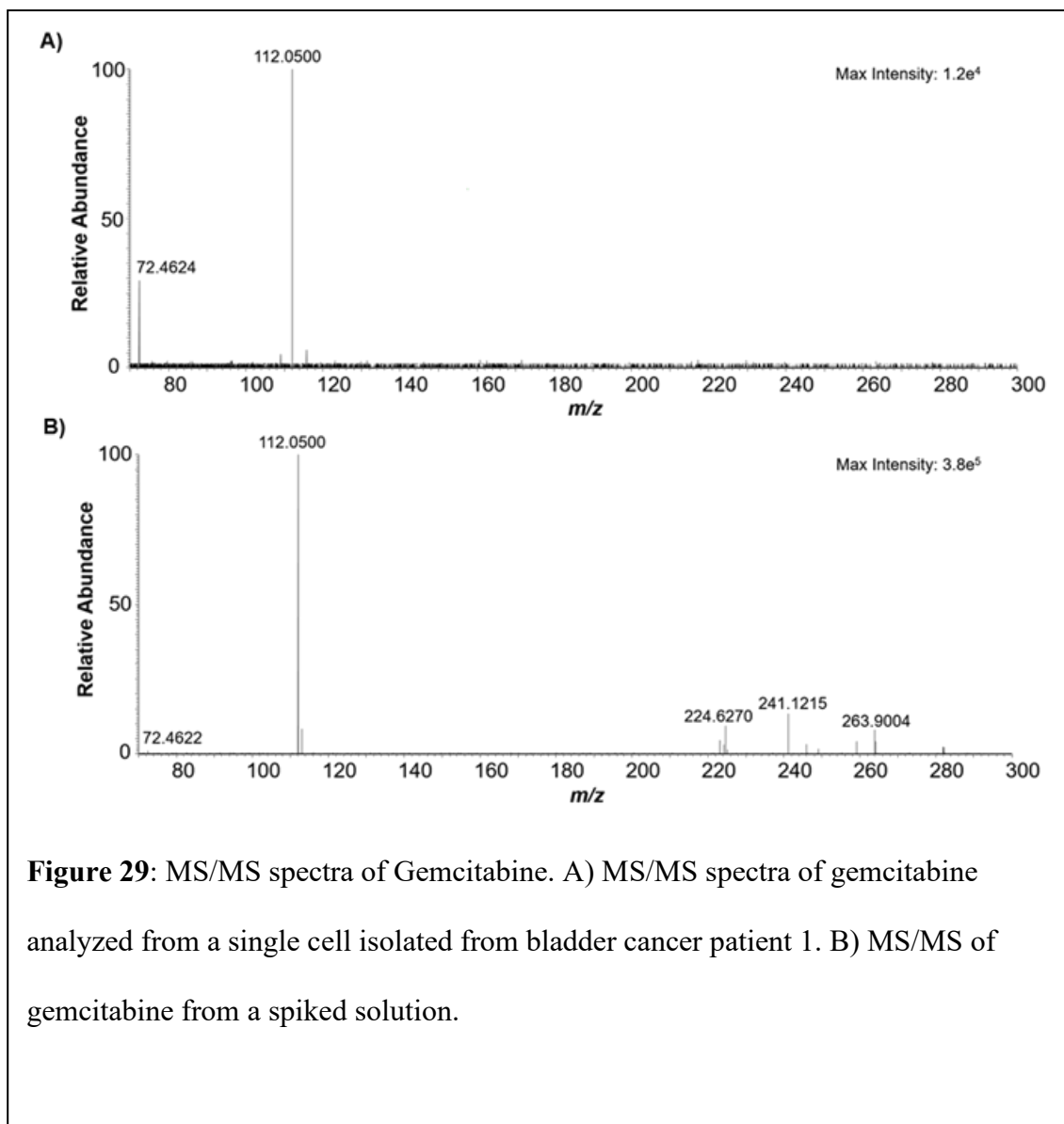


Figure 29: MS/MS spectra of Gemcitabine. A) MS/MS spectra of gemcitabine analyzed from a single cell isolated from bladder cancer patient 1. B) MS/MS of gemcitabine from a spiked solution.

The spherical, suspended K562 cell line was also used to quantify the absolute concentration of intracellular gemcitabine inside each individual cell. Each cell's diameter was measured by measuring the inner diameter of the cell selection probe. With a calculated cell volume, the concentration of gemcitabine in the K562 cells was determined. The intracellular concentrations of gemcitabine are significantly increased in a concentration dependent pattern ($p < 0.05$) (**Table 2**).

A further level of validation was taken by comparing the SCMS calculated concentration levels of gemcitabine in K562 cells to a LCMS quantification of gemcitabine. LCMS is the gold standard for determining intracellular drug concentration by considering both the total cell count in the lysate and the estimated cellular volume (2.8 pL). The calculated LCMS results are the average intracellular drug concentration in single cells. The LCMS results showed similar comparison to the SCMS results using the Single-probe/ICMP setup. This further signifies the potential of this methodology for quantifying drug accumulation in single cells.

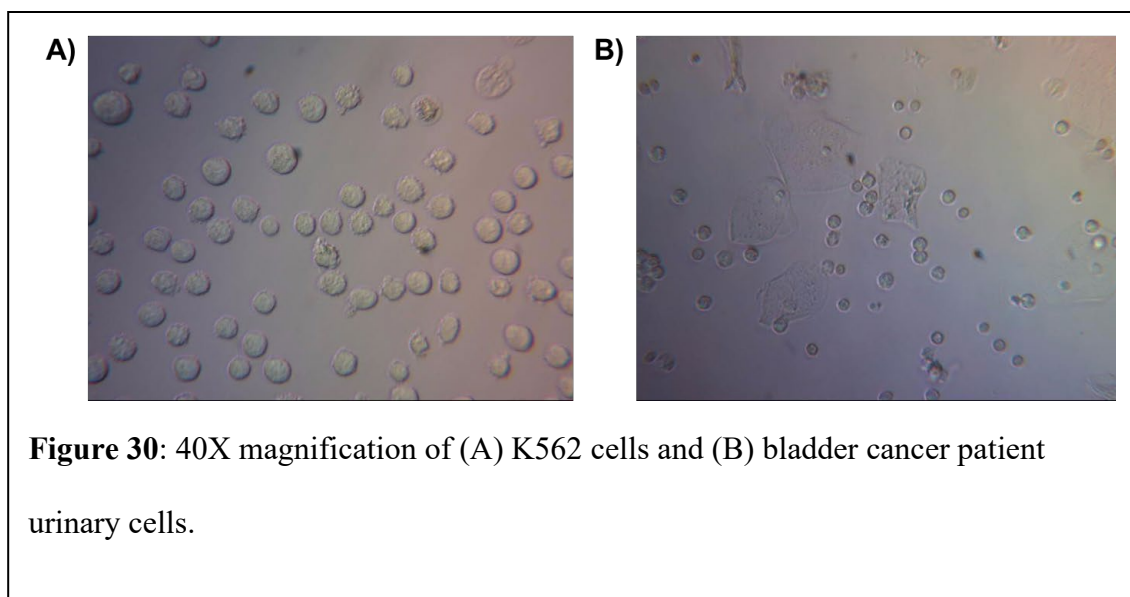
Table 2: Concentration of intracellular gemcitabine in K562 cells using SCMS and LCMS.

| Treatment Conc. | SCMS (μM) | LCMS (μM) |
|-------------------|------------------------|------------------------|
| 0.1 μM | 10.9 ± 7.1 | 17.4 ± 5.0 |
| 1 μM | 17.9 ± 11.9 | 18.1 ± 5.8 |
| 10 μM | 37.3 ± 26.1 | 28.0 ± 12.6 |

4.3.5 Clinical Single-Cell Patient Isolated Drug Quantification

Following the validation *in vitro*, the Single-probe/ICMP methodology was used to quantify the amount of gemcitabine from non-invasively isolated cells from the urine of bladder cancer patients. A total of four individual bladder cancer patients were analyzed (**Figure 30**). Two of them comprised the control group (No treatment) and two comprised the experimental group (Gemcitabine treated). Urine was collected from the control group, and the cells were isolated and subjected to the Single-probe/ICMP.

Numerous lipid peaks were identified and correlated with previously identified PC peaks, signifying the ability of the method to detect intracellular metabolites from individual cells *in vivo* (**Figure 28**). The experimental group was administered 1000 mg/ m² of gemcitabine. The urine from the treated patients were collected 1 h after the infusion.



Gemcitabine was detected in both patients and validated through MS/MS fragmentation as compared to the standard solution (**Figure 27, Figure 29**). Gemcitabine was detected only from the patients who underwent chemotherapy but was not present in cells from the untreated patients. A limited gemcitabine quantification data set was compiled consisting of no more than 15 cells quantified per infusion. The amount of intracellular drug measured from individual cells from Patient 1 was 473 ± 188 and $1,557 \pm 1004$ attomole following the second and fourth infusions, respectively. Patient 2 had a significantly lower amount of drug uptake than Patient 1, having 45.8 ± 39.4 and 79.4 ± 50.9 attomole of intracellular gemcitabine following the first and second infusions, respectively. The measurement of intracellular drug concentration was not conducted due to the inability to accurately measure the dimensions of irregularly shaped patient cells.

4.4 Discussion

We've developed a bio-analytical method capable of quantifying the amount of drug accumulation inside live, single cultured cells and cells isolated from bladder cancer patients. The spherical physiology of the suspended cells allowed for the quantification of intracellular drug concentration in real time on a cell to cell basis, providing an ideal measurement of drug accumulation inside individual cancer cells. The Single-Probe/ICMP system was comparable to an LCMS analysis on cellular lysate, validating the capability of this method on the single-cell level (**Table 2**).

Single cell gemcitabine drug quantification was performed from two different bladder cancer patients following two infusions of gemcitabine, respectively. Gemcitabine is a standard of care chemotherapeutic compound for bladder cancer and is easily ionizable in positive ion mode making it an ideal compound for mass spectrometry identification. Gemcitabine (dFdC) is pro-drug, which either gets deaminated into its inactive metabolite, dFdU, or phosphorylated into its active metabolites dFdCMP/ dFdCDP/ dfFdCTP.¹⁸¹ dFdU was able to be identified through our Single-Probe/ICMP method providing another molecule to monitor for cellular accumulation, however, we were unable to identify any of the active phosphorylated metabolites (dFdCMP/ dFdCDP/ dfFdCTP), possibly due to their incorporation into DNA, ultimately leading to cellular toxicity.

The Single-Probe/ICMP system is capable of detecting many different metabolites isolated from cells from a variety of different solutions and bodily fluids with little sample preparation. This technique could potentially be applied to hematological cancers (e.g., Leukemias/ Lymphomas) in addition to bladder cancer. Upon isolating

blood samples, the Single-Probe/ICMP system could quantify the amount of cancer therapeutics accumulating inside individual cancer cells in a real time readout, resulting in an optimal personalized drug monitoring method with minimal invasiveness.

In addition to quantitative drug accumulation, the Single-Probe/ICMP system is able to qualitatively measure a vast degree of small molecules. This capability could be applied and developed for metabolomic analysis of clinically isolated cells, potentially following drug treatment, to identify drug cellular physiology and dynamics *in situ*. Furthermore, this technique could be used to identify certain biomarkers (i.e., intracellular molecules that are significantly changed upon a drug treatment) to produce another level of detecting compound efficacy on the single-cell level.

4.5 Conclusions

Altogether, the Single-Probe/ICMP system was developed and applied for the quantification of the chemotherapeutic, gemcitabine, inside individual clinically isolated bladder cancer cells. This methodology could be further applied for the quantification of other drug compounds in addition to qualitatively analyzing numerous other metabolites from various different cancers.

Chapter 5: Conclusions and Future Outlook

My dissertation research was focused on identifying and characterizing druggable targets and developing new bioanalytical methods translatable for use in the emerging era of personalized medicine. The work presented in **Chapter 2** detailed my contribution to the discovery of a potential route for broad spectrum antiviral replication inhibition through a unique mechanism of targeting a host protein, rather than a viral associated molecule target. The discovery of that OSW-1 represses OSBP protein levels, leading to a prophylactic antiviral response, could lead to a broad-spectrum treatment of pathogenic viral infections. Although the mechanism of long-term repression was not identified, the OSW-1-induced repression of OSBP is not due to the obvious potential cellular mechanisms such as residual OSW-1 compound, calpain activity, proteasome degradation, autophagy, or transcription inhibition.¹⁰⁷ Furthermore, the OSW-1-induced reduction of OSBP is specific to OSBP.¹⁰⁸

Future work needs to be conducted into identification of the biological mechanism into the repression of the OSBP protein. Such a finding could have significant impacts into drug development for a wide range diseases. Such a mechanism could be a miRNA mediated targeted repression of the OSBP mRNA transcript, although the how binding of a small molecule to a protein (i.e., OSW-1 binding to OSBP) would initiate such a response, is unknown. The discovery of the mechanism, however, has obvious benefits to human health and drug development.

My work in studying ORP4 as a potential precision target in ovarian cancer (**Chapter 3**) showed the potential of the OSW-1-compound as personalized medicine.

We demonstrated that the ORP4 expression was ubiquitous among all four ovarian cancer cell lines tested in both a 2D and 3D models. The OSW-1 compound showed superior antiproliferative activity compared to the ovarian standard of care compounds paclitaxel and cisplatin in both ovarian monolayer and spheroid models. The cytotoxicity of the OSW-1 compound correlated to the degradation of the ORP4L protein, supporting the claim that the ORP4 protein is the cytotoxic target, rather than the OSBP protein. Of important significance, the OSW-1 compound was significantly more potent in the absences of extracellular lipids and attenuated by the addition of exogenous cholesterol. This phenomenon could potentially be exploited for the precision targeting of tumors, which are nutrient deprived. In this model, the targeting of both OSBP and ORP4 are additive in cytotoxic effects due to the cholesterol depletion in tumors. If true, this should make normal tissue with adequate cholesterol less responsive to OSW-1 compounds.

More research is needed to validate that the significant increase in cytotoxicity specifically to the OSW-1 compound is caused by the degradation of OSBP, and if it is, needs to be translated to an *in vivo* model. The implications of this research are profound, as it identifies biological targets to produce an ideal, precision medicine that targets the cancer cells, specifically tumors, with a large therapeutic window with efficacy against a broad range of cancers.

Beyond studying new druggable cellular targets, my dissertation research also encompassed new bioanalytical technology to measure drug compounds in cancer cells. This application of single cell mass spectrometry in drug quantification could lead to personalization of drug administration in way not currently possible. We have developed the Single-probe/ICMP qSCMS system to determine the concentration of

chemotherapeutic drugs in single suspended cells *in vitro*, and then used this system to quantify the amount of intracellular gemcitabine in cells isolated from bladder cancer patients. The Single-probe/ICMP qSCMS method can be further developed to quantify the amount of many different intracellular molecules of interest (e.g., drug compounds, lipids, metabolites, etc.) and to discriminate cell types based on metabolomic features of individual clinical cells, such as normal vs. cancerous cells. This method can potentially be used to measure therapeutically informative levels of drug compounds within cells in order to develop precision drug monitoring and administration. Single-cell quantification of drug compounds isolated from non-invasive patient samples is a major advancement for the development of single cell pharmacology. Single cell pharmacology could lead to understanding the action of drugs on the level of individual disease cells and provide a new paradigm in the development and better administration of drug compounds in patients.

Further development is still needed on the technology for it be incorporated into a clinical setting. Intensive validation and precision need to be optimized and methodology for discriminating cells in an efficient method needs to be implemented. One such method could be a FACS methodology through flow cytometry to discriminate cancer from non-cancerous cells. Furthermore, if blood samples are used rather than epithelial bladder cancers, a spherical cell output could be obtained and sorted through FACS. This would produce an ideal cell population to use our technology to quantify the cellular drug concentration in individual cancer cells compared to normal cells to produce a real-time output reading of drug monitoring and personalized chemotherapeutic administration regiment.

References

- (1) Vogenberg, F. R.; Barash, C. I.; Pursel, M. *P and T*. MediMedia, USA October 2010, p 560.
- (2) Krzyszczyk, P.; Acevedo, A.; Davidoff, E. J.; Timmins, L. M.; Marrero-Berrios, I.; Patel, M.; White, C.; Lowe, C.; Sherba, J. J.; Hartmanshenn, C.; O'Neill, K. M.; Balter, M. L.; Fritz, Z. R.; Androulakis, I. P.; Schloss, R. S.; Yarmush, M. L. *TECHNOLOGY* **2018**, 6 (03n04), 79–100.
- (3) Drew, L. *Nature* **2016**, 537 (7619), S60–S62.
- (4) McDonnell, PharmD, BCOP, A. M.; Dang, PharmD, BCPS, C. H. *J. Adv. Pract. Oncol.* **2013**, 4 (4), 263.
- (5) Druker, B. J. *Trends Mol. Med.* **2002**, 8 (4), S14–S18.
- (6) Sliwkowski, M. X.; Lofgren, J. A.; Lewis, G. D.; Hotaling, T. E.; Fendly, B. M.; Fox, J. A. *Semin. Oncol.* **1999**, 26 (4 Suppl 12), 60–70.
- (7) Kang, J. S.; Lee, M. H. *Korean Journal of Internal Medicine*. Korean Association of Internal Medicine 2009, pp 1–10.
- (8) Duhme, D. W.; Greenblatt, D. J.; Koch-Weser, J. *Ann. Intern. Med.* **1974**, 80 (4), 516–519.
- (9) Atkinson, J.; Nordstrom, K. *Clinical Pharmacology and Therapeutics*. October 1996, pp 363–367.
- (10) Shenfi;eld, G. M. *Br. J. Clin. Pharmacol.* **2001**, 52 (S1), 3–4.
- (11) Glazko, A. J. *Epilepsia* **1975**, 16 (2), 367–391.
- (12) Steijns, L. S. W.; Bouw, J.; Van der Weide, J. *Ther. Drug Monit.* **2002**, 24 (3), 432–435.

- (13) Alnaim, L. *Journal of Oncology Pharmacy Practice*. December 2007, pp 207–221.
- (14) Bardin, C.; Veal, G.; Paci, A.; Chatelut, E.; Astier, A.; Levêque, D.; Widmer, N.; Beijnen, J. *Eur. J. Cancer* **2014**, *50* (12), 2005–2009.
- (15) Balkwill, F. R.; Capasso, M.; Hagemann, T. *J. Cell Sci.* **2012**, *125* (23), 5591–5596.
- (16) Lopes-Rodrigues, V.; Sousa, E.; Vasconcelos, M. *Pharmaceuticals* **2016**, *9* (4), 71.
- (17) Kentala, H.; Weber-Boyvat, M.; Olkkonen, V. M. In *International Review of Cell and Molecular Biology*; Elsevier Inc., 2016; Vol. 321, pp 299–340.
- (18) Pietrangelo, A.; Ridgway, N. D. *Cellular and Molecular Life Sciences*. Birkhauser Verlag AG September 1, 2018, pp 3079–3098.
- (19) Taylor, F. R.; Saucier, S. E.; Shown, E. P.; Parish, E. J.; Kandutsch, A. A. *J. Biol. Chem.* **1984**, *259* (20), 12382–12387.
- (20) Taylor, F. R.; Kandutsch, A. A. *Chem. Phys. Lipids* **1985**, *38* (1–2), 187–194.
- (21) Lagace, T. A.; Byers, D. M.; Cook, H. W.; Ridgway, N. D. *Biochem. J.* **1997**, *326* (1), 205–213.
- (22) Ridgway, N. D.; Lagace, T. A.; Cook, H. W.; Byers, D. M. *J. Biol. Chem.* **1998**, *273* (47), 31621–31628.
- (23) Storey, M. K.; Byers, D. M.; Cook, H. W.; Ridgway, N. D. *Biochem. J.* **1998**, *336* (1), 247–256.
- (24) Lagace, T. A.; Byers, D. M.; Cook, H. W.; Ridgway, N. D. *J. Lipid Res.* **1999**, *40* (1), 109–116.

- (25) Clare, K.; Hardwick, S. J.; Carpenter, K. L.; Weeratunge, N.; Mitchinson, M. J. *Atherosclerosis* **1995**, *118* (1), 67–75.
- (26) Ong, J. M.; Aoki, A. M.; Seigel, G. M.; Sacerio, I.; Castellon, R.; Nesburn, A. B.; Kenney, M. C. *Neurochem. Res.* **2003**, *28* (6), 883–891.
- (27) Olkkonen, V. M.; Li, S. *Progress in Lipid Research*. October 2013, pp 529–538.
- (28) Yan, D.; Olkkonen, V. M. In *International Review of Cytology*; Academic Press Inc., 2008; Vol. 265, pp 253–285.
- (29) Olkkonen, V. M.; Béaslas, O.; Nissilä, E. *Biomolecules*. MDPI AG February 15, 2012, pp 76–103.
- (30) Weber-Boyvat, M.; Zhong, W.; Yan, D.; Olkkonen, V. M. *Biochemical Pharmacology*. Elsevier Inc. July 1, 2013, pp 89–95.
- (31) Im, Y. J.; Raychaudhuri, S.; Prinz, W. A.; Hurley, J. H. *Nature* **2005**, *437* (7055), 154–158.
- (32) Kandutsch, A. A.; Shown, E. P. *J. Biol. Chem.* **1981**, *256* (24), 13068–13073.
- (33) Kandutschs, A. A.; Thompson⁸, E. B. *Cytosolic Proteins That Bind Oxygenated Sterols CELLULAR DISTRIBUTION, SPECIFICITY, AND SOME PROPERTIES**; 1980; Vol. 255.
- (34) Wyles, J. P.; McMaster, C. R.; Ridgway, N. D. *J. Biol. Chem.* **2002**, *277* (33), 29908–29918.
- (35) Charman, M.; Colbourne, T. R.; Pietrangelo, A.; Kreplak, L.; Neale, D. **2014**, *4*.
- (36) Wang, C.; JeBailey, L.; Ridgway, N. D. *Biochem. J.* **2002**, *361* (3), 461–472.
- (37) A four-step cycle driven by PI(4)P hydrolysis directs sterol/PI(4)P exchange by the ER-Golgi tether OSBP. - PubMed - NCBI

<https://www.ncbi.nlm.nih.gov/pubmed/24209621> (accessed Apr 8, 2020).

- (38) Ridgway, N. D.; Dawson, P. A.; Ho, Y. K.; Brown, M. S.; Goldstein, J. L. *J. Cell Biol.* **1992**, *116* (2), 307–319.
- (39) Levine, T. P.; Munro, S. *Curr. Biol.* **1998**, *8* (13), 729–739.
- (40) Mesmin, B.; Bigay, J.; Moser von Filseck, J.; Lacas-Gervais, S.; Drin, G.; Antonny, B. *Cell* **2013**, *155* (4), 830–843.
- (41) Perry, R. J.; Ridgway, N. D. *Mol Biol Cell* **2006**.
- (42) Goto, A.; Liu, X.; Robinson, C. A.; Ridgway, N. D. *Mol. Biol. Cell* **2012**, *23* (18), 3624–3635.
- (43) Wang, P. Y.; Weng, J.; Anderson, R. G. W. *Science* (80-.). **2005**, *307* (5714), 1472–1476.
- (44) Romeo, G. R.; Kazlauskas, A. *J. Biol. Chem.* **2008**, *283* (15), 9595–9605.
- (45) Roberts, B. L.; Severance, Z. C.; Bensen, R. C.; Le-McClain, A. T.; Malinky, C. A.; Mettenbrink, E. M.; Nuñez, J. I.; Reddig, W. J.; Blewett, E. L.; Burgett, A. W. G. *Antiviral Res.* **2019**, *170*.
- (46) Albulescu, L.; Strating, J. R. P. M.; Thibaut, H. J.; Van Der Linden, L.; Shair, M. D.; Neyts, J.; Van Kuppeveld, F. J. M. *Antiviral Res.* **2015**, *117*, 110–114.
- (47) Bauer, L.; Ferla, S.; Head, S. A.; Bhat, S.; Pasunooti, K. K.; Shi, W. Q.; Albulescu, L.; Liu, J. O.; Brancale, A.; van Kuppeveld, F. J. M.; Strating, J. R. P. M. *Antiviral Res.* **2018**, *156*, 55–63.
- (48) Albulescu, L.; Bigay, J.; Biswas, B.; Weber-Boyvat, M.; Dorobantu, C. M.; Delang, L.; van der Schaar, H. M.; Jung, Y. S.; Neyts, J.; Olkkonen, V. M.; van Kuppeveld, F. J. M.; Strating, J. R. P. M. *Antiviral Res.* **2017**, *140*, 37–44.

- (49) WANG, C.; JeBAILEY, L.; RIDGWAY, N. D. *Biochem. J.* **2002**, *361* (3), 461–472.
- (50) WANG, C.; JeBAILEY, L.; RIDGWAY, N. D. *Biochem. J.* **2002**, *361* (3), 461 LP-472.
- (51) Zhong, W.; Yi, Q.; Xu, B.; Li, S.; Wang, T.; Liu, F.; Zhu, B.; Hoffmann, P. R.; Ji, G.; Lei, P.; Li, G.; Li, J.; Li, J.; Olkkonen, V. M.; Yan, D. *Nat. Commun.* **2016**, *7*.
- (52) Zhong, W.; Xu, M.; Li, C.; Zhu, B.; Cao, X.; Li, D.; Chen, H.; Hu, C.; Li, R.; Luo, C.; Pan, G.; Zhang, W.; Lai, C.; Wang, T.; Du, X.; Chen, H.; Xu, G.; Olkkonen, V. M.; Lei, P.; Xu, J.; Yan, D. *Cell Rep.* **2019**, *26* (8), 2166–2177.e9.
- (53) Zhong, W.; Xu, M.; Li, C.; Zhu, B.; Cao, X.; Li, D.; Chen, H.; Hu, C.; Li, R.; Luo, C.; Pan, G.; Zhang, W.; Lai, C.; Wang, T.; Du, X.; Chen, H.; Xu, G.; Olkkonen, V. M.; Lei, P.; Xu, J.; Yan, D. *Cell Rep.* **2019**, *26* (8), 2166–2177.e9.
- (54) Charman, M.; Colbourne, T. R.; Pietrangelo, A.; Kreplak, L.; Ridgway, N. D. *J. Biol. Chem.* **2014**, *289* (22), 15705–15717.
- (55) Li, J. W.; Xiao, Y. L.; Lai, C. F.; Lou, N.; Ma, H. L.; Zhu, B. Y.; Zhong, W. Bin; Yan, D. G. *Oncotarget* **2016**, *7* (40), 65849–65861.
- (56) Cao, X.; Chen, J.; Li, D.; Xie, P.; Xu, M.; Lin, W.; Li, S.; Pan, G.; Tang, Y.; Xu, J.; Olkkonen, V. M.; Yan, D.; Zhong, W. *FASEB J.* **2019**, fj201900933RR.
- (57) Garcia-Prieto, C.; Ahmed, K. B. R.; Chen, Z.; Zhou, Y.; Hammoudi, N.; Kang, Y.; Lou, C.; Mei, Y.; Jin, Z.; Huang, P. *J. Biol. Chem.* **2013**, *288* (5), 3240–3250.
- (58) Kubo, S.; Mimaki, Y.; Terao, M.; Sashida, Y.; Nikaido, T.; Ohmoto, T. *Phytochemistry* **1992**, *31* (11), 3969–3973.

- (59) Mimaki, Y.; Kuroda, M.; Kameyama, A.; Sashida, Y.; Hirano, T.; Oka, K.; Maekawa, R.; Wada, T.; Sugita, K.; Beutler, J. A. *Bioorganic Med. Chem. Lett.* **1997**, 7 (5), 633–636.
- (60) Burgett, A. W. G.; Poulsen, T. B.; Wangkanont, K.; Anderson, D. R.; Kikuchi, C.; Shimada, K.; Okubo, S.; Fortner, K. C.; Mimaki, Y.; Kuroda, M.; Murphy, J. P.; Schwalb, D. J.; Petrella, E. C.; Cornella-Taracido, I.; Schirle, M.; Tallarico, J. A.; Shair, M. D. *Nat. Chem. Biol.* **2011**, 7 (9), 639–647.
- (61) Albulescu, L.; Strating, J. R. P. M.; Thibaut, H. J.; Van Der Linden, L.; Shair, M. D.; Neyts, J.; Van Kuppeveld, F. J. M. *Antiviral Res.* **2015**, 117, 110–114.
- (62) Albulescu, L.; Bigay, J.; Biswas, B.; Weber-Boyvat, M.; Dorobantu, C. M.; Delang, L.; van der Schaar, H. M.; Jung, Y. S.; Neyts, J.; Olkkonen, V. M.; van Kuppeveld, F. J. M.; Strating, J. R. P. M. *Antiviral Res.* **2017**, 140, 37–44.
- (63) Arita, M.; Kojima, H.; Nagano, T.; Okabe, T.; Wakita, T.; Shimizu, H. *J. Virol.* **2013**, 87 (8), 4252–4260.
- (64) Strating, J. R. P. M.; van der Linden, L.; Albulescu, L.; Bigay, J.; Arita, M.; Delang, L.; Leyssen, P.; van der Schaar, H. M.; Lanke, K. H. W.; Thibaut, H. J.; Ulferts, R.; Drin, G.; Schlinck, N.; Wubbolts, R. W.; Sever, N.; Head, S. A.; Liu, J. O.; Beachy, P. A.; DeMatteis, M. A.; Shair, M. D.; Olkkonen, V. M.; Neyts, J.; van Kuppeveld, F. J. M. *Cell Rep.* **2015**, 10 (4), 600–615.
- (65) Boggio, K. J.; Obasuyi, E.; Sugino, K.; Nelson, S. B.; Agar, N. Y. R.; Agar, J. N. *Expert Review of Proteomics*. October 2011, pp 591–604.
- (66) Onjiko, R. M.; Moody, S. A.; Nemes, P. *Proc. Natl. Acad. Sci. U. S. A.* **2015**, 112 (21), 6545–6550.

- (67) Duncan, K. D.; Fyrestam, J.; Lanekoff, I. *Cite this Anal.* **2019**, *144*, 782.
- (68) Zhang, L.; Vertes, A. *Angewandte Chemie - International Edition*. Wiley-VCH Verlag April 16, 2018, pp 4466–4477.
- (69) Dueñas, M. E.; Essner, J. J.; Lee, Y. J. *Sci. Rep.* **2017**, *7* (1).
- (70) Redeker, V.; Toullec, J. Y.; Vinh, J.; Rossier, J.; Soye, D. *Anal. Chem.* **1998**, *70* (9), 1805–1811.
- (71) Rubakhin, S. S.; Garden, R. W.; Fuller, R. R.; Sweedler, J. V. *Nat. Biotechnol.* **2000**, *18* (2), 172–175.
- (72) Zhang, X. C.; Wei, Z. W.; Gong, X. Y.; Si, X. Y.; Zhao, Y. Y.; Yang, C. D.; Zhang, S. C.; Zhang, X. R. *Sci. Rep.* **2016**, *6*.
- (73) Wei, Z.; Zhang, X.; Si, X.; Gong, X.; Zhang, S.; Zhang, X. In *Methods in Molecular Biology*; Humana Press Inc., 2020; Vol. 2064, pp 31–59.
- (74) Gong, X.; Zhao, Y.; Cai, S.; Fu, S.; Yang, C.; Zhang, S.; Zhang, X. *Anal. Chem.* **2014**, *86* (8), 3809–3816.
- (75) Wilm, M.; Shevchenko, A.; Houthaeve, T.; Breit, S.; Schweigerer, L.; Fotsis, T.; Mann, M. *Nature* **1996**, *379* (6564), 466–469.
- (76) Tian, Q.; Li, D.; Barbacci, D.; Schwartz, S. J.; Patil, B. S. *Rapid Commun. Mass Spectrom.* **2003**, *17* (22), 2517–2522.
- (77) Comi, T. J.; Do, T. D.; Rubakhin, S. S.; Sweedler, J. V. *Journal of the American Chemical Society*. American Chemical Society March 22, 2017, pp 3920–3929.
- (78) Phelps, M.; Hamilton, J.; Verbeck, G. F. *Rev. Sci. Instrum.* **2014**, *85* (12).
- (79) Fujii, T.; Matsuda, S.; Tejedor, M. L.; Esaki, T.; Sakane, I.; Mizuno, H.; Tsuyama, N.; Masujima, T. *Nat. Protoc.* **2015**, *10* (9), 1445–1456.

- (80) Shimizu, T.; Miyakawa, S.; Esaki, T.; Mizuno, H.; Masujima, T.; Koshiba, T.; Seo, M. *Plant Cell Physiol.* **2015**, *56* (7), 1287–1296.
- (81) Hiyama, E.; Ali, A.; Amer, S.; Harada, T.; Shimamoto, K.; Furushima, R.; Abouleila, Y.; Emara, S.; Masujima, T. *Anal. Sci.* **2015**, *31* (12), 1215–1217.
- (82) Masujima, T. *Analytical Sciences*. Japan Society for Analytical Chemistry 2009, pp 953–960.
- (83) Zhang, L.; Foreman, D. P.; Grant, P. A.; Shrestha, B.; Moody, S. A.; Villiers, F.; Kwak, J. M.; Vertes, A. *Analyst* **2014**, *139* (20), 5079–5085.
- (84) Pan, N.; Rao, W.; Kothapalli, N. R.; Liu, R.; Burgett, A. W. G.; Yang, Z. *Anal. Chem.* **2014**, *86* (19), 9376–9380.
- (85) Sun, M.; Tian, X.; Yang, Z. *Anal. Chem.* **2017**, *89* (17), 9069–9076.
- (86) Liu, R.; Pan, N.; Zhu, Y.; Yang, Z. *Anal. Chem.* **2018**, *90* (18), 11078–11085.
- (87) Rao, W.; Pan, N.; Yang, Z. *J. Am. Soc. Mass Spectrom.* **2015**, *26* (6), 986–993.
- (88) Sun, M.; Yang, Z. *Anal. Chem.* **2019**, *91* (3), 2384–2391.
- (89) Rao, W.; Pan, N.; Yang, Z. *J. Vis. Exp.* **2016**, *2016* (112).
- (90) Roberts, B. L.; Severance, Z. C.; Bensen, R. C.; Le, A. T.; Kothapalli, N. R.; Nuñez, J. I.; Ma, H.; Wu, S.; Standke, S. J.; Yang, Z.; Reddig, W. J.; Blewett, E. L.; Burgett, A. W. G. *ACS Chem. Biol.* **2019**, *14* (2), 276–287.
- (91) Tapparel, C.; Siegrist, F.; Petty, T. J.; Kaiser, L. *Infection, Genetics and Evolution*. March 2013, pp 282–293.
- (92) Lugo, D.; Krogstad, P. *Current Opinion in Pediatrics*. Lippincott Williams and Wilkins February 1, 2016, pp 107–113.
- (93) Abzug, M. J. *J. Infect.* **2014**, *68* (SUPPL1), S108-14.

- (94) Hixon, A. M.; Yu, G.; Leser, J. S.; Yagi, S.; Clarke, P.; Chiu, C. Y.; Tyler, K. L. *PLoS Pathog.* **2017**, *13* (2), e1006199.
- (95) Amako, Y.; Syed, G. H.; Siddiqui, A. *J. Biol. Chem.* **2011**, *286* (13), 11265–11274.
- (96) Meutiawati, F.; Bezemer, B.; Strating, J. R. P. M.; Overheul, G. J.; Žusinaite, E.; van Kuppeveld, F. J. M.; van Cleef, K. W. R.; van Rij, R. P. *Antiviral Res.* **2018**, *157*, 68–79.
- (97) Melia, C. E.; Peddie, C. J.; de Jong, A. W. M.; Snijder, E. J.; Collinson, L. M.; Koster, A. J.; van der Schaar, H. M.; van Kuppeveld, F. J. M.; Bárcena, M. *MBio* **2019**, *10* (3).
- (98) Strating, J. R.; van Kuppeveld, F. J. *Current Opinion in Cell Biology*. Elsevier Ltd August 1, 2017, pp 24–33.
- (99) Belov, G. A.; Van Kuppeveld, F. J. *Current Opinion in Virology*. Elsevier B.V. December 2012, pp 740–747.
- (100) Belov, G. A.; Altan-Bonnet, N.; Kovtunovych, G.; Jackson, C. L.; Lippincott-Schwartz, J.; Ehrenfeld, E. *J. Virol.* **2007**, *81* (2), 558–567.
- (101) Hsu, N. Y.; Ilnytska, O.; Belov, G.; Santiana, M.; Chen, Y. H.; Takvorian, P. M.; Pau, C.; van der Schaar, H.; Kaushik-Basu, N.; Balla, T.; Cameron, C. E.; Ehrenfeld, E.; van Kuppeveld, F. J. M.; Altan-Bonnet, N. *Cell* **2010**, *141* (5), 799–811.
- (102) Arita, M. *Microbiol. Immunol.* **2014**, *58* (4), 239–256.
- (103) Pounds, R.; Leonard, S.; Dawson, C.; Kehoe, S. *Oncology Letters*. Spandidos Publications 2017, pp 2587–2597.

- (104) Lestner, J.; Hope, W. W. *Expert Opin. Drug Metab. Toxicol.* **2013**, *9* (7), 911–926.
- (105) Gao, Q.; Yuan, S.; Zhang, C.; Wang, Y.; Wang, Y.; He, G.; Zhang, S.; Altmeyer, R.; Zou, G. *Antimicrob. Agents Chemother.* **2015**, *59* (5), 2654–2665.
- (106) Hannedouche, S.; Zhang, J.; Yi, T.; Shen, W.; Nguyen, D.; Pereira, J. P.; Guerini, D.; Baumgarten, B. U.; Roggo, S.; Wen, B.; Knochenmuss, R.; Noël, S.; Gessier, F.; Kelly, L. M.; Vanek, M.; Laurent, S.; Preuss, I.; Miault, C.; Christen, I.; Karuna, R.; Li, W.; Koo, D. I.; Suply, T.; Schmedt, C.; Peters, E. C.; Falchetto, R.; Katopodis, A.; Spanka, C.; Roy, M. O.; Detheux, M.; Chen, Y. A.; Schultz, P. G.; Cho, C. Y.; Seuwen, K.; Cyster, J. G.; Sailer, A. W. *Nature* **2011**, *475* (7357), 524–527.
- (107) Roberts, B. L.; Severance, Z. C.; Bensen, R. C.; Le, A. T.; Kothapalli, N. R.; Nuñez, J. I.; Ma, H.; Wu, S.; Standke, S. J.; Yang, Z.; Reddig, W. J.; Blewett, E. L.; Burgett, A. W. G. *ACS Chem. Biol.* **2019**, *14* (2), 276–287.
- (108) Roberts, B. L.; Severance, Z. C.; Bensen, R. C.; Le, A. T.; Malinky, C. A.; Mettenbrink, E. M.; Nuñez, J. I.; Reddig, W. J.; Blewett, E. L.; Burgett, A. W. G. *Antiviral Res.* **2019**, 104548.
- (109) Torre, L. A.; Trabert, B.; DeSantis, C. E.; Miller, K. D.; Samimi, G.; Runowicz, C. D.; Gaudet, M. M.; Jemal, A.; Siegel, R. L. *CA. Cancer J. Clin.* **2018**, *68* (4), 284–296.
- (110) Howlader, N.; Noone, A.; Krapcho, M.; Noone, A.; Neyman, N.; Aminou, R.; Altekruse, S.; Kosary, C.; Altekruse, S. F.; Kosary, C. L.; Ruhl, J.; Tatalovich, Z.; Cho, H.; Afifi, A. M.; Garshell, J.; Yu, M. January 1, 2012.

- (111) Lengyel, E. *American Journal of Pathology*. Elsevier Inc. September 1, 2010, pp 1053–1064.
- (112) Armstrong, D. K.; Bundy, B.; Wenzel, L.; Huang, H. Q.; Baergen, R.; Lele, S.; Copeland, L. J.; Walker, J. L.; Burger, R. A. *N. Engl. J. Med.* **2006**, *354* (1), 34–43.
- (113) Ahmed, N.; Stenvers, K. L. *Front. Oncol.* **2013**, *3 SEP*, 256.
- (114) Shield, K.; Riley, C.; Quinn, M. A.; Rice, G. E.; Ackland, M. L.; Ahmed, N. J. *Carcinog.* **2007**, *6* (1), 11.
- (115) Chaicharoenaudomrung, N.; Kunhorm, P.; Noisa, P. *World Journal of Stem Cells*. Baishideng Publishing Group Co December 1, 2019, pp 1065–1083.
- (116) Mehta, G.; Hsiao, A. Y.; Ingram, M.; Luker, G. D.; Takayama, S. *J. Control. Release* **2012**, *164* (2), 192–204.
- (117) Pampaloni, F.; Reynaud, E. G.; Stelzer, E. H. K. *Nature Reviews Molecular Cell Biology*. October 2007, pp 839–845.
- (118) Sontheimer-Phelps, A.; Hassell, B. A.; Ingber, D. E. *Nat. Rev. Cancer* **2019**, *19* (2), 65–81.
- (119) Paullin, T.; Powell, C.; Menzie, C.; Hill, R.; Cheng, F.; Martyniuk, C. J.; Westerheide, S. D. *PLoS One* **2017**, *12* (8), e0182930.
- (120) Souza, A. G.; Silva, I. B. B.; Campos-Fernandez, E.; Barcelos, L. S.; Souza, J. B.; Marangoni, K.; Goulart, L. R.; Alonso-Goulart, V. *Curr. Pharm. Des.* **2018**, *24* (15), 1689–1694.
- (121) Ghosh, S.; Spagnoli, G. C.; Martin, I.; Ploegert, S.; Demougin, P.; Heberer, M.; Reschner, A. *J. Cell. Physiol.* **2005**, *204* (2), 522–531.

- (122) Xing, H.; Wang, S.; Hu, K.; Tao, W.; Li, J.; Gao, Q.; Yang, X.; Weng, D.; Lu, Y.; Ma, D. *J. Cancer Res. Clin. Oncol.* **2005**, *131* (8), 511–519.
- (123) Yang, Y.; Li, S.; Sun, Y.; Zhang, D.; Zhao, Z.; Liu, L. *Onco. Targets. Ther.* **2019**, *12*, 897–906.
- (124) Nunes, A. S.; Barros, A. S.; Costa, E. C.; Moreira, A. F.; Correia, I. J. *Biotechnology and Bioengineering*. John Wiley and Sons Inc. January 1, 2019, pp 206–226.
- (125) Zhou, Y.; Garcia-Prieto, C.; Carney, D. A.; Xu, R.; Pelicano, H.; Kang, Y.; Yu, W.; Lou, C.; Kondo, S.; Liu, J.; Harris, D. M.; Estrov, Z.; Keating, M. J.; Jin, Z.; Huang, P. *J. Natl. Cancer Inst.* **2005**, *97* (23), 1781–1785.
- (126) Huang, J.; Mousley, C. J.; Dacquay, L.; Maitra, N.; Drin, G.; He, C.; Ridgway, N. D.; Tripathi, A.; Kennedy, M.; Kennedy, B. K.; Liu, W.; Baetz, K.; Polymenis, M.; Bankaitis, V. A. *Dev. Cell* **2018**, *44* (3), 378–391.e5.
- (127) Banerji, S.; Ngo, M.; Lane, C. F.; Robinson, C. A.; Minogue, S.; Ridgway, N. D. *Mol. Biol. Cell* **2010**, *21* (23), 4141–4150.
- (128) Perry, R. J.; Ridgway, N. D. *Mol. Biol. Cell* **2006**, *17* (6), 2604–2616.
- (129) Goto, A.; Charman, M.; Ridgway, N. D. *J. Biol. Chem.* **2016**, *291* (3), 1336–1347.
- (130) Udagawa, O.; Ito, C.; Ogonuki, N.; Sato, H.; Lee, S.; Tripvanuntakul, P.; Ichi, I.; Uchida, Y.; Nishimura, T.; Murakami, M.; Ogura, A.; Inoue, T.; Toshimori, K.; Arai, H. *Genes to Cells* **2014**, *19* (1), 13–27.
- (131) Elias, K. M.; Emori, M. M.; Papp, E.; Macduffie, E.; Konecny, G. E.; Velculescu, V. E.; Drapkin, R. *Gynecol. Oncol.* **2015**, *139* (1), 97–103.

- (132) Kelm, J. M.; Timmins, N. E.; Brown, C. J.; Fussenegger, M.; Nielsen, L. K. *Biotechnol. Bioeng.* **2003**, *83* (2), 173–180.
- (133) Raghavan, S.; Ward, M. R.; Rowley, K. R.; Wold, R. M.; Takayama, S.; Buckanovich, R. J.; Mehta, G. *Gynecol. Oncol.* **2015**, *138* (1), 181–189.
- (134) Vinci, M.; Gowan, S.; Boxall, F.; Patterson, L.; Zimmermann, M.; Court, W.; Lomas, C.; Mendiola, M.; Hardisson, D.; Eccles, S. A. *BMC Biol.* **2012**, *10* (1), 29.
- (135) WARTENBERG, M.; DÖNMEZ, F.; LING, F. C.; ACKER, H.; HESCHELER, J.; SAUER, H. *FASEB J.* **2001**, *15* (6), 995–1005.
- (136) Friedrich, J.; Seidel, C.; Ebner, R.; Kunz-Schughart, L. A. *Nat. Protoc.* **2009**, *4* (3), 309–324.
- (137) Raghavan, S.; Mehta, P.; Horst, E. N.; Ward, M. R.; Rowley, K. R.; Mehta, G. *Oncotarget* **2016**, *7* (13), 16948–16961.
- (138) Amaral, R. L. F.; Miranda, M.; Marcato, P. D.; Swiech, K. *Front. Physiol.* **2017**, *8* (AUG).
- (139) Riss, T.; Valley, M.; Kupcho, K.; Zimprich, C.; Leippe, D.; Niles, A.; Vidugiriene, J.; Cali, J.; Kelm, J.; Moritz, W.; Lazar, D. *Toxicol. Lett.* **2014**, *229* (229), S145.
- (140) Kijanska, M.; Kelm, J. *In vitro 3D Spheroids and Microtissues: ATP-based Cell Viability and Toxicity Assays*; Eli Lilly & Company and the National Center for Advancing Translational Sciences, 2004.
- (141) Lewis, C. A.; Brault, C.; Peck, B.; Bensaad, K.; Griffiths, B.; Mitter, R.; Chakravarty, P.; East, P.; Dankworth, B.; Alibhai, D.; Harris, A. L.; Schulze, A.

- Oncogene* **2015**, *34* (40), 5128–5140.
- (142) Raychaudhuri, S.; Prinz, W. A. *Annu. Rev. Cell Dev. Biol.* **2010**, *26* (1), 157–177.
- (143) Pan, N.; Standke, S. J.; Kothapalli, N. R.; Sun, M.; Bensen, R. C.; Burgett, A. W. G.; Yang, Z. *Anal. Chem.* **2019**, *91* (14), 9018–9024.
- (144) Wang, D.; Bodovitz, S. *Trends Biotechnol.* **2010**, *28* (6), 281–290.
- (145) Heath, J. R.; Ribas, A.; Mischel, P. S. *Nat. Publ. Gr.* **2016**.
- (146) Schmid, A.; Kortmann, H.; Dittrich, P. S.; Blank, L. M. *Curr. Opin. Biotechnol.* **2010**, *21* (1), 12–20.
- (147) Boggio, K. J.; Obasuyi, E.; Sugino, K.; Nelson, S. B.; Agar, N. Y.; Agar, J. N. *Expert Rev. Proteomics* **2011**, *8* (5), 591–604.
- (148) Rubakhin, S. S.; Romanova, E. V.; Nemes, P.; Sweedler, J. V. *Nat. Methods* **2011**, *8* (4), S20–S29.
- (149) Fan, H. C.; Fu, G. K.; Fodor, S. P. A. *Science (80-.)*. **2015**, *347* (6222), 1258367.
- (150) Stuart, T.; Satija, R. *Nature Reviews Genetics*. Nature Publishing Group May 1, 2019, pp 257–272.
- (151) Qiu, X.; Hill, A.; Packer, J.; Lin, D.; Ma, Y. A.; Trapnell, C. *Nat. Methods* **2017**, *14* (3), 309–315.
- (152) Giustacchini, A.; Thongjuea, S.; Barkas, N.; Woll, P. S.; Povinelli, B. J.; Booth, C. A. G.; Sopp, P.; Norfo, R.; Rodriguez-Meira, A.; Ashley, N.; Jamieson, L.; Vyas, P.; Anderson, K.; Segerstolpe, Å.; Qian, H.; Olsson-Strömberg, U.; Mustjoki, S.; Sandberg, R.; Jacobsen, S. E. W.; Mead, A. J. *Nat. Med.* **2017**, *23* (6), 692–702.
- (153) Kalisky, T.; Quake, S. R. *Nat. Methods* **2011**, *8* (4), 311–314.

- (154) Shapiro, E.; Biezuner, T.; Linnarsson, S. *Nat. Rev. Genet.* **2013**, *14* (9), 618–630.
- (155) Yan, L.; Yang, M.; Guo, H.; Yang, L.; Wu, J.; Li, R.; Liu, P.; Lian, Y.; Zheng, X.; Yan, J.; Huang, J.; Li, M.; Wu, X.; Wen, L.; Lao, K.; Li, R.; Qiao, J.; Tang, F. *Nat. Struct. Mol. Biol.* **2013**, *20* (9), 1131–1139.
- (156) Lecault, V.; White, A. K.; Singhal, A.; Hansen, C. L. *Curr. Opin. Chem. Biol.* **2012**, *16* (3–4), 381–390.
- (157) Passarelli, M. K.; Ewing, A. G.; Winograd, N. *Anal. Chem.* **2013**, *85* (4), 2231–2238.
- (158) Rubakhin, S. S.; Lanni, E. J.; Sweedler, J. V. *Curr. Opin. Biotechnol.* **2013**, *24* (1), 95–104.
- (159) Zhang, L.; Vertes, A. *Angew. Chemie Int. Ed.* **2018**, *57* (17), 4466–4477.
- (160) Duncan, K. D.; Fyrestam, J.; Lanekoff, I. *Analyst*. Royal Society of Chemistry February 7, 2019, pp 782–793.
- (161) Mizuno, H.; Tsuyama, N.; Harada, T.; Masujima, T. *J. Mass Spectrom.* **2008**, *43* (12), 1692–1700.
- (162) Masujima, T. *Anal. Sci.* **2009**, *25* (8), 953–960.
- (163) Urban, P. L.; Schmid, T.; Amantonico, A.; Zenobi, R. *Anal. Chem.* **2011**, *83* (5), 1843–1849.
- (164) Greving, M. P.; Patti, G. J.; Siuzdak, G. *Anal. Chem.* **2011**, *83* (1), 2–7.
- (165) Miura, D.; Fujimura, Y.; Wariishi, H. .
- (166) Zemski Berry, K. A.; Hankin, J. A.; Barkley, R. M.; Spraggins, J. M.; Caprioli, R. M.; Murphy, R. C. *Chem. Rev.* **2011**, *111* (10), 6491–6512.
- (167) Chughtai, K.; Heeren, R. M. A. *Chem. Rev.* **2010**, *110* (5), 3237–3277.

- (168) CRISTOFANILLI, M. *Semin. Oncol.* **2006**, 33 (3 Suppl 9), 9–14.
- (169) Gerlinger, M.; Rowan, A. J.; Horswell, S.; Larkin, J.; Endesfelder, D.; Gronroos, E.; Martinez, P.; Matthews, N.; Stewart, A.; Tarpey, P.; Varela, I.; Phillimore, B.; Begum, S.; McDonald, N. Q.; Butler, A.; Jones, D.; Raine, K.; Latimer, C.; Santos, C. R.; Nohadani, M.; Eklund, A. C.; Spencer-Dene, B.; Clark, G.; Pickering, L.; Stamp, G.; Gore, M.; Szallasi, Z.; Downward, J.; Futreal, P. A.; Swanton, C. *N. Engl. J. Med.* **2012**, 366 (10), 883–892.
- (170) Marusyk, A.; Almendro, V.; Polyak, K. *Nat. Rev. Cancer* **2012**, 12 (5), 323–334.
- (171) Gonzalez de Castro, D.; Clarke, P. a; Al-Lazikani, B.; Workman, P. *Clin. Pharmacol. Ther.* **2013**, 93 (3), 252–259.
- (172) Alnaim, L. *J. Oncol. Pharm. Pract.* **2007**, 13 (4), 207–221.
- (173) Bardin, C.; Veal, G.; Paci, A.; Chatelut, E.; Astier, A.; Levêque, D.; Widmer, N.; Beijnen, J. *Eur. J. Cancer* **2014**, 50 (12), 2005–2009.
- (174) Gurney, H. *Br. J. Cancer* **2002**, 86 (8), 1297–1302.
- (175) Lowe, V. J.; Dunphy, F. R.; Varvares, M.; Kim, H.; Wittry, M.; Dunphy, C. H.; Dunleavy, T.; McDonough, E.; Minster, J.; Fletcher, J. W.; Boyd, J. H. *Head Neck* **1997**, 19 (8), 666–674.
- (176) Pan, N.; Rao, W.; Kothapalli, N. R.; Liu, R.; Burgett, A. W. G.; Yang, Z. *Anal. Chem.* **2014**, 86 (19), 9376–9380.
- (177) Sun, M.; Yang, Z. *Anal. Chem.* **2019**, 91 (3), 2384–2391.
- (178) Pan, N.; Standke, S. J.; Kothapalli, N. R.; Sun, M.; Bensen, R. C.; Burgett, A. W. G.; Yang, Z. *Anal. Chem.* **2019**, acs.analchem.9b01311.
- (179) Standke, S. J.; Colby, D. H.; Bensen, R. C.; Burgett, A. W. G.; Yang, Z. *Anal.*

Chem. **2019**, *91* (3), 1738–1742.

- (180) Chou, T. S.; Heath, P. C.; Patterson, L. E.; Poteet, L. M.; Lakin, R. E.; Hunt, A. H. *Synthesis (Stuttg)*. **1992**, 565–570.
- (181) De Sousa Cavalcante, L.; Monteiro, G. *European Journal of Pharmacology*. Elsevier October 15, 2014, pp 8–16.
- (182) Griffiths, W. J.; Abdel-Khalik, J.; Crick, P. J.; Yutuc, E.; Wang, Y. *Journal of Steroid Biochemistry and Molecular Biology*. Elsevier Ltd September 1, 2016, pp 4–26.

Appendix 1: Chapter 2 Supplemental

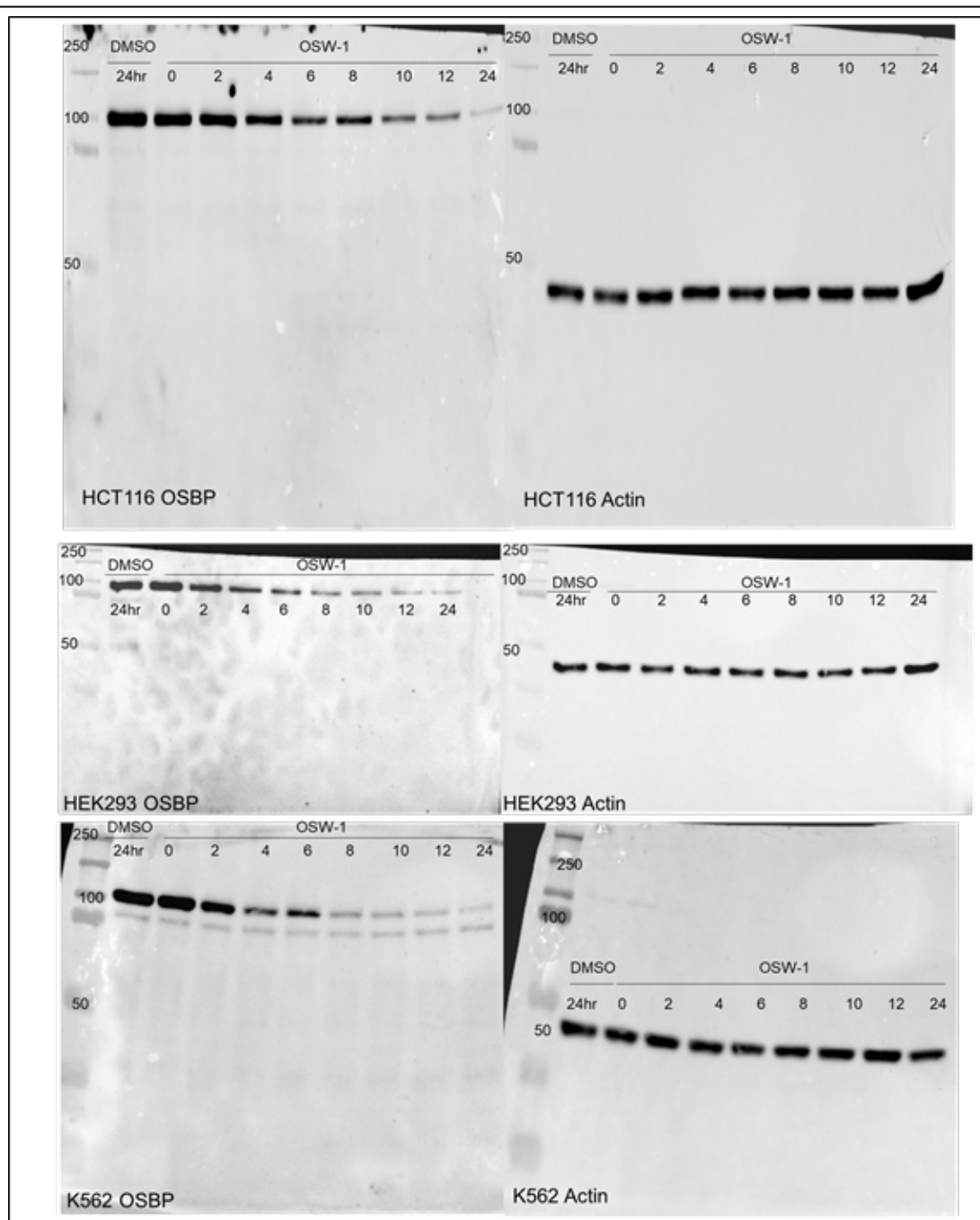


Figure 31: Full blots from Figure 5

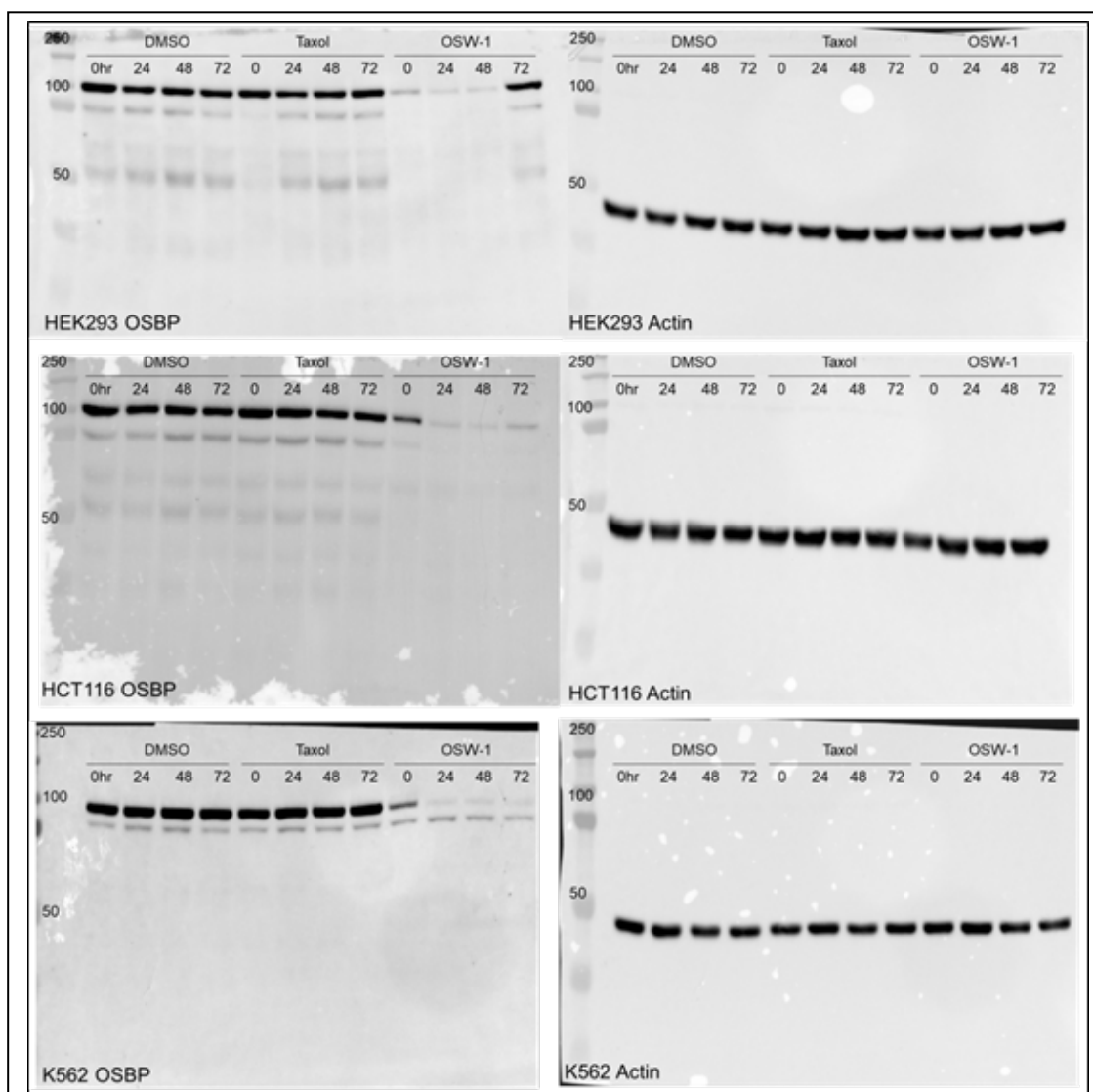


Figure 32: Full blots from Figure 5

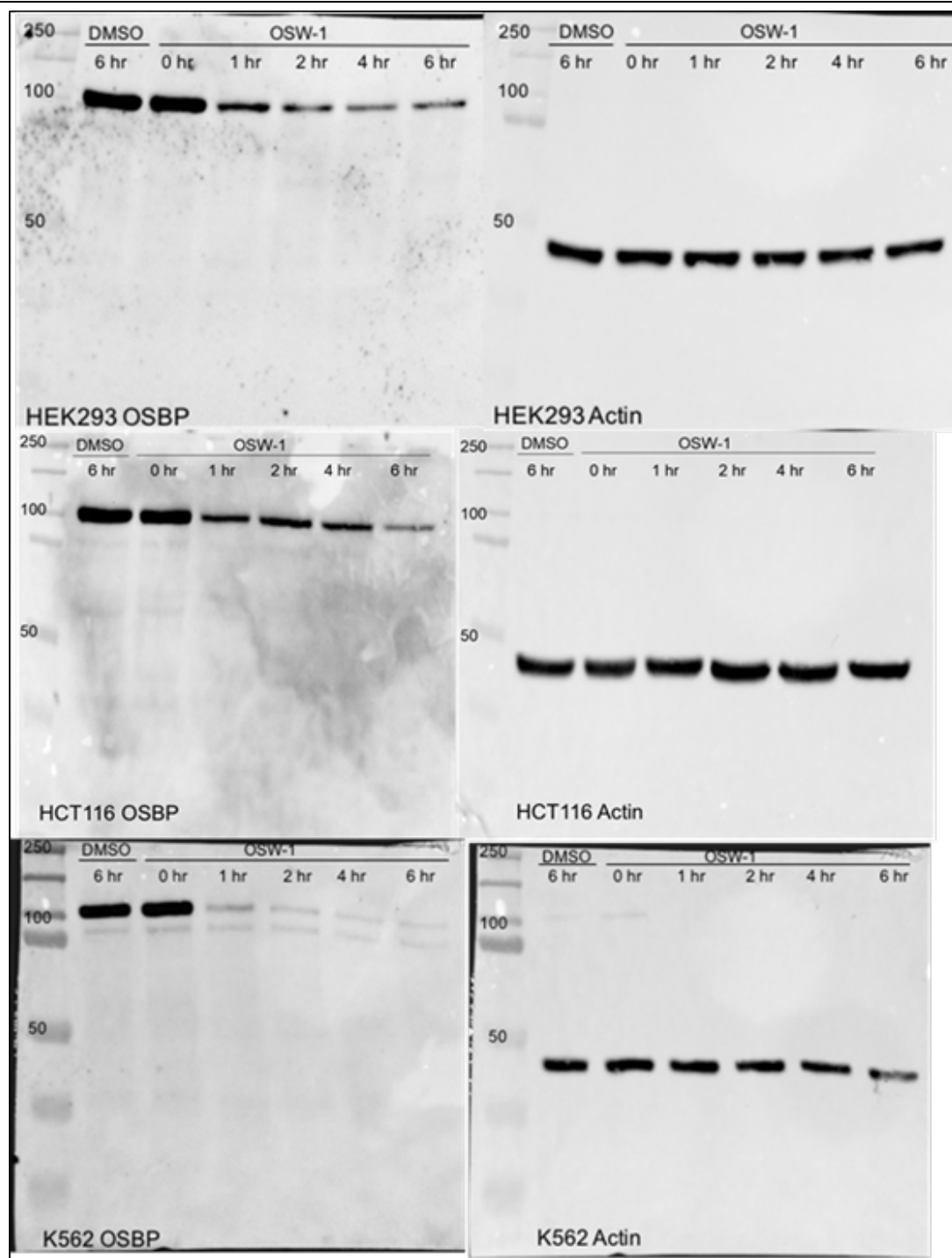


Figure 33: Full blots from Figure 5

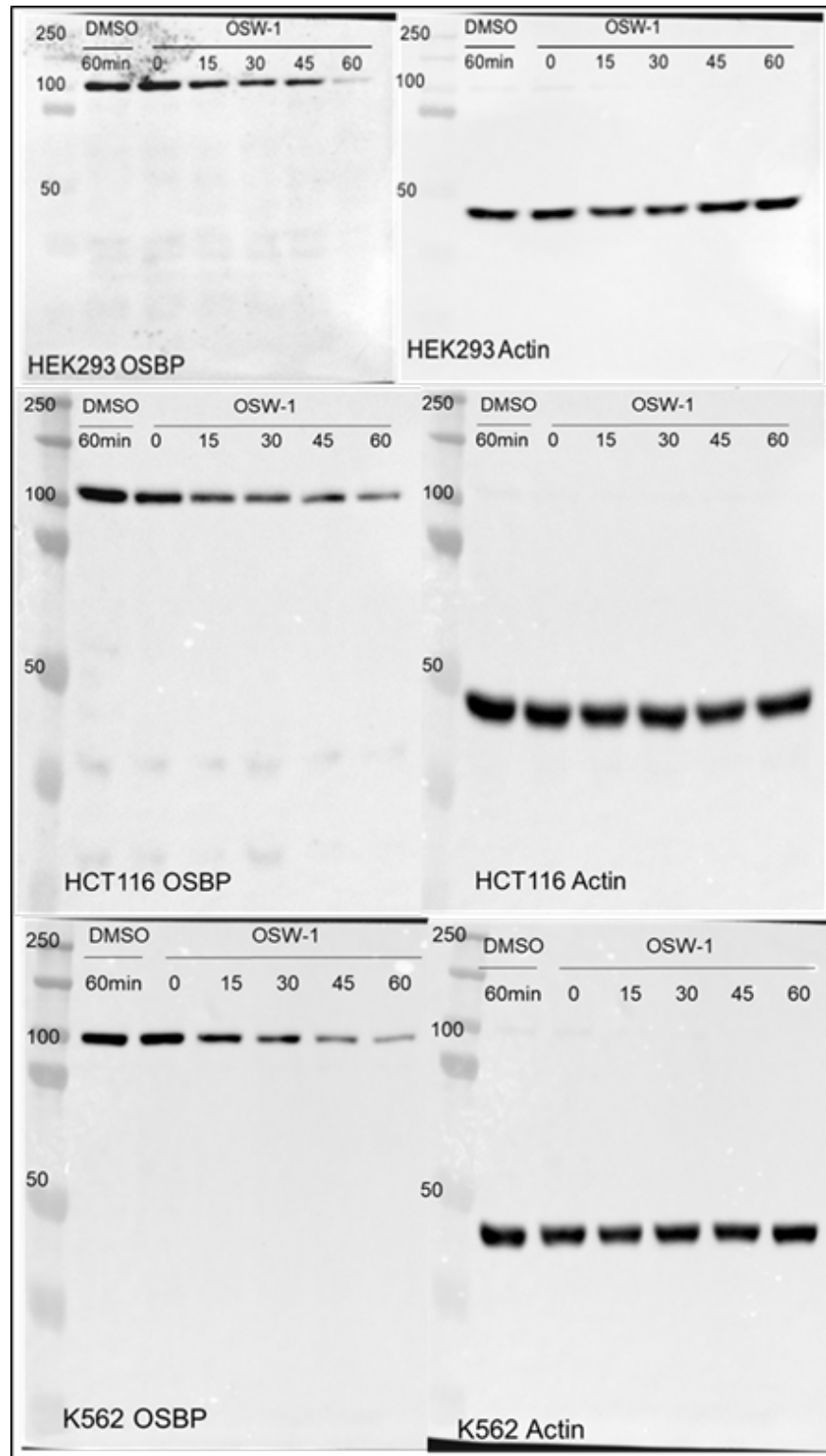


Figure 34: Full blots from Figure 5

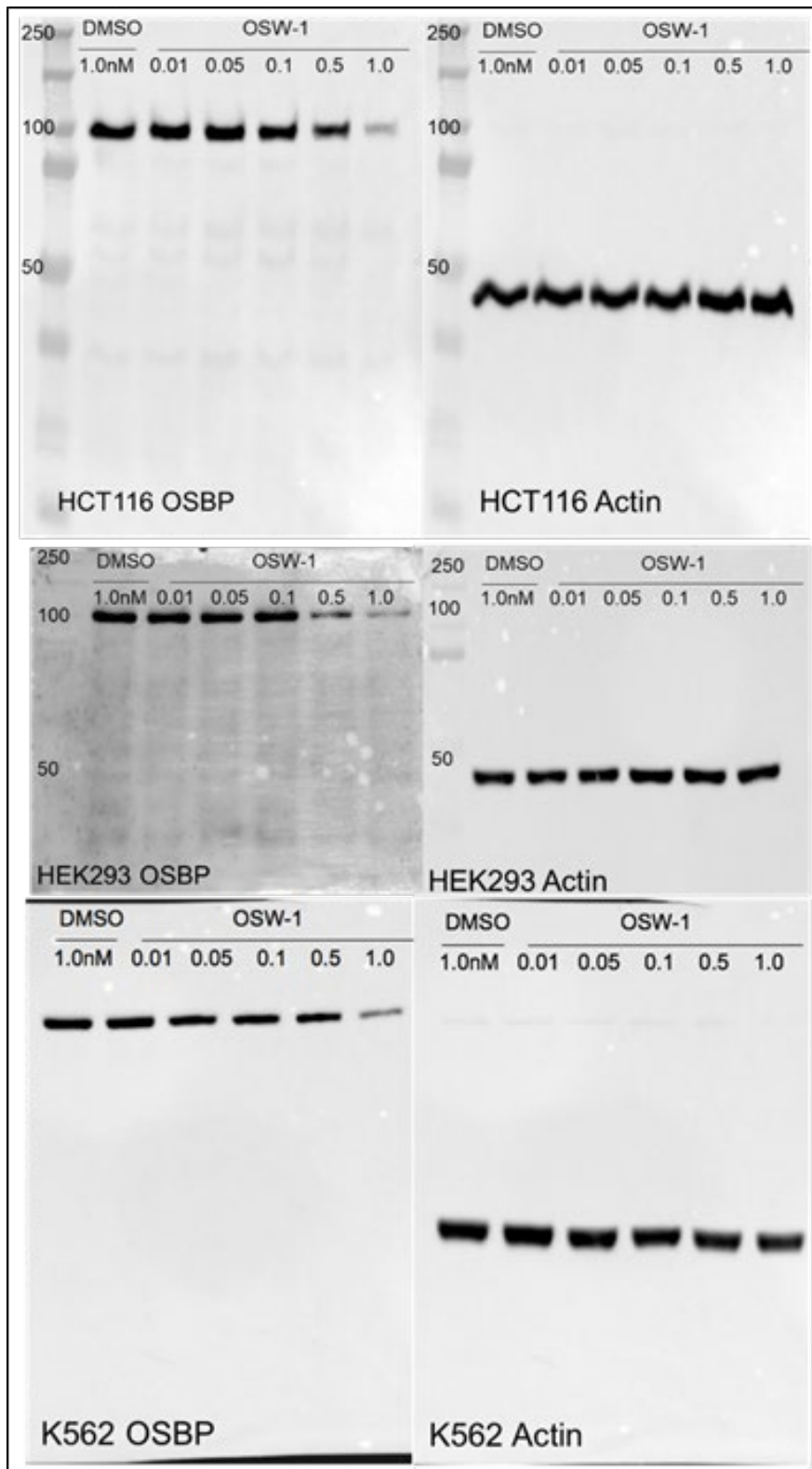


Figure 35: Full blots from Figure 5

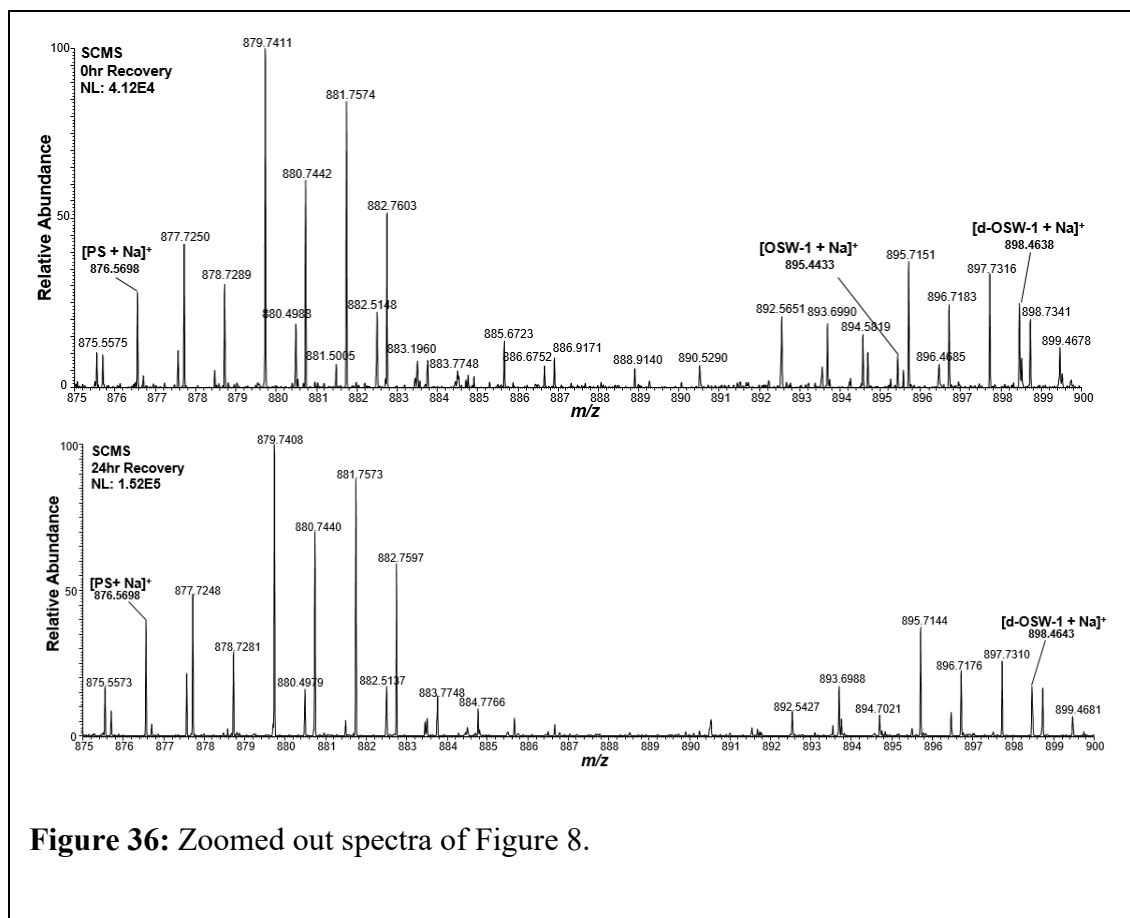
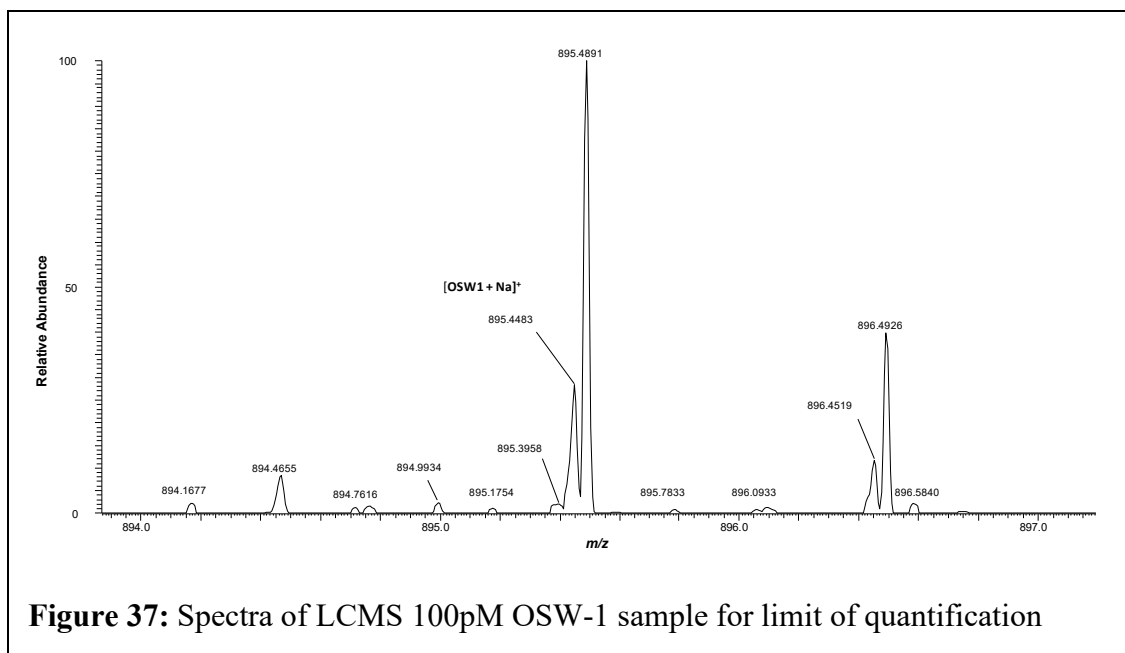


Figure 36: Zoomed out spectra of Figure 8.



Appendix 2: Chapter 3 Supplemental

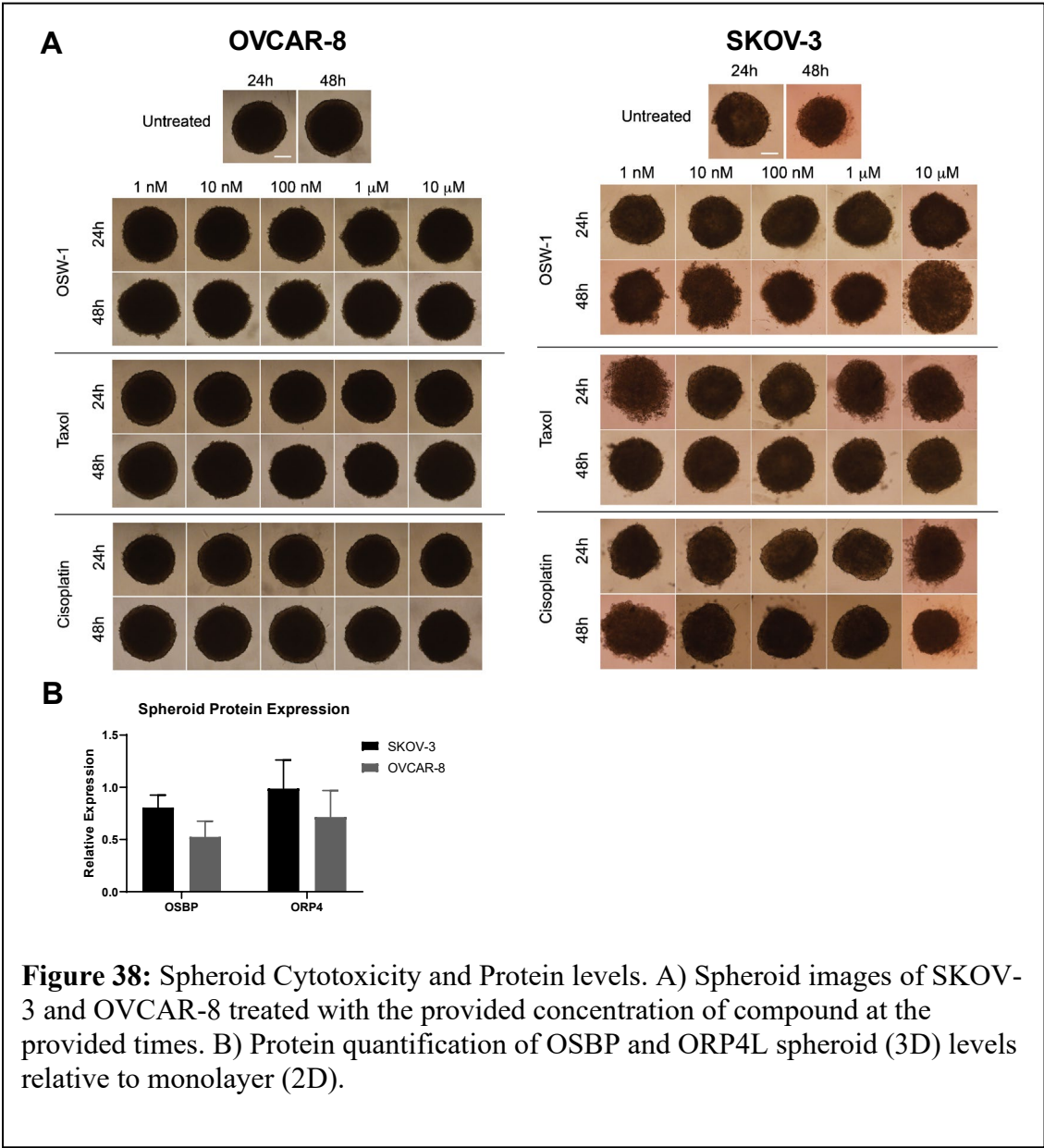


Figure 38: Spheroid Cytotoxicity and Protein levels. A) Spheroid images of SKOV-3 and OVCAR-8 treated with the provided concentration of compound at the provided times. B) Protein quantification of OSBP and ORP4L spheroid (3D) levels relative to monolayer (2D).

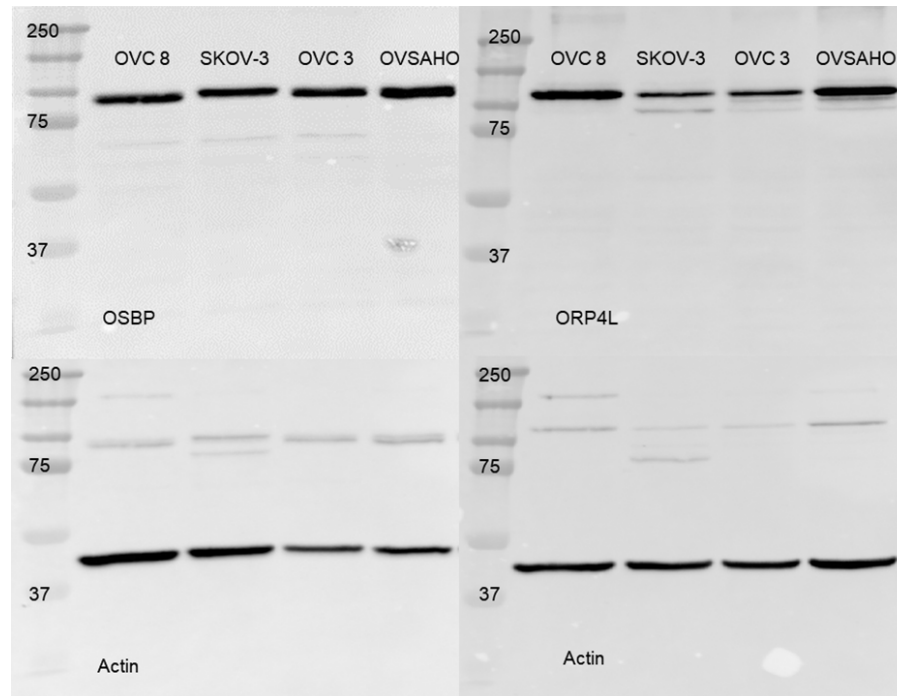
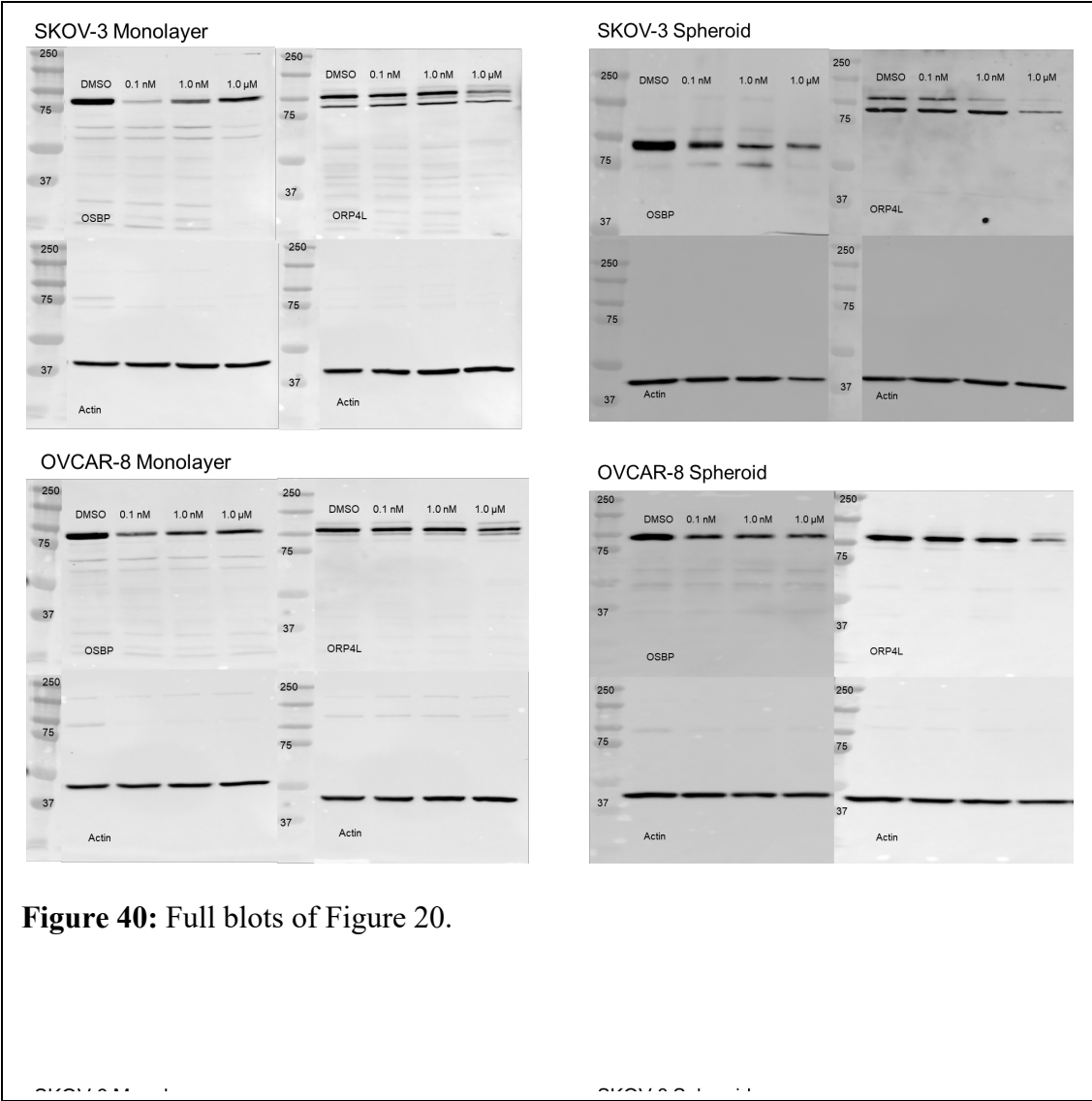
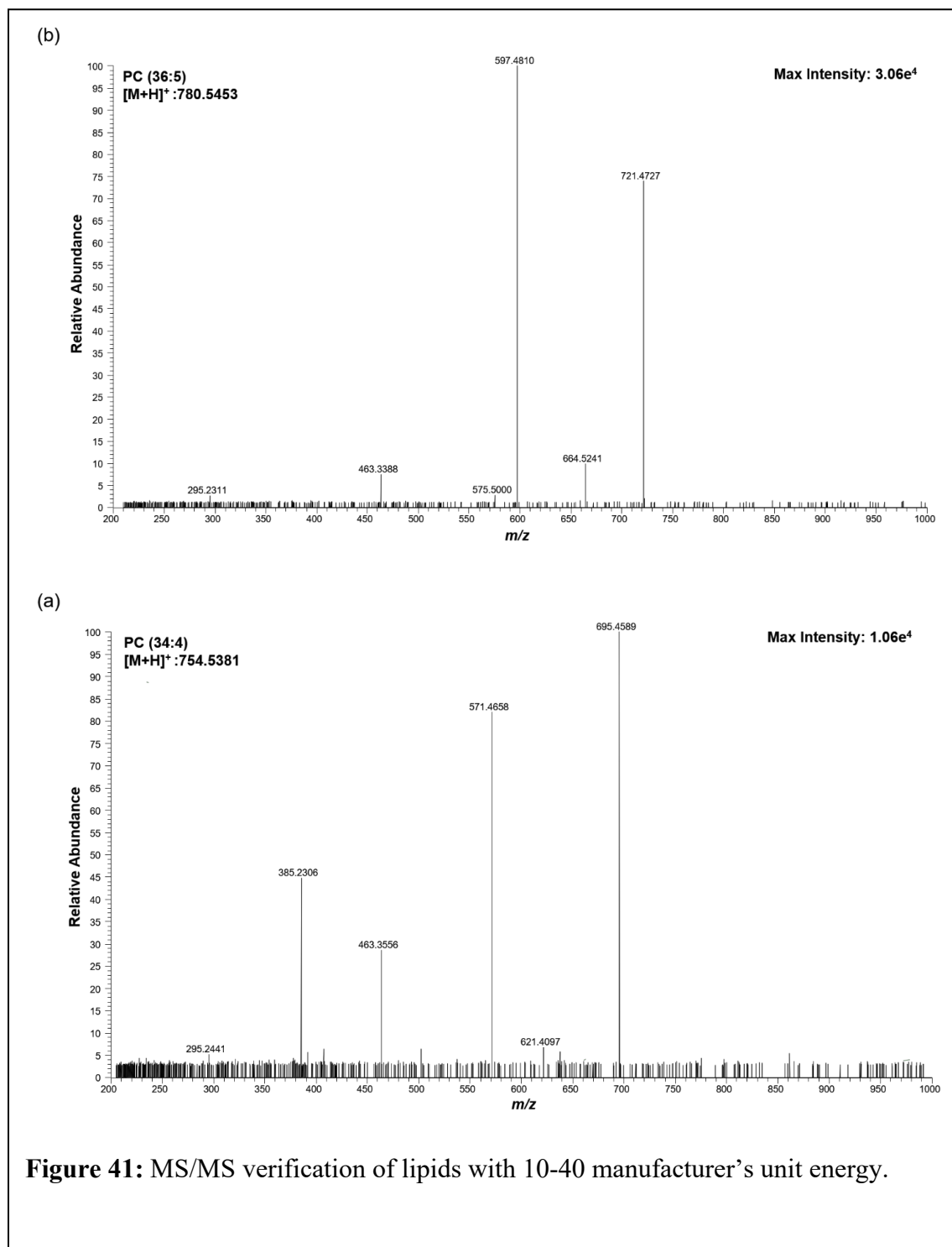


Figure 39: Full blot of Figure 15.



Appendix 3: Chapter 4 Supplemental



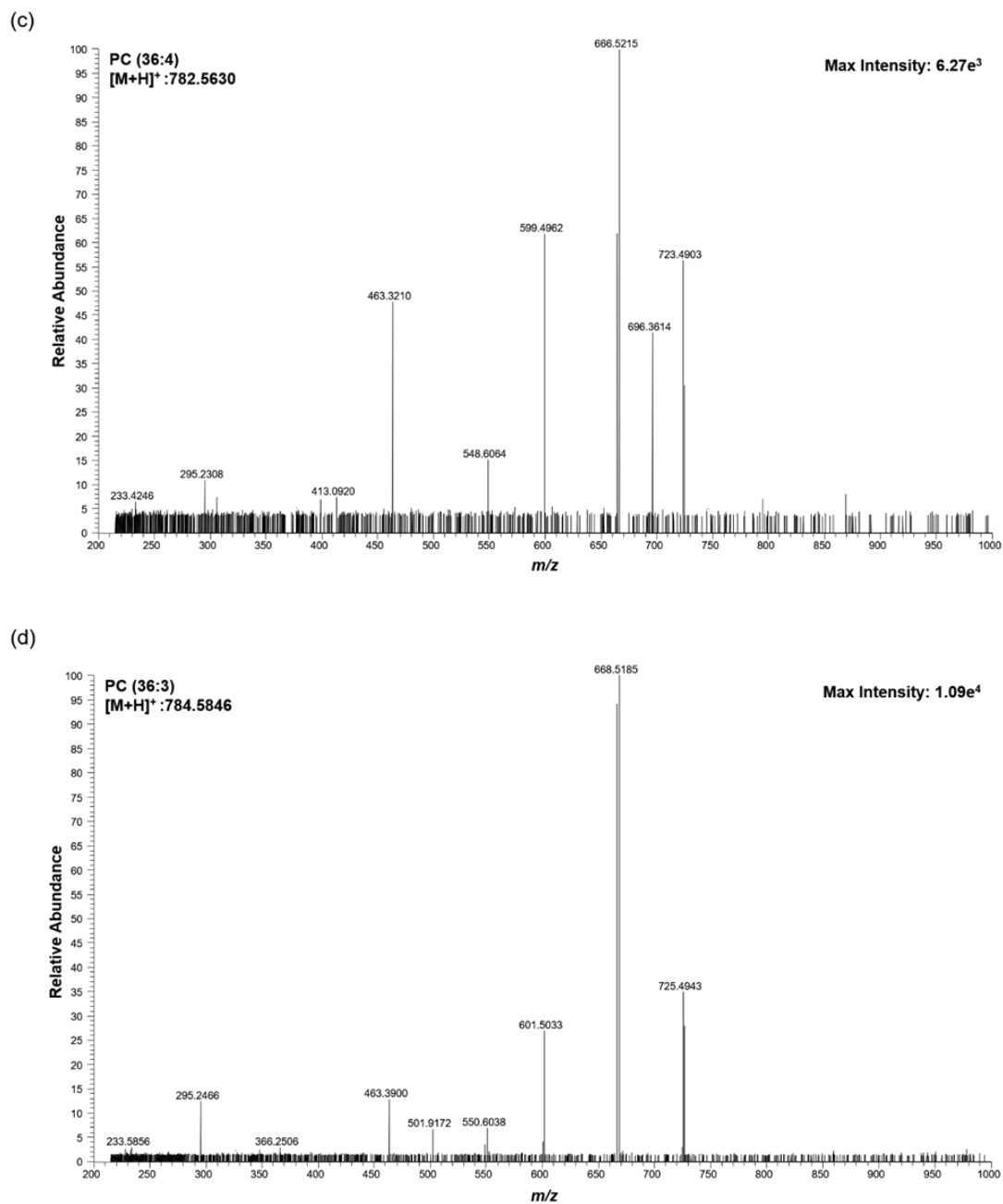


Figure 42: MS/MS verification of lipids with 10-40 manufacturer's unit energy.

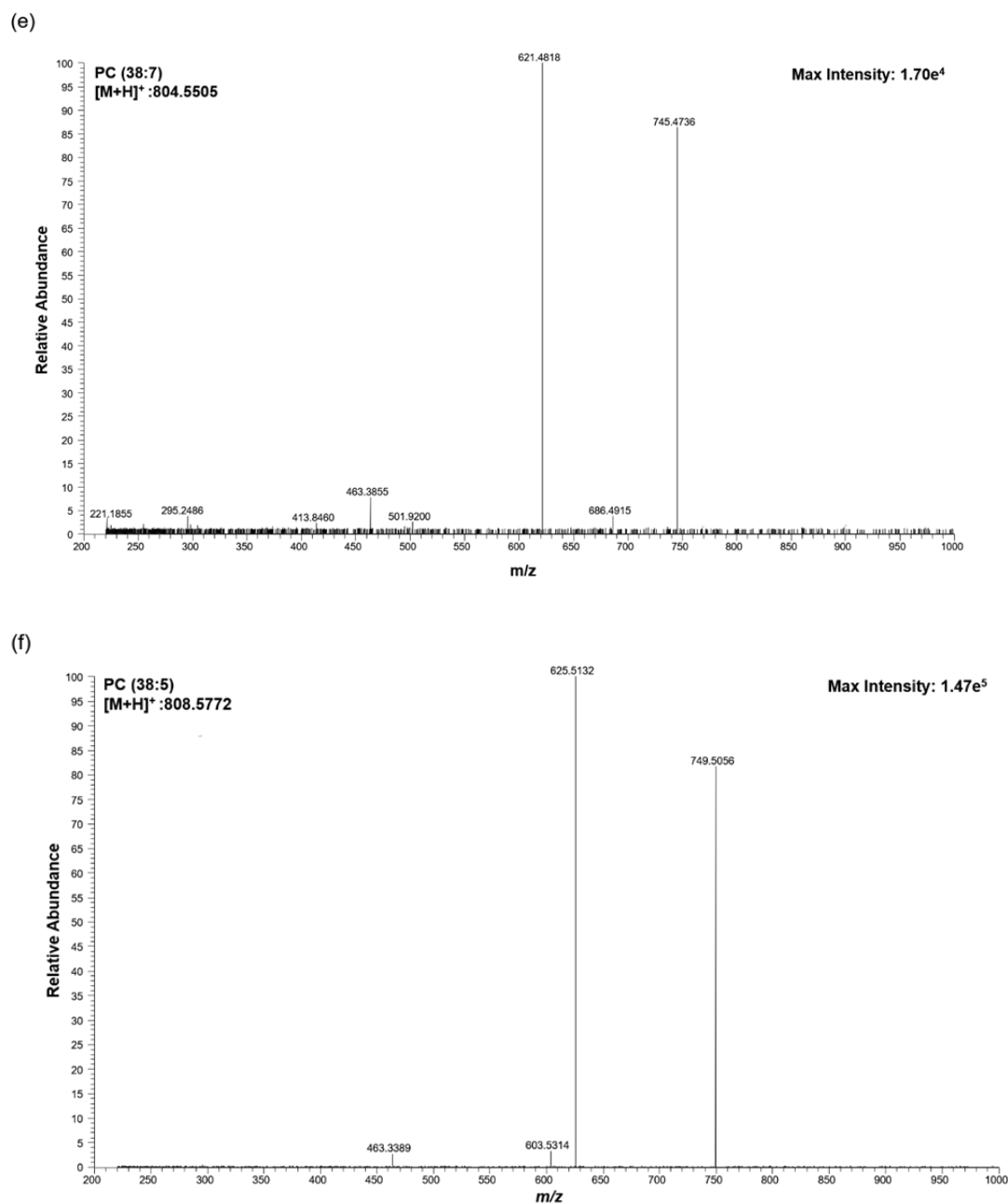


Figure 43: MS/MS verification of lipids with 10-40 manufacturer's unit energy.

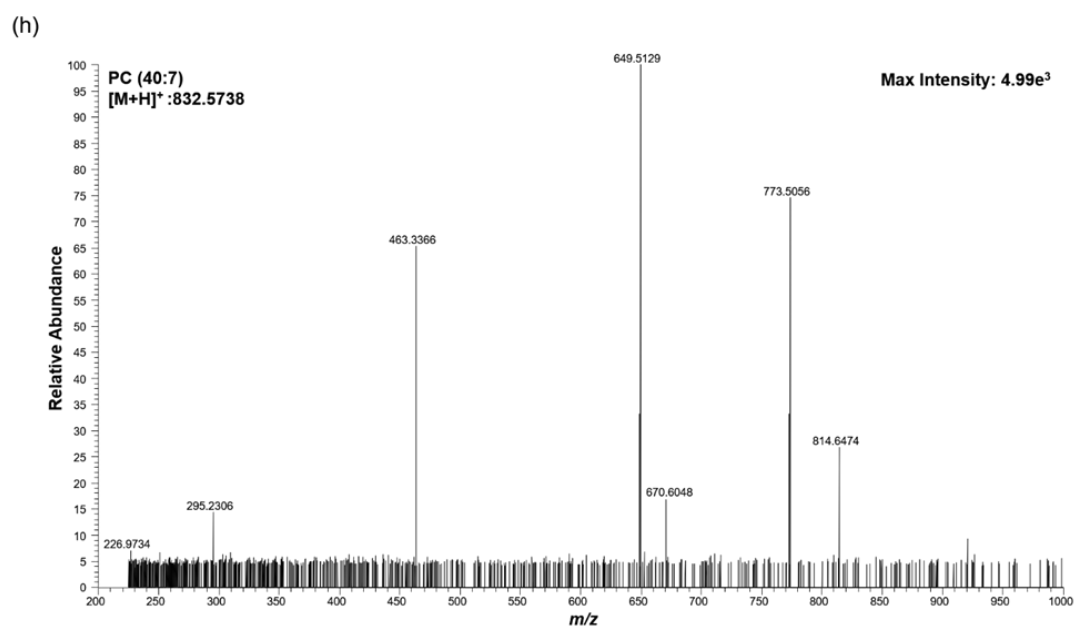
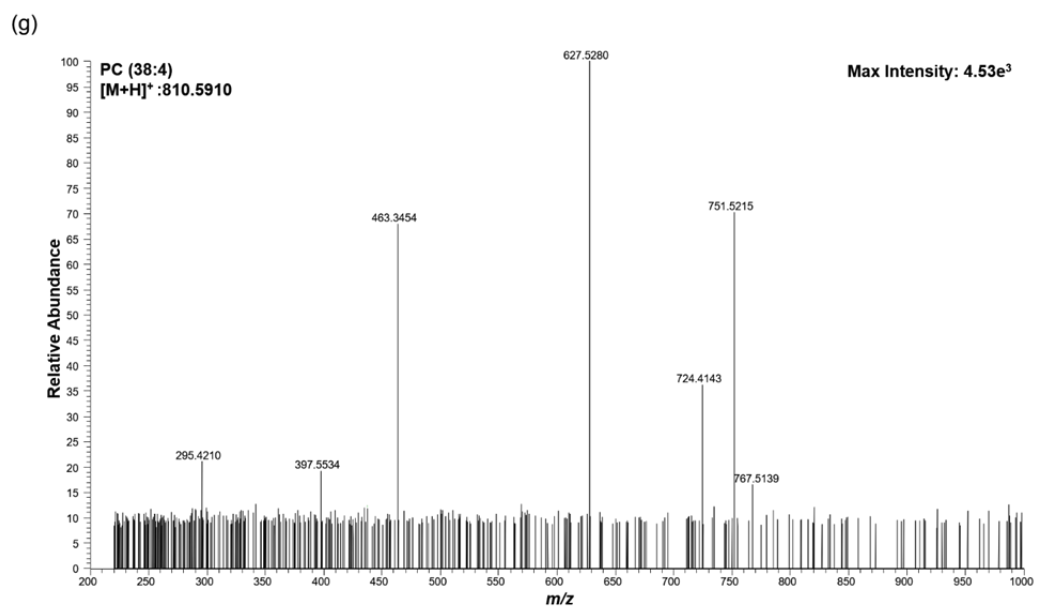


Figure 44: MS/MS verification of lipids with 10-40 manufacturer's unit energy.

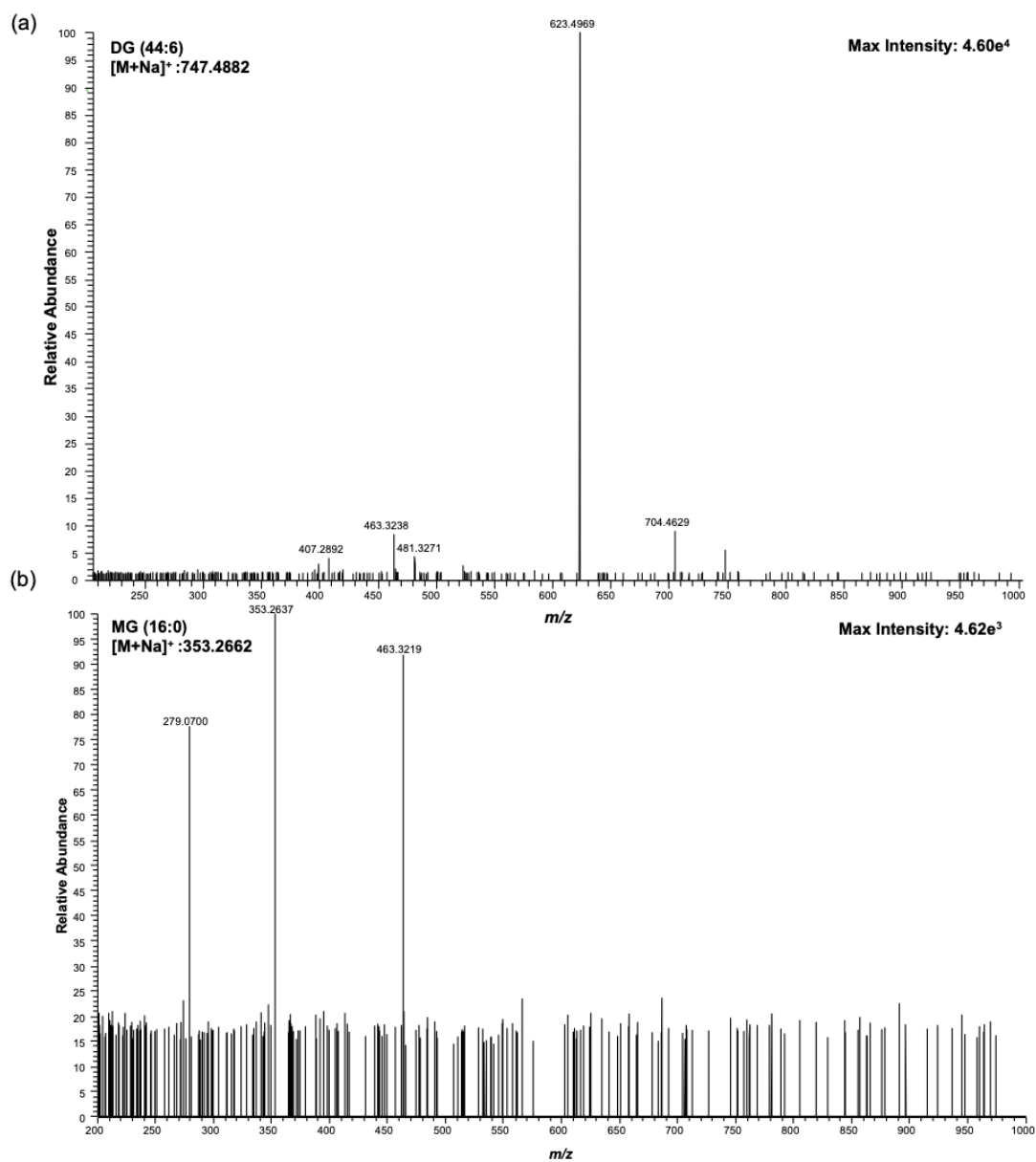
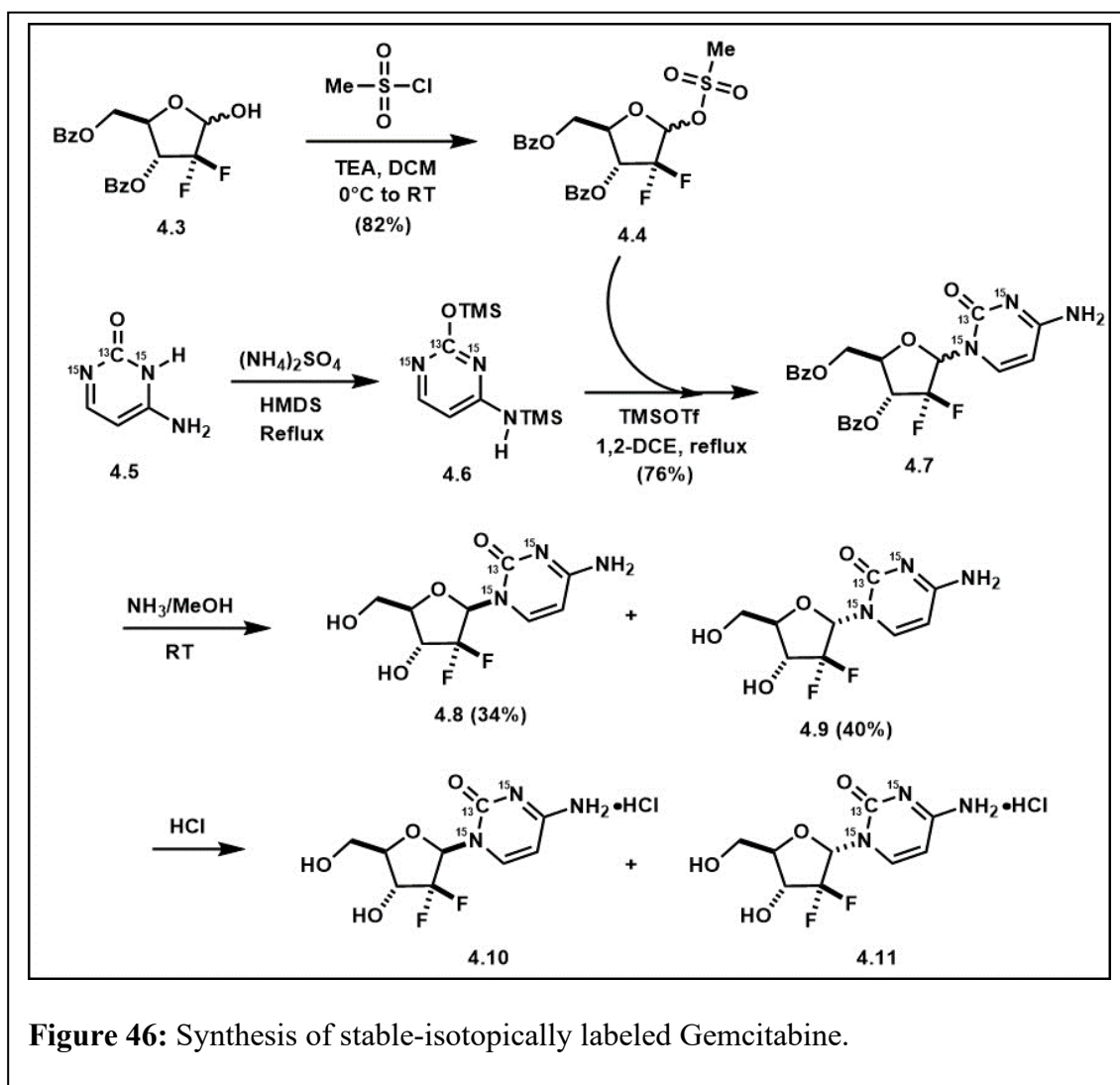


Figure 45: MS/MS verification of lipids with 10-40 manufacturer's unit energy.



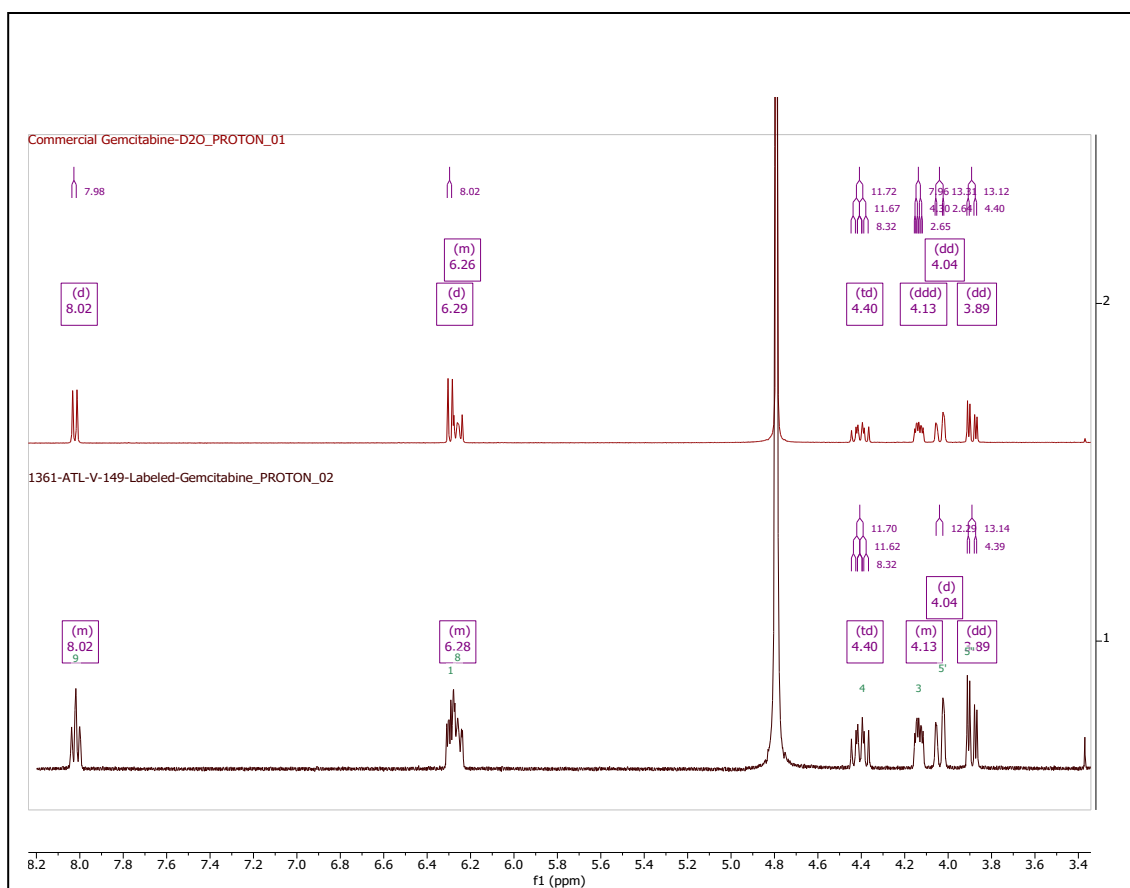


Figure 47: ^1H NMR spectra of non-labeled gemcitabine (top) and labeled gemcitabine (bottom).

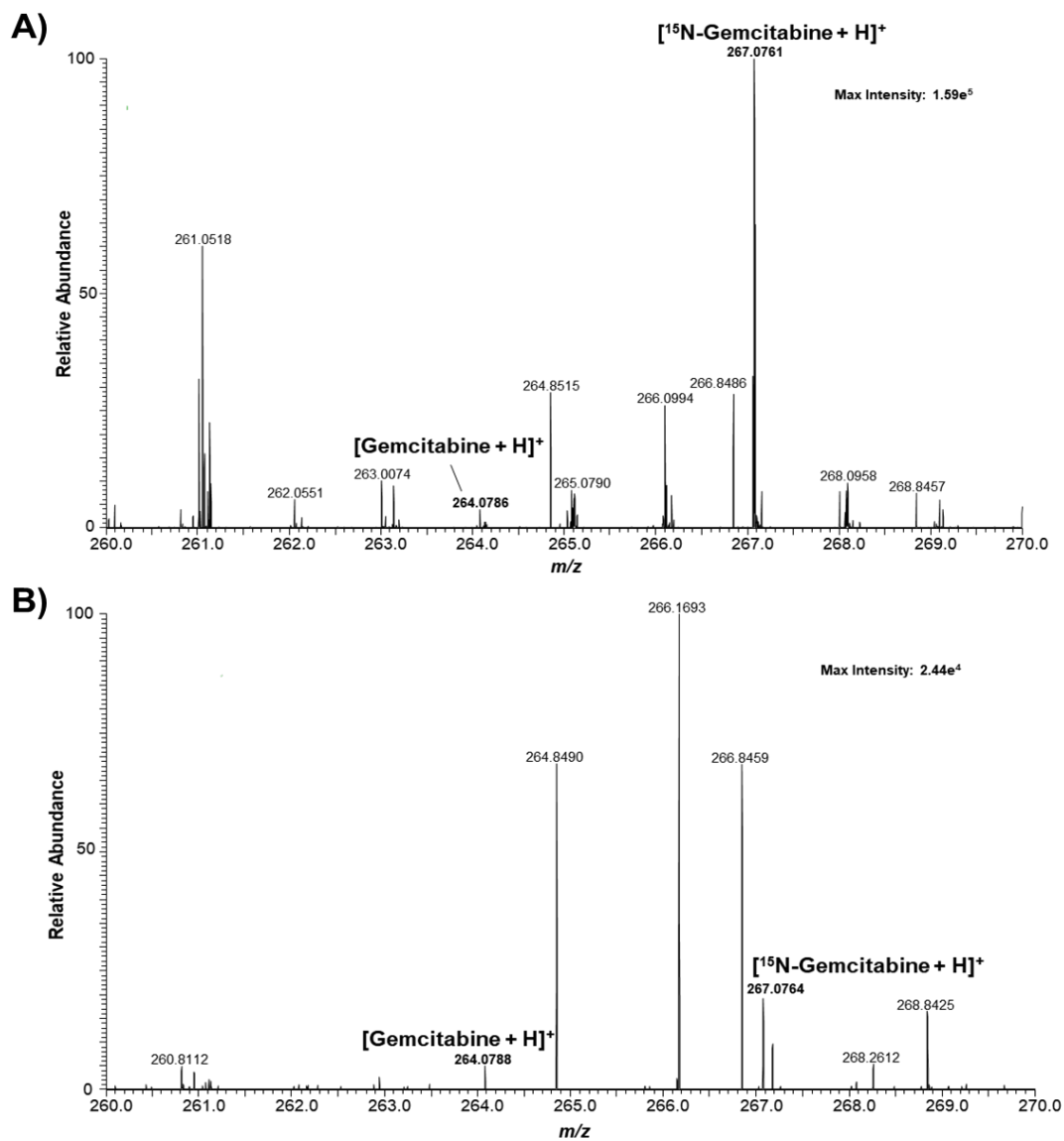


Figure 48: Mass spectrum of gemcitabine and $^{15}\text{N}_3$ -gemcitabine. (A) Spectra from a single T24 cell following 1 h 10 μM Gemcitabine treatment. (B) Spectra from a single K562 cell following 1 h 10 μM Gemcitabine treatment.

